

UNIVERSIDAD AUTÓNOMA DE BAJA CALIFORNIA  
FACULTAD DE CIENCIAS MARINAS  
INSTITUTO DE INVESTIGACIONES OCEANOLÓGICAS



"CIRCULACIÓN SUPERFICIAL EN LA BAHÍA DE TODOS SANTOS  
OBSERVADA POR RADARES DE ALTA FRECUENCIAS"

TESIS  
QUE PARA CUBRIR PARCIALMENTE LOS REQUISITOS NECESARIOS  
PARA OBTENER EL GRADO DE

DOCTOR EN CIENCIAS EN OCEANOGRÁFÍA COSTERA

PRESENTA

LUIS FELIPE NAVARRO OLACHE

ENSENADA BAJA CALIFORNIA, MÉXICO, Agosto 17 DEL 2019

"CIRCULACIÓN SUPERFICIAL EN LA BAHÍA DE TODOS SANTOS  
OBSERVADA POR RADARES DE ALTA FRECUENCIAS"

TESIS

QUE PARA CUBRIR PARCIALMENTE LOS REQUISITOS PARA  
OBTENER EL GRADO DE DOCTOR EN CIENCIAS

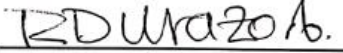
PRESENTA

Luis Felipe Navarro Olache

Aprobada por:

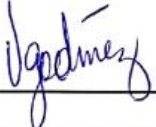


\_\_\_\_\_  
Dr. Rafael Hernández Walls  
Director



\_\_\_\_\_  
Dr. Reginaldo Durazo Arvizu

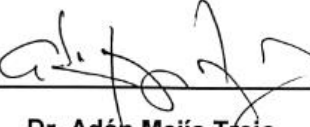
Co-Director



\_\_\_\_\_  
Dr. Victor M. Godínez Sandoval  
Sinodal



\_\_\_\_\_  
Dr. Martín Hernández Ayón  
Sinodal



\_\_\_\_\_  
Dr. Adán Mejía Trejo  
Sinodal

**“CIRCULACIÓN SUPERFICIAL EN LA BAHÍA DE TODOS SANTOS  
OBSERVADA POR RADARES DE ALTA FRECUENCIAS”**

## **AGRADECIMIENTOS**

Gracias a la Universidad Autónoma de Baja California, México por recibirme en el doctorado de Oceanografía Costera de la Facultad de Ciencias Marinas y del Instituto de Investigaciones Oceanológicas, por otorgarme todas las facilidades para realizar este trabajo. Deseo también agradecer a todos aquellos que dejaron su valiosa aportación para la este trabajo. Efraín Abraham Gutiérrez Galindo, Isaí Pacheco Ruiz y Asdrúbal Martínez Díaz de León.

Al Dr. Rafael Hernández Walls y Dr. Reginaldo Durazo por haberme aceptado como estudiante, dándome su confianza al tomar la Dirección de mi trabajo, y aportando tiempo, conocimiento y dedicación para la realización de los análisis de este. En especial a Rafael Hernández por su desinteresado generosa y desprendida dosis de líneas de programación ideas y recursos que en ningún momento me reservo.

Agradezco a los Doctores Adán Mejía, Rubén Castro Valdez y Xavier Flores por haberme ayudado a resolver muchos de los problemas que se fueron presentando y seguir trabajando en sus soluciones. Al Dr. Martin Hernández Ayón por su disponibilidad hasta el último momento, y por su siempre animosa lucha contra el tiempo, muchas gracias.

Agradezco al Dr. Víctor Godínez por su entusiasmo y valioso apoyo que durante todo el proceso de este trabajo me brindo, sin ningún interés y siempre en busca de un mejor trabajo. Gracias a un verdadero profesional en su campo, un amigo ejemplar y una persona extraordinaria.

Muchas gracias a todos los miembros del Laboratorio de oceanografía operacional y radares Jesús, Andy, Lalo y Eduardo Gil por su ayuda y asistencia en la realización de esta investigación en particular al próximo Doctor en ciencias Isaac Rodríguez Padilla quien colaboró en el análisis de datos de este trabajo.

Debo agradecer a muchas personas más y pido me disculpen por la omisión.

## **Dedicatoria**

**A Don Walde y Mayita, motores amorosos de cualquiera de mis caóticas trayectorias**

**A mis timones, hermanos de cuna Waldemar, Mayela, Eduardo y hermanos de vida Armando, Canito, Rubén y Víctor**

**Para mis hijas mis grandes tesoros motivo de mis alegrías Ana Karen y Pamela por su compresión por el tiempo robado, las amo.**

**A mi amada esposa Lucy por su fortaleza sacrificio e impulso para llevar a buen puerto esta tarea, para mi titánica. Te amo.**

**Al creador, impulsor del todo, quien se ha encargado de que el tiburón siempre ronde en mi bañera.**

## Tabla de Contenido

|  |          |
|--|----------|
| <i>Capítulo I.</i>   | <hr/> 1  |
| Medición de corrientes superficiales en el océano mediante radares de alta frecuencia  | <hr/> 1  |
| <i>Capítulo II</i>   | <hr/> 11 |
| Santa Ana's winds influence over the surface circulation of Todos Santos Bay, Baja California,<br>México                     | <hr/> 11 |
| <i>Capítulo III</i>  | <hr/> 47 |
| Kinematic parameters within Todos Santos Bay using the surface current velocity obtained with<br>high frequency radars       | <hr/> 47 |
| <i>Capítulo IV.</i>  | <hr/> 77 |
| Efecto de estructuras Coherentes Lagrangeanas de meso-escala sobre la circulación superficial de la<br>Bahía de Todos Santos | <hr/> 77 |

# Capítulo I.

## Medición de corrientes superficiales en el océano mediante radares de alta frecuencia

Luis F. Navarro Olache, Rafael Hernández Walls, Reginaldo Durazo.

Universidad Autónoma de Baja California UABC,

### 1. Introducción

Los movimientos de fluidos en el océano son el resultado de diferentes fuerzas que combinadas, permiten el transporte de agua y sus propiedades de un lugar a otro, llamadas corrientes marinas. El esfuerzo del viento, mareas y gradientes de densidad, acopladas con la rotación terrestre trasladan agua, calor y propiedades en forma de corrientes marinas a lo largo y ancho de los océanos. Una gran parte de las corrientes en el mundo son conocidas por sus características promedio de dirección predominante y principales propiedades de trasporte y mezcla. El sistema de la Corriente de California, la Corriente de Kuroshio, la Corriente del Golfo o la Corriente Circumpolar Antártica, solo por mencionar algunas (Figura 1.1).

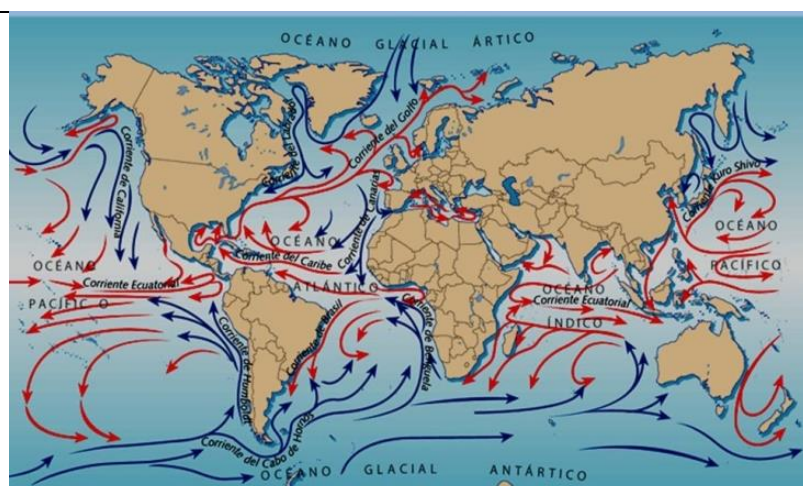


Figura 1.1. Corrientes superficiales del mundo, mostrando la dirección promedio de flujo, de

(<https://www.meteorologiaenred.com/corrientes-marinas.html>)

Mediante observaciones se ha generado el concepto de que los flujos en la superficie del océano presentan un comportamiento promedio que se muestra en la figura 1.1, sin embargo en el detalle, las trayectorias de partículas individuales en estos flujos son altamente dependientes del tiempo, el espacio y la posición inicial. Por ejemplo, si dos elementos o partículas son colocados a la deriva, en un flujo como el que se esquematiza en figura 1.2A, podemos predecir que por un tiempo, ambos elementos se desplazara manteniendo una razón de separación más o menos constante, y con velocidades similares. Después de un tiempo, siguiendo el flujo de la estructura, los elementos cambiaran su trayectoria y la distancia que existe entre ellos, aumentando o disminuyendo de acuerdo a su posición de origen. En este ejemplo los elementos, marcados en la figura, se alejaran notablemente, para invertir el sentido del movimiento inicial, siguiendo la estructura de flujo en forma de dipolo. En este caso diferente posición inicial podría genera una trayectoria diferente. Con estas características, las observaciones detalladas de corrientes en el medio natural son complejas y ambiguas, sobre todo cuando se confía en metodología tradicional, ya sea metodología Lagrangeana (boyas de deriva) o Eulereanas (puntos fijos). Conocer detectar y predecir trayectorias de elementos particulares es clave en estudios del comportamiento de manchas de contaminación, dispersión de petróleo, distribución de larvas o semillas e incluso en labores de búsqueda y rescate. Podemos imaginar que serían necesarios seguir cientos o miles de boyas de deriva o innumerables instrumentos fijos para distinguir las trayectorias reales capaces de representar las trayectorias que se simulan mediante escenarios numéricos (Figura 1.2B). En este trabajo se describe una técnica efectiva y confiable de monitorear corrientes superficiales del océano, utilizando una red de radares de alta frecuencia. Los Radares de alta frecuencia proveen una base de datos de alta resolución en tiempo y espacio del campo de velocidad superficial, el cual puede ser utilizado para describir no solo patrones de movimiento sino además describir con un alto grado de confiabilidad algunos patrones cinemáticos de esta circulación, como la divergencia la vorticidad y la deformación del flujo. El método ha sido probado en USA y por algunos años en las costas norte del Pacífico mexicano

esperando que en un futuro se pueda construir una base de información nacional en tiempo real para observar las corrientes cercanas a la costa de nuestro País.

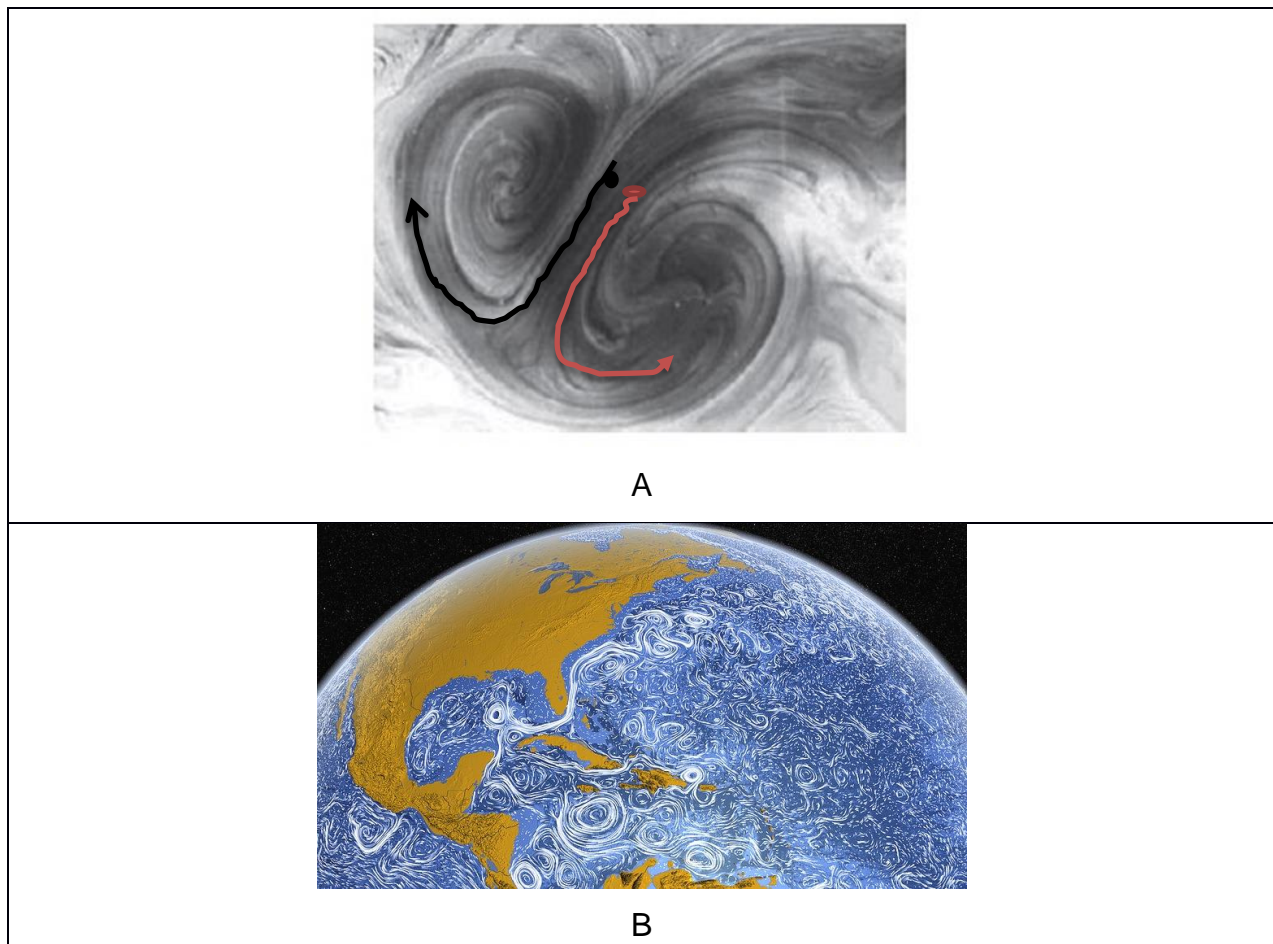


Figura 1.2. A) Representación gráfica de la trayectoria de dos partículas sobre un flujo tipo vórtice dipolo en el laboratorio, fuente Voropayev y Afanasyev (1994). B) Simulación numérica de la circulación superficial del Océano Atlántico (<http://managingwholes.com/images/paradigms/oceancurrents.jpg>)

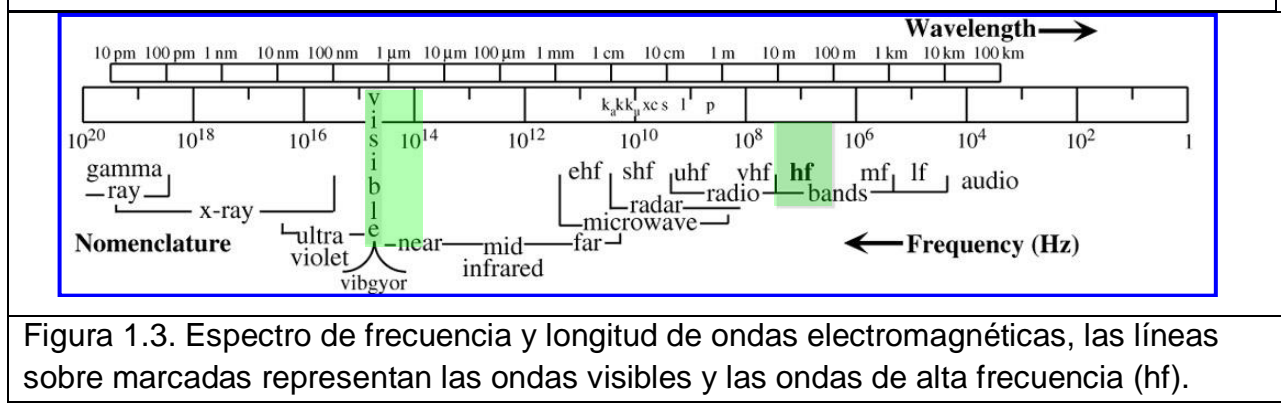


Figura 1.3. Espectro de frecuencia y longitud de ondas electromagnéticas, las líneas sobre marcadas representan las ondas visibles y las ondas de alta frecuencia (hf).

## Radares de Alta frecuencia

La velocidad de las corrientes superficiales calculadas por radares se basa en la trasmisión de ondas electromagnéticas (radiofrecuencia) desde un punto fijo sobre la costa, en dirección del océano. Estas bandas de frecuencia están entre los 3 a 50 MHz (HF) con longitudes de onda ( $L=C/f$ ) entre 100 a 6 metros, donde  $C$  es la velocidad de la luz (Figura 1.3). Estas bandas de frecuencias caen en las ondas habituales de radio de amplitud modulada (~1MHz) y frecuencia modulada (~100 MHz) por lo que también los radares son llamados radio escaterómetros. Aunque el método teórico se desarrolló hace más de 50 años, su carácter de prototipos los había mantenido al margen como instrumentos oceanográficos hasta hace algunas décadas, cuando se iniciaron campañas de medición de velocidades con aplicaciones militares y después por universidades, en particular en las costas de Estados Unidos, Canadá, Alemania, Filipinas, y China. A la fecha la costa este y oeste de Estados Unidos cuenta con un sistema costero de corrientes superficiales que es utilizado para aplicaciones académicas y de seguridad e incluso como auxiliares las labores de búsqueda y rescate para militares y guardacostas ver por ejemplo:

<https://cordc.ucsd.edu/projects/mapping/global/> y  
<http://cordc.ucsd.edu/projects/mapping/maps/>

## Operación

Los radares operan con fundamento en la llamada ley de Bragg, presentada en 1912 por William Henry y William Lawrence Bragg sobre el análisis de la estructura de cristales por medio de propiedades de difracción de rayos X. Los Bragg, padre e hijo, encontraron que, bajo ciertos ángulos de incidencia de rayos de luz, proyectada sobre un cristal, se producían picos intensos de radiación, conocidos ahora como picos Bragg y no son otra cosa que ondas que entran en resonancia o interferencias constructivas de la longitud de onda incidente a determinados ángulos de ataque. A los Bragg esto les permitió encontrar la estructura atómica de cristales y los llevó a ganar el premio Novel de física. Con el mismo principio Crombie (1955) observó interferencias constructivas al transmitir y recibir ondas de radar incidiendo en el océano. En los

experimentos de Crombie la onda emitida con frecuencia y longitud de onda conocida se reflejaba efectivamente en las perturbaciones de la capa del océano (Figura 1.4) con una variedad de frecuencias. Aunque la mayoría de las perturbaciones (olas) refleja en forma difusa, llamó la atención algunas olas que entraban en resonancia con las ondas transmitidas, en forma similar a los picos Bragg. El oleaje resonante fue exactamente la mitad de la onda trasmitada por el radar (figura 1.4) por lo que por ésta similitud de resonancia a la ley de Bragg se le conoce también como pico Bragg y corresponde a una interferencia constructiva en el pico de mayor energía reflejada (Figura 1.5).

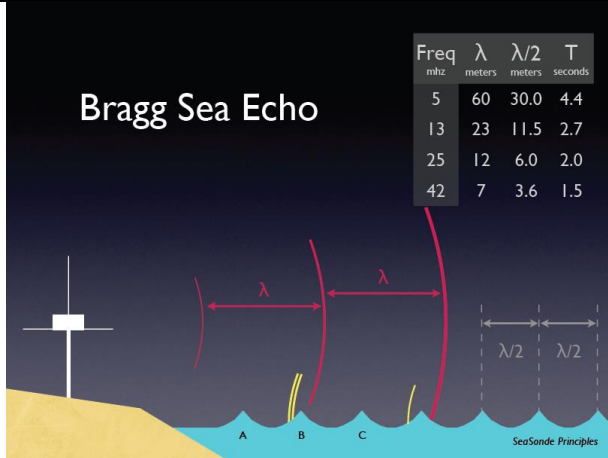
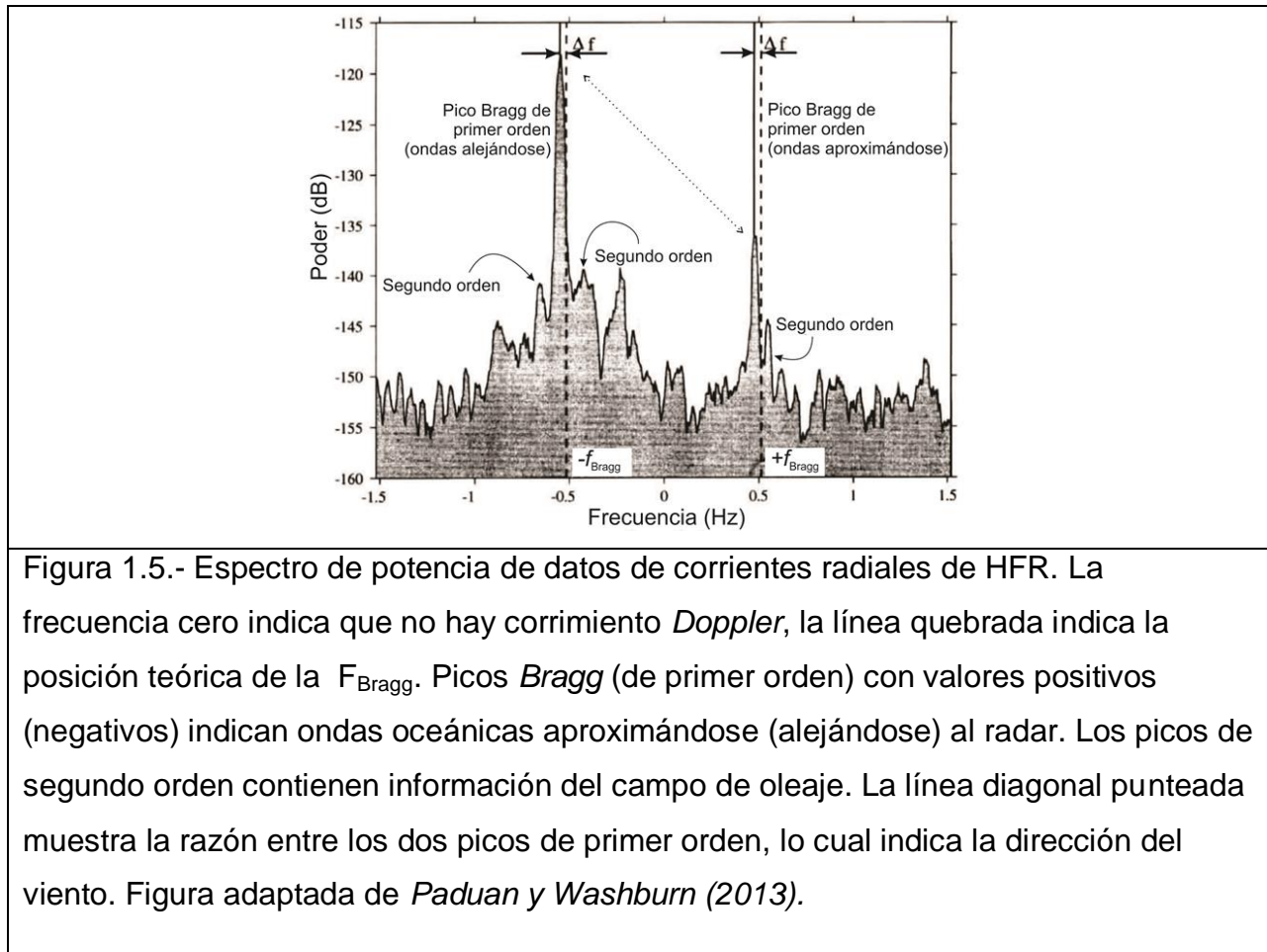


Figura 1.4. Esquema de trasmisiones con una señal de radar hacia el océano con longitud de onda  $\lambda$ . y su refección de forma especular por olas gravitacionales cuya longitud es exactamente  $\lambda/2$ . El recuadro muestra la frecuencia de trasmisión (MHz), longitudes de trasmisión y de olas en resonancia (m) además del periodo (s) (tomada de HFRadar CNR-ISMAR network).

El análisis de la señal de Crombie mostró que el pico Bragg presentaba un corrimiento en la señal ( $\Delta f$  en la **figura 1.5**) el cual lo asocio con trenes de olas alejándose en resonancia acercándose o hacia el radar debido a interacción con alguna corriente en el mar. Esta diferencia  $\Delta f$  entre la velocidad teórica del oleaje y el pico Bragg determinar la velocidad de la corriente debida al efecto Doppler. El desfase  $\Delta f$  está directamente relacionado con la velocidad radial de la corriente (Paduan et al, 1997, 2013). Con un radar se pueden detectar corrientes radiales, hacia la fuente o alejándose de ella, (ver Figura 1.6A), mientras que, con dos radares, se puede formar

un campo vectorial en dos dimensiones como se muestra en el arreglo dispuesto en la Bahía de Todos Santos (Figura 1.6B).



Los datos de dos o más radares generan mallas de velocidad superficiales con alta resolución y rango de cobertura, esto se logra por medio de la frecuencia de la onda emitida. Las frecuencias más bajas 8 MHz, tienen un rango de hasta 200 km fuera de la costa y una resolución gruesa de alrededor de 2 km entre cada punto de velocidad. Las frecuencias más altas, que pueden llegar a 80 MHz son utilizadas en aplicaciones de escala pequeñas tales como ríos esteros o incluso puertos. En estas frecuencias, la resolución espacial es fina de 1 a 10 metros, sin embargo su alcance es limitado, del orden de un kilómetro. Frecuencias intermedias se utilizan en otros rangos de acuerdo a las aplicaciones costeras que se deseé alcanzar. En la bahía de Todos Santos por ejemplo operan tres radares de 25 MHz con un alcance de 20 km. La resolución espacial es de entre 500-800 metros. Mediante radares además de las velocidades en

la superficie, se pueden extraer información de la dirección y magnitud de viento además de características de la energía del oleaje arribando a la costa.

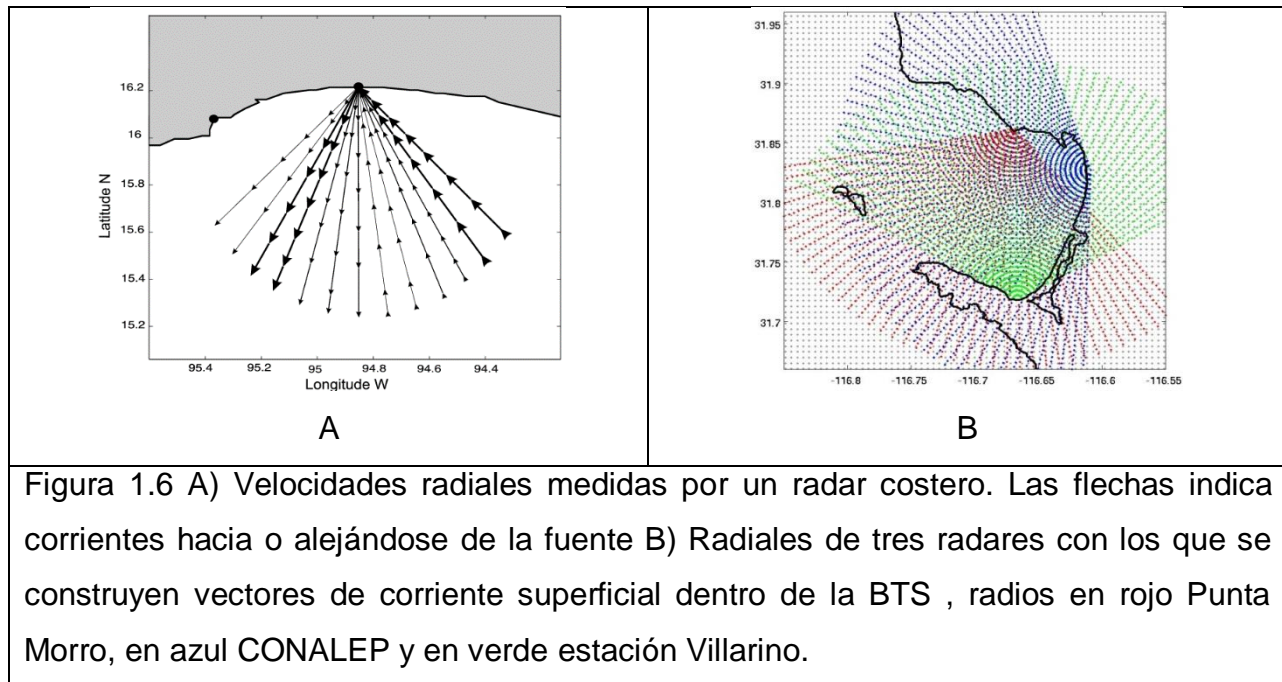


Figura 1.6 A) Velocidades radiales medidas por un radar costero. Las flechas indican corrientes hacia o alejándose de la fuente B) Radiales de tres radares con los que se construyen vectores de corriente superficial dentro de la BTS , radios en rojo Punta Morro, en azul CONALEP y en verde estación Villarino.

El uso de radares representa una ventaja sobresaliente sobre otras técnicas de medición de corrientes en el océano, incluyendo la simulación numérica. Sin embargo los datos solo muestran la capa superficial del océano. La alta resolución espacio y temporal, permite obtener información sobre las propiedades cinemáticos de los flujos, como la divergencia, la vorticidad y la deformación del campo horizontal, que proporcionan información adicional sobre cómo se mueve, dispersan y mezclan las propiedades dentro de la primera capa del océano. El observatorio regional costero de la Universidad Autónoma de Baja California genera desde finales de 2009 datos horarios del campo de corrientes en la Bahía de Todos Santos. El observatorio está localizado en la región NW de México (Figura 1.6B) y genera una malla de 22x22 nodos usando 2 radares y de 78x80 nodos utilizando 3 radares, para obtener una resolución espacial de entre 500-800 m (Flores Vidal et al., 2015; Figura 1.6B). El arreglo de radares transmite en una frecuencia de alrededor de 25 MHz (Figura 1.7A) con una precisión radial de  $0.06 \text{ m s}^{-1}$ , promediadas cada hora (Flores-Vidal et al., 2015).

En la Figura 1.7 se muestran algunos ejemplos de los datos de corriente superficial en la bahía. El promedio de la hora 19 del día 1º de enero del 2010, muestra los efectos de un evento de Santa Ana, con flujos de viento hacia afuera de la costa y el correspondiente flujo de la corriente superficial, a partir de 2 radares también hacia afuera de la costa. Estos flujos hacia afuera de la costa responden a pulsos de viento de frecuencia diurna, intensos y de corta duración que ocurre con frecuencia durante otoño e invierno (Navarro et al 2017, 2018). En este mes la variabilidad de las corrientes en la bahía muestra zonas de calma en el interior y zonas de altas velocidades en la frontera abierta. El promedio de este mes está asociado a eventos de tormentas invernales, 2 eventos de vientos de Santa Ana ocurridas en el mes enero de 2010 y los sistemas de brisa locales. En este caso el promedio de la circulación de la bahía, muestra un dominante giro ciclónico, el cual sigue el contorno de la bahía (Figura 1.7B).

El método de radares presenta ventajas sobresalientes en la obtención de datos de corriente superficiales, comparado a cualquier otro método para medir corrientes en el océano. Esto permite incursionar en otras áreas para resolver problemas más complejos, como seguir la forma y dispersión de manchas de contaminantes, como el petróleo, la forma y proyección de descargas de aguas residuales y otros flujos complejos en el océano. Los datos y la metodología de radares son usados en labores de búsqueda, en localización de embarcaciones y objetos sobre la superficie como embarcaciones o hielo, además ofrecen una cobertura de datos de velocidad en zonas donde los sensores remotos (satélites) y embarcaciones oceanográficas están limitados por la cercanía de la costa y profundidad. El método mide el campo de velocidades en la superficie, muy cerca de la costa y con una densidad de datos que puede ser generada por datos tradicionales. Los radares aseguran que el conocimiento de la circulación superficial avance y que nuevos métodos sean implementados, para obtener una visión más holista de la circulación en los océanos.

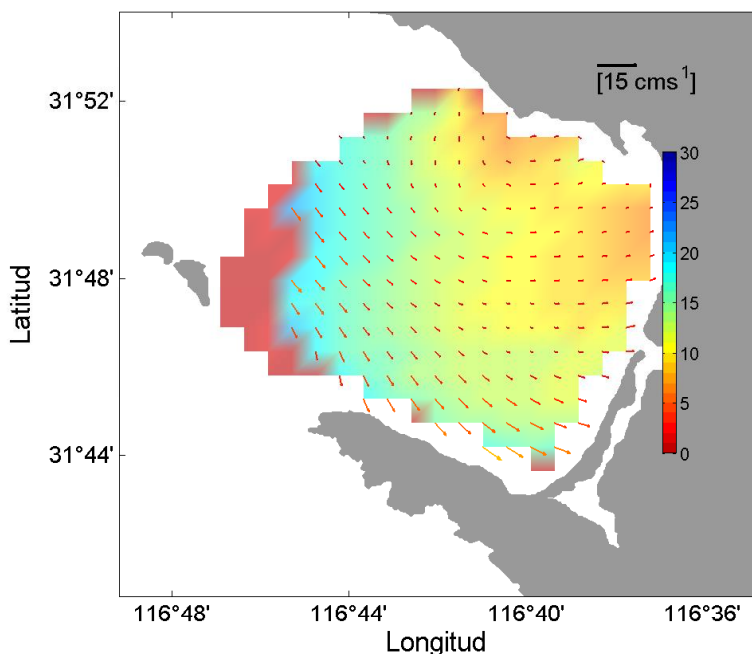
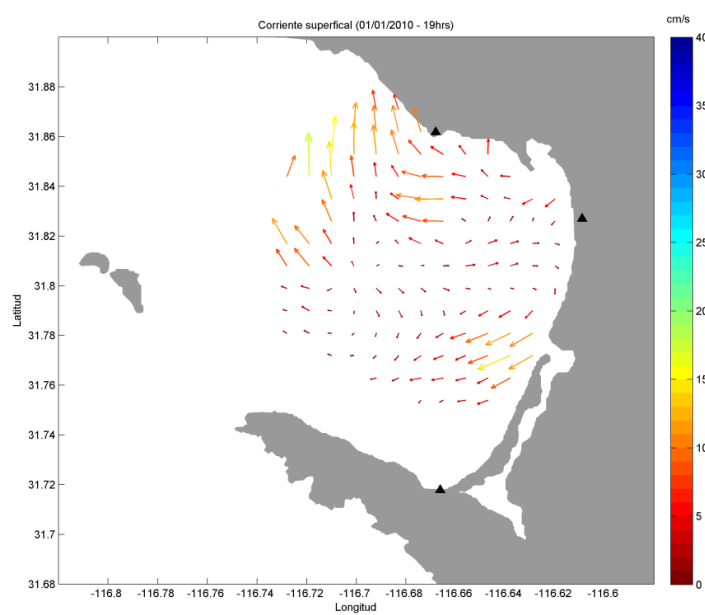


Figura 1.7. Mapas promedio de velocidades superficiales en la Bahía de Todos Santos  
A) Promedio de velocidad para la hora 19 del 1º de enero 2010 durante un evento de viento Santa Ana. B) Promedio de velocidad para el mes de enero 2010 vientos del NW (tormenta de invierno). La barra de colores es la variabilidad respecto a la raíz cuadrática media de la velocidad.

## Referencias

- Crombie, D. D., "Doppler spectrum of sea echo at 13.56 Mc/s," *Nature*, vol. 175, pp. 681–682, 1955.
- Flores-Vidal X, Durazo R, Castro R, Navarro Olache LF, Dominguez F, Gil-Silva E. 2015. Fine scale tidal and sub-tidal variability on an upwelling influenced bay as measured by the 2 Mexican High Frequency Radar Observing System. "Coastal Observing Systems". Elsevier.
- Paduan, J. D. y Graber, H. C. (1997). Introduction to high frequency radar: Reality and myth. *Oceanography*, 10(2).
- Paduan JD, Washburn L, 2013. High-Frequency Radar Observations of Ocean Surface Currents. *Annu. Rev. Mar. Sci.* (5):115–36
- Voropayev y Afanasyev (1994) Vortex Structures in a Stratified Fluid. En Chapman S & Hall, 230 pp. Volume 276 , J. S. Turner

## **Capítulo II:**

### **Santa Ana's winds influence over the surface circulation of Todos Santos Bay, Baja California, México**

<sup>1</sup>Navarro-Olache LF, <sup>2</sup>Castro Rubén <sup>2\*</sup>, Durazo R, <sup>2</sup>Hernández-Walls R, , Mejía-Trejo A,

<sup>1</sup>Flores-Vidal X.

<sup>1</sup>Universidad Autónoma de Baja California, Instituto de Investigaciones Oceanológicas.

Carretera Ensenada-Tijuana No. 3917, zona Playitas, C.P. 22860, Ensenada, B.C.,

México

<sup>2</sup>Universidad Autónoma de Baja California, Facultad de Ciencias Marinas. Carretera

Ensenada-Tijuana No. 3917, zona Playitas, C.P. 22860, Ensenada, B.C., México

(Corresponding author): Dr. Reginaldo Durazo

Correo electrónico (email): rdurazo@uabc.edu.mx

(Running title): Santa Ana's winds influence over the surface of Todos Santos Bay...

## **Abstract**

The influence of easterly north-easterly dry and warm Santa Ana winds (SAw) on the surface circulation of Todos Santos Bay (TSB), Mexico, is studied from surface currents obtained with HF radars and wind data measured during the most extreme periods of activity (autumn-winter season) between 2009 and 2015. Atmospheric variables allowed grouping 122 SAw, each lasting for 3-5 days, and some reaching bursts of  $\sim 20 \text{ ms}^{-1}$ . The study shows that SAw events yield an influence that in some, occasions enough intensity to cause an inversion on the surface circulation of the bay's background flow, from cyclonic sense to an anti-cyclonic one. The data also suggests that even when the relation of wind intensity to currents occurs in short intervals, the frequency of occurrence of SAw can have a significant impact on the inner bay surface currents. It was found that approximately 22% of the SAw events analyzed exhibited sufficient wind intensity to change the bay circulation. At its maximum strength, winds caused an intensification of the surface current to maximal velocities between  $20\text{-}40 \text{ cms}^{-1}$ .

**Keywords:** 1) Santa Ana winds, 2) Surface currents, 3) High-Frequency radars, 4) Todos Santos Bay

## **1 Introduction**

The atmospheric high-pressure center located in the North Pacific (NPH) links the oceanographic characteristics of southern California (USA) and Baja California, Mexico (Romero-Centeno, 2007, Castro and Martínez, 2010). The NPH produces prevailing alongshore equatorward winds that maintain the eastern boundary wind-induced current known as the California Current (CC). Seasonality in the wind regulates the CC flow and provides a weather classification in the coastal areas of California, the USA, and Baja California, Mexico, a dry season from April to September and a wet season from October to March. During the dry season, northwesterly winds induce coastal upwelling as a balance for the offshore Ekman divergence (Winant and Dorman 1997; Dorman and Winant 2000; Castro and Martinez, 2010, Durazo 2015). During winter the NPH weakens and migrates towards the south (Romero-Centeno, 2007), a process that allows low-pressure systems into California and Baja California producing cycles of rain during this season (Westerling et al., 2004, Hughes and Hall, 2010). Although relatively cool northwesterly to westerly winds dominate during the wet season,(more than 80% Alvarez-Sanchez, 1977), intense, short-timed easterly or northeasterly wind occurs in the area with a variable frequency during years. These events known as Santa Ana entirely change the climate of the coastal regions because of their continental origin and atypical characteristics (Conil and Hall, 2006).

S<sub>A</sub>w typical scale is  $\sim 10^3$  km and originates in the North Pacific Ocean approximately on latitude 42° N (Abatzoglou et al., 2013, Hughes and Hall 2009, Raphael 2003). They continue through the desert plains of California and generate a strong pressure gradient between the desert and the Pacific Ocean which drive the wind downhill to the west

(Guzmán-Morales et al. 2016, Hughes and Hall 2009, Miller and Schlegel 2006). SAE is characterized by relatively hot and dry offshore winds that last between 1 to 6 days (Miller and Schlegel 2006; Hughes and Hall 2009; Guzmán-Morales et al. 2016). Over the nearby coastal ocean, the wind is particularly intensified over canyons and creeks to values up to  $30 \text{ ms}^{-1}$  (Miller and Schlegel 2006, Fowell and Cao, 2017). Along the coast winds increase ambient temperatures to  $\sim 35^\circ\text{C}$  and drastically reduce relative humidity. Remote sensing images identify easterly winds by signals such as continental dust over the ocean and/or smoke from forest fires (Westerling, et al., 2004, Castro et al., 2006, Fowell and Cao, 2017). The meteorological events on land are well described (Raphael et al., 2004, Hughes and Hall 2009, Guzman-Morales et al., 2016), and the dangers they pose are recognized through Santa Anna Wind Alerts (Westerling, et al., 2004).

As SA winds arrive in the coastal zone they produce changes on the surface circulation, mainly on shallower areas and coastal bodies of water. This paper studies the effects of such intense continental winds over the background circulation of Todos Santos Bay (TSB), with an area of approximately  $250 \text{ km}^2$  and a mean depth of 50 m (Fig. 1). The typical northwesterly winds and the influence of the equatorward California Current, along the open boundary, induce a mean cyclonic circulation inside the bay (Alvarez-Sánchez, 1988, Larrañaga, 2013, Flores-Vidal et al., 2015, 2018). Average surface currents of  $5 \text{ cms}^{-1}$  (Alvarez Sanchez, et al., 1988). Here we hypothesize that if winds change direction to that of SAW events, then the internal circulation may also change, particularly during intense and sustained SAW episodes. Although numerical experiments (Hernandez-Walls, 1986, Argote et al., 1991, Mateos et al., 2006) have suggested that changes in the circulation occur during Santa Ana winds, the lack of in-

field observations hampered their results from being conclusive. In this work, we analyze the effect of SAW events on the surface circulation of TSB using hourly surface currents measured with high-frequency radars (HFR) during the peak of events in the wet season.

## 2 Materials and Methods

Surface ocean currents (0.5m depth) used in this work were obtained from a high-frequency radar(HFR) network located North, East, and South of TSB (Fig. 1) and operated from 2009 to 2015. Surface current velocities between October and March were selected for the analysis, because it is during this period that the most frequent SAW events take place. However, two late SAW events occurred during late April and middle May 2014, were also considered. Two sets of data were analyzed over the six-year period of the study. The first data set was obtained by a system of 2 radars of the "direction finding" type (~ 25 MHz, CODAR) installed in the North and East of the bay during the period October 2009 to December 2013 (Fig 1). The second set of velocity observations includes the use of an additional unit. This radar is a WERA "beamforming" type radar (~ 24.5 - 27.3 MHz, Flores-Vidal et al., 2018) located in the southern region of TSB (Fig. 1) and was operational during the period from January 2013 to December 2015. In both systems arrays, the radial reach is ~ 20 km with a spatial resolution of around 0.8 km and uncertainty of  $0.06 \text{ ms}^{-1}$  (Gurgel et al., 1999, Flores-Vidal et al., 2015). Current velocities calculated at each radar site provided hourly data on a Cartesian mesh of ~1 km of spatial resolution. The spatial coverage of

the first array (CODAR) was represented by a regular mesh of 22 x 22 cells, while the mesh with three radars was 76 x 88, thus increasing the coverage area.

Meteorological observations were obtained using a DAVIS weather station, located north of the TSB at 10 m altitude (Fig. 1). Hourly wind magnitude and direction, relative humidity, and air temperatures used here. To identify SAW events, we selected only data with relative humidity below a threshold of 45% and wind speed over  $7 \text{ ms}^{-1}$ . This classification follows the latest SAW criteria in the southern California area.(Guzmán-Morales et al., 2016)

Regional remotely sensed wind data, for some days during a Saw event, were obtained from the Cross-Calibrated Multi-Platform (CCMP) wind vector analysis product (Atlas et al., 2011; Wentz et al., 2015). The CCMP wind data used have a spatial and temporal resolution of  $0.25^\circ$  and 6 h, respectively. We also used level 2 Chlorophyll-a images from the MODIS (Moderate Resolution Imaging Spectrum-radiometer) instrument aboard the Terra (EOS AM) and Aqua (EOS PM) satellites. Additional chlorophyll time series were obtained from daily means of the global reanalysis ocean product ( $0.25^\circ \times 0.25^\circ$ ) from COPERNICUS Marine environmental monitoring service (<http://marine.copernicus.eu>).

### 3. Results

Meteorological data showed the typical seasonal signature on air temperature for Todos Santos Bay TSB (Fig. 2a). Temperature average ( $20^\circ\text{C} \pm 7^\circ\text{C}$  during winter and  $27 \pm 3^\circ\text{C}$  during summer. Pacific coast shows the characteristic high relative humidity over 70%, with air velocities in the range of light breeze  $3 \pm 3 \text{ ms}^{-1}$  during winter and  $2.5 \pm 1$

$\text{ms}^{-1}$  during summer. Maximal temperature 38 °C registered during late summer and early autumn (August-September, dry season) during short time heat wave events. During winter short time heat waves events also occurred, associated with a severe decrease in relative humidity and sometimes intense continental winds, wind intensity in the range of near gale (Figs 2b, 3b). These events are known as Santa Ana winds (SAw). SAw reaches the Pacific Coast from a dominant NE to E direction (Figs 3b,4), modify the coastal environment at this latitude. Dry and hot air (less than 40% of relative humidity) change the coastal area, most frequently dominated by the NW to W Pacific Ocean air system (Alvarez-Sanchez, 1977, Durazo, 2015), Figs. 2a and 3b. and a small number of winter storms that occurred in the area with an average speed of 4-6  $\text{ms}^{-1}$  and gusts of wind over 10  $\text{ms}^{-1}$ (Figs. 2b, 3a).

SAw occurred on a regional scale. Continental winds flow down the hill to the ocean, modifying the coastal environment (Raphael 2003, Westerling et al., 2012). An example of this occurred between May 13-15, 2014 (Fig.4). This figure present 6 h snapshots of wind data, during characteristics SAw event in the Southern California and Baja California region (Fig. 4). During the approximately 3 days event SAw apparently displace the Pacific marine layer along a ~600 km flank and ~100 km offshore into the Pacific Ocean. SAw field showed sustained speeds of more than 10  $\text{ms}^{-1}$ , in the direction of the ocean. Notwithstanding SAw occurred in regional scale, figure 4 shows that wind intensity has maximal value during the day, and subsequent days, May 14 and 15 (not showed here). Winds reach higher speeds during daylight decreasing overnight particularly between latitude 30° to 32° North where marine layers seem to be hurled offshore (Fig. 4).

To illustrate its effects of SAW events on the TSB circulation we presented the mean winter surface circulation during winter, using the HF radar's surface velocities with CODAR (Fig. 5a) and WERA arrays (Fig. 5b). Note that WERA showed more coverage area, due to the number of radars used. In general, both average maps showed the surface circulation of the bay interior to be cyclonic. Speeds are of the order of 5-10  $\text{cms}^{-1}$ . The figure shows more variability on the bay open boundary, adjacent to Todos Santos Island, likely associated with the influence of the California Current towards the equator. Data showed that variability in the bay interior is low, particularly near the city and port facility (Figs. 5a and b).

On the other hand, to observe the surface circulation influenced by SAW, we extracted and averaged selected events using CODAR and WERA arrays (Figs. 5c,d). Surface currents obtained with CODAR were calculated using, nine events (Fig 5c). Data depicted two eddies not very well defined, cyclonic in the north, clockwise in the south, converging around the center of the bay (Fig. 5c). On TSB open boundary, surface velocity is slightly larger than inside the bay and with the same direction of the CC. Surface currents obtained with WERA were calculated using four events (Fig. 5d). Data depicted an anticyclonic eddy covering much of the TSB. Data showed on the open boundary, higher surface velocities and a northward offshore flow (Fig. 5d). This is opposite to the CC direction observed on Figs. 5a-c. Inside Todos Santos Bay, surface currents were slightly faster than Fig 5b. A flow parallel to the coast is also observed, bonding the large vortex around the bay.

Continental wind forming the SA circulation inside the bay shows three main directions in the NE quadrant (Fig. 3b), which could result in different surface current patterns. To

illustrate this, we selected three examples of SAW occurred in the area and depict the resulting currents inside the bay.

The first SAW event selected occurred on December 14-21, 2011 (Fig. 6). In general the average surface current drift offshore (Fig 6a) along the northern and southern coasts. The main wind direction was northeasterly (Fig. 6b), with wind speeds ranging from ~2 to above  $10 \text{ ms}^{-1}$  (Figs. 6b,c). A drastic decreasing in relative humidity (~70-30%) marked the event, which started on December 14 and lasted six days (Fig. 6c). During the event, winds maximal speeds seem to oscillate with a diurnal variability, variability that was also observed in the regional scale (Fig. 4). Average surface currents in an area south of TSB (Fig. 6c) also depicted diurnal intensification pulses, from 20 to 30  $\text{cms}^{-1}$ , lagging the wind by 6-8 hours. However, not all wind bursts derived in the current intensification (Fig. 6c). Maximum wind speeds were observed from December 15 to 17. These velocities faded down as relative humidity increased and the air temperature dropped to normal winter temperatures (Fig.2).

In the second SAW event, considered here the relative humidity drop from 80% to 20% in a lapse of a few hours (Fig. 7b). This event occurred between April 29 and May 5, 2014. Surface average currents showed a dominant flow offshore along the bay's southern region, showing maximal velocities of  $25 \text{ cms}^{-1}$  between the island and continent (Fig 6a). Average surface currents from an area south of the bay ( $-116^{\circ}, 40'$ ,  $31^{\circ}46' \text{ N}$ ) showed an intensification of the currents during the first three days of the event, April 29 to May 3 (Fig.6c), responded to the northeasterly winds distributed in TSB (Fig. 6b). Wind speed reaches  $\sim 10 \text{ ms}^{-1}$ , oscillating with an approximately diurnal frequency (continuous blue line on Fig. 7c).

The third SAw event considered presented E-NE winds, it occurred between May 11 to 16 2104, few days after event number 2.. The average surface current showed a closed cyclonic circulation around TSB. Stronger offshore can be observed south of the bay and along the open boundary towards the north. Maximal values on the open boundary reach average of  $30 \text{ cms}^{-1}$ (Fig 8a) Average surface currents from an section (-116° 40", 31°46' N) showed surface currents diurnal pulses during the days of the event , with a maximal signal reaching a maximal of  $40 \text{ cms}^{-1}$ (Fig 8c). This surface currente, apparently responding to a wind intensity maximum over  $12 \text{ ms}^{-1}$  observed at this day (Fig. 4, and 8c).

SAw event during April and May 2014 illustrated good examples of how the continental wind modifies the TSB circulation. Considering four points along a line near the coast (Fig. 9a) that show the wind and surface current velocity during the events. Wind speed (blue line, Fig. 9b) showed increasing diurnal pulses with values up to  $10$  and  $14 \text{ ms}^{-1}$  during two SAw events occurring on the period. Current speeds also show increases, following approximately the same diurnal pattern that was observed during the arrival of both SAw events, from calm to  $40 \text{ cms}^{-1}$ .

The examples provided show that SAw transports surface water outside TSB, which might generate a mechanism to promote upwelling in the area and as a consequence an increase in the chlorophyll concentration. Evidence of the relationship is a filament of approximately 70 km off the coast, observed in the MODIS images on Fig. 10a, just outside TSB. The figure shows that during the last days of April 2014 a large plume of chlorophyll-a spin-out from the coast, as a result of the continental SAw. Chlorophyll-a concentration increase considerably from almost null cell concentration to values 5.5 to

$6.5 \text{ mgm}^{-3}$  during the events between April to May 2014 (Fig. 10b). The peak in cell concentrations in an area just outside the bay ( $-116^{\circ} 48' \text{ W}$ ,  $31^{\circ} 44' \text{ N}$ ) corresponds with the maximal wind velocity, during SA events. The large concentration of chlorophyll-a observed during the event decreasing rapidly in the area. Larger concentration could be seen to the south of TSB (Fig. 10a) responding to strong wind forcing as seen in Figure 4.

#### **4. Discussion**

In this paper, we present the effects of SAW (NE-E) on the surface currents circulation at TSB. The use of HF radars provided a fine scale velocity field data in space ( $\sim 1 \times 1 \text{ km}$ ) and time (hourly), and evidence of the effects of the wind in the resulting circulation of TSB. Previous works in TSB surface circulation had suggested this circulation through drifting buoys (Álvarez et al., 1979, Durazo-Arvizu et al., 1988), and numerical simulations, that included SAW conditions as initial forcing (Hernandez-Walls 1986, Argote et al., 1991). In this work, using HF radar data, we add concrete information of the surface circulation, including a change in TSB circulation as a result of wind intensification during SA continental winds in the bay. The change in rotation observed from a cyclonic, during most time of the year (Fig. 5a and 5b) to anti-cyclonic rotation (Fig. 5c and 5d) was evident. This change in the current rotation inside TSB has not been previously documented. Figures showed that as a result of the offshore wind forcing, areas of relative calm became activated, during the events, in particular, shallow areas near the coast that usually present speeds lower than  $.05 \text{ ms}^{-1}$  (Alvarez-Sánchez et al., 1978, Durazo et al., 1988, Flores Vidal et al., 2015,2017).

Additionally, in agreement with documented satellite data during SA events (Trasviña et al., 2003; Castro et al., 2003, 2006) our data showed that a relatively large area shifted offshore, as continental dry and warm wind burst in the area (Fig 4). In the same context, surface velocity data show that surface water exchange between TSB and ocean waters (Figs. 5c y 5d), in the same direction of the wind. Water exchange along the coast and in TSB could be associated with the development of coastal upwelling (Sosa-Avalos et al, 2005) because as suggested on Figs 4 and 9a, Santa Ana wind shifted coastal water more than 50 km from the coast, supplementing nutrients on the surface that eventually increase the chlorophyll cells concentration, maximal cell concentration shows highs with values larger than  $10 \text{ mgm}^{-3}$  during April 30, 2014 (Fig.10a). This was also observed just outside TSB(Fig.10b), in a time series located in (-116.75 W, 31.75 N). Two peaks of maximal concentration ( 5.5 and  $6.5 \text{ mgm}^{-3}$ ) are in good agreement with the maximal winds observed during a SAw event, supporting the idea of the importance of these events, occurring consistently in the Pacific Coast during spring, fall and winter.

Contrary to the close cyclonic circulation observed in TSB (Larrañaga, 2013) under NW and W winds (Figs. 5a,b). Surface currents associated with SAw events depicted water flowing outside the bay, through the north and south boundary. HF CODAR surface velocity data show surface water, following the flow of two eddies in the northern boundary (Fig 5c). On the other hand, HF WERA surface velocity data showed the water off the bay following the direction of a larger eddy in the southern side of the bay (Fig. 5d). The variation of the offshore flow direction may be explained by velocity resolution, larger using WERA radars system than CODAR, documented in methods.

However, there is a possibility as well that the form and number of eddies inside the bay may be related to the direction in which winds arrive in TSB during SA events. Data shows that some SAW events enter from the NE direction and other from the E direction (see for example Fig. 7b), apparently guided by the distribution of the regional high pressure center (Raphael, 2005), and ultimately funneled through the two main topographical depression inside TSB, with height below 50 m, one near the city port and the other south of the bay at Maneadero Valley (see figure 1 from Alvarez, 1977).

A similar relationship between SAW events and surface currents in the ocean has also been observed in California, USA Santana Events, as SA winds flow guided by coastal depressions over the ocean (Hu and Liu, 2003). In both cases, surface water is forced out, improving the water quality in TSB, as surface water may be vertically and horizontally replacement. This exchange may help to explain the surface temperature decrease, documented (Hu and Liu, 2003, Trasviña et al., 2003, Castro et al, 2006) and the increase of chlorophyll associated with the arrival of Santa Ana events in the area (Hu and Liu, 2003, Sosa-Avalos et al., 2005, Castro et al., 2006), as it was previously presented on May 28 and 30 (Figures 10a,b).

Winter average cyclonic circulation, not including SAW events, showed surface currents velocity values between 5-10 cms<sup>-1</sup>. This circulation pattern tends to keep particles inside the bay area, for large periods of time (Larrañaga, 2013, Flores Vidal et al., 2015). An estimation of residence time (Graham and Largier, 1997), using typical temperature gradients between air-ocean heat fluxes gives water residence times of ~6-8 days. Considering SAW events characteristic it is possible that temperature gradients may be stronger and surface velocities are also larger (~0.3-0.5 ms<sup>-1</sup>) which may

reduce the residence time to four days. However more in site data may be required to corroborate this conclusion. With less residence time, surface water would play a role in the sanitizing of surface water, particularly on areas in which water seems to be trapped, inside the center of the cyclonic eddy or near the city port. In those areas the current variability and the speed are low (Fig. 5a,b) compared with values during Santa Ana events.

Data (atmosphere-ocean) suggests that during SAw events, the surface winds seem to weaken and intensity during the day (Fig. 4), which could be associated with the variability on the High Basin (Durazo 2015) and with the interaction between SAw and the local diurnal processes such as breezes (Alvarez Sanchez, 1977, Reyes Coca et al., 1983, Pavia y Reyes, 1983). The diurnal variability was also observed as wind and current intensity pulses, observed in the meteorological station and HF surface velocities (Figs. 5- 8). We suggest that as temperature increases during the day a local low pressure builds up, generating an obstacle that swerves the apparently continuous wind flows in the upper strata, shown in satellite images. This phenomenon of daytime breeze is sometimes shown as a thermal inversion that causes mirages in the bay (Hernández-Walls et al., 2011), or by the presence of low mist generated by warm fronts between air and water (Pillie et al., 1979).

## 5. Conclusions

During the time of observations, 50% of the SAw events showed null to calm conditions with wind velocities lower than  $5 \text{ ms}^{-1}$ , 26% of SAw events presented intermediate range, and 22% were intense, with wind speeds higher than  $7 \text{ ms}^{-1}$ . Although intense

SAw seems to transport important amount of surface water off the bay additional meteorological data may be necessary to observe the initial stages of SA events and the location of initial forcing, as it may be key to understand the difference in the number of vortexes formed inside the bay.

Intense SA events showed sustained wind pulses of 7 hours over the bay surface, during events lasting three to five days. In most cases, low humidity and high air temperature endured longer than the wind, in the coastal region for 5 to 7 days. At its maximum strength, SAw events (NE-E) caused an acceleration of the Bay's surface current that leads to maximal velocities between  $20\text{-}40 \text{ cms}^{-1}$

The winds and currents described during the Santa Ana events in the TSB change the Todos Santos Bay curse of rotation, from cyclonic to anticyclonic, during a period of three to four days. During SAw events surface water is forced off TSB, increasing the horizontal and vertical water exchange between coastal and the open ocean. Todos Santos Bay water quality may improve during SAw events as coastal stagnant water might be replaced from shallow areas inside the bay (Figs 5- 8). Data suggest that Santa Ana Events may be an important contributor to enhance the coastal zone primary productivity as an increase in productivity is stronger linked with these events.

Nonetheless, velocities calculated using high-frequency radars represent a thin layer in the vast TSB area, the amount high resolution in time and space present HF radar velocities as a robust tool to solve a problem not previously addressed such as dispersion of particles, mixing and transfer of Lagrangeanas properties.

## References

- Abatzoglou JT, Barbero R, Nauslar, NJ 2013. Diagnosing Santa Ana Winds in Southern California with synoptic-scale analysis. *Weather and Forecasting*, 28: 704–710, doi: 10.1175/WAF-D-13-00002.1
- Adams DK and Comrie, AC. 1997 The North American Monsoon. Bulletin of the American Meteorological Society. [https://doi.org/10.1175/1520-0477\(1997\)078<2197:TNAM>2.0.CO;2](https://doi.org/10.1175/1520-0477(1997)078<2197:TNAM>2.0.CO;2)
- Alvarez-Sánchez LG. 1977. Vientos en la Bahía de Todos Santos, Baja California. Revista Ciencias Marinas, UABC. 4(1):81-89: : <http://dx.doi.org/10.7773/cm.v4i1.301>
- Álvarez-Sánchez LG, Hernández-Walls R, Durazo-Arvizu R. 1988. Drift patterns of Lagrangian tracers in Todos Santos Bay. Ciencias Marinas, 14: 135–162
- Argote-Espinoza ML, Gavidia-Medina FJ, Amador-Buenrostro A. 1991. Wind-induced circulation in Todos Santos Bay, B.C., México. *Atmósfera*, 4:101-115.
- Atlas R., R. N. Hoffman, J. Ardizzone, S. M. Leidner, J. C. Jusem, D. K. Smith, D. Gombos, 2011: A cross-calibrated, multiplatform ocean surface wind velocity product for meteorological and oceanographic applications. Bull. Amer. Meteor. Soc., 92, 157-174. doi: 10.1175/2010BAMS2946.1
- Castro R, Parés-Sierra A, Marinone SG. 2003. Evolution and extension of the Santa Ana winds of February 2002 in front of California and the Baja California Peninsula. *Ciencias Marinas*, 29: 275–281.

- Castro R, Mascarenhas A, Martínez-Díaz-de-León A, Durazo R, Gil-Silva E. 2006. Spatial influence and oceanic thermal response to Santa Ana events along the Baja California peninsula. *Atmósfera*, 19:195-211.
- Castro R, Martínez A. 2010. Variabilidad espacial y temporal del campo de viento frente a la península de Baja California. In: Gaxiola-Castro G., Durazo R. (Eds.), Dinámica del Ecosistema Pelágico Frente a Baja California, 1997–2007. Instituto Nacional de Ecología-CICESE-UABC, México, 504 pp.
- Conil S, Hall A. 2006. Local regimes of atmospheric variability: A case study of southern California. *Journal of Climate*, 19, 4308–4325, doi: 10.1175/JCLI3837.1.
- Dorman CE, Winant CD. 2000. The structure and variability of the marine atmosphere around the Santa Barbara channel. *Monthly Weather Review*, 128:261–282.
- Durazo Arvizu R y Alvarez Sánchez, LG. 1988. Kinematics of the Southem Region of Bahía de Todos Santos, BC. Ciencias Marinas, 14: 95-114. Doi <http://dx.doi.org/10.7773/cm.v14i1.558>
- Durazo R. 2015. Seasonality of the transitional region of the California Current System off Baja California. *Journal of Geophysical Research-Oceans*, 120:1173–1196, doi: 10.1002/2014JC010405.
- Flores-Vidal X, Durazo R, Castro R, Navarro LF, Dominguez F, Gil E. 2015. Chapter 12. Fine-scale tidal and sub-tidal variability of an upwelling-influenced bay as measured by the Mexican high-frequency radar observing system. In: Coastal Ocean Observing

Systems: Advances and Syntheses. Academic Press, 209-228, doi: 10.1016/B978-0-12-802022-7.00012-2.

Flores-Vidal X, González-Montes S, Zertuche-Chances R, Rodriguez-Padilla I, Martí CL, Imberger J, Mejía-Trejo A, Durazo R, Navarro-Olache L. 2018. Three-dimensional exchange flows in a semi-enclosed bay: Numerical simulations and high-frequency radar observations. *Estuarine Coastal and Shelf Science* 210: 26-35, doi: 10.1016/j.ecss.2018.05.027.

Fowell RG, Cao Y. 2017 The Santa Ana winds of Supthern California Winds, gust, and the 2007 Witch fire. Wind amd Structures. 24(6) 529-564. DOI: <http://doi.org/10.12989/was.2017.24.6.529>

Guzman-Morales J, Gershunov A, Theiss J, Li H, Cayan D. 2016. Santa Ana Winds of southern California: Their climatology, extremes, and behavior spanning six and a half decades. *Geophysical Research Letters*, 43:2827–2834, doi: 10.1002/2016GL067887.

Graham WM, Largier JL. 1997. Upwelling shadows as nearshore retention sites: the example of north Monterey Bay. *Continental Shelf Research*, 17: 509-532.

Hemández-Walls, R. 1986. Circulación inducida por el viento en la zona costera. BSc Thesis. Universidad Autónoma de Baja California, 73 pp.

Hernandez-Walls R, Castro R, Pinet-Placencia R, Gil-Silva E, Yepiz R. 2011. Registro de un espejismo superior en la Bahía de Todos Santos, B.C. Mexico, bajo la condición de vientos Santa Ana. *GEOS*, 31: 1-8.

Hu H. and Lui W.T. 2003. Oceanic thermal and biological response to Santa Ana winds. *Geophysical Research Letters*, Vol. 30 no.11. 50-1,50-4 doi:10.1029/2003GL017208.

Hughes M, Hall A. 2009. Local and synoptic mechanisms causing Southern California's Santa Ana winds. *Climate Dynamics*, 34:847-857, doi: 10.1007/s00382-009-0650-4.

Larrañaga-Fu M. 2013. Variabilidad de la circulación superficial en la Bahía de Todos Santos, Baja California, México. BSc Thesis. Universidad Autónoma de Baja California, 67pp.

Mateos E, Marinone SG, Parés-Sierra A. 2009. Towards the numerical simulation of the summer circulation in Todos Santos Bay, Ensenada, B. C., Mexico. *Ocean Modeling*, 27: 107-112, doi: 10.1016/j.ocemod.2008.11.002.

Mateos E, Marinone SG, Lavín MF. 2013. Numerical Modeling of the coastal circulation off northern Baja California and southern California. *Continental Shelf Research*, 58: 50-66.

Miller NL, Schlegel NJ. 2006. Climate change projected fire weather sensitivity: California Santa Ana wind occurrence. *Geophysical Research Letters*, 33:1–5, doi: 10.1029/2006GL025808.

NASA Goddard Space Flight Center, Ocean Ecology Laboratory, Ocean Biology Processing Group. Moderate-resolution Imaging Spectroradiometer (MODIS) Aqua Ocean Color Data; 2018 Reprocessing. NASA OB.DAAC, Greenbelt, MD, USA. doi: 10.5067/AQUA/MODIS/L2/OC/2018.

Pavia E y Reyes S. 1983. Variaciones espaciales y estacionales del viento superficial en la Bahía de Todos Santos, B.C. Revista Ciencias Marinas. UABC. 9(1) 151-167: <http://dx.doi.org/10.7773/cm.v9i1.405>

Pillie RJ, Mack EJ, Rogers CW, Kate U, Kocmond WC. 1979. The formation of marine fog and the development of fog-status system along California Coast. *Journal of Applied Meteorology*, 18:1275-1286.

Raphael MN. 2003. The Santa Ana winds of California. *Earth Interactions*, 7:1–13, doi: 10.1175/1087-3562(2003)007<0001:TSAWOC>2.0.CO;2.

Reyes S, Vogel G, Pavía E and Parés A. 1983 Synoptic Effects on the Local Winds in Todos Santos Bay: A Case Study. Monthly Weather Review. American Meteorological Society, 111:1494-1500.: [https://doi.org/10.1175/1520-0493\(1983\)111<1494:SEOTLW>2.0.CO;2](https://doi.org/10.1175/1520-0493(1983)111<1494:SEOTLW>2.0.CO;2)

Romero Centeno R, Zavala-Hidalgo J., and Raga GB. 2007. Midsummer Gap Winds and Low-Level Circulation over the Eastern Tropical Pacific American Meteorological Society. 20: 3768-3784.

Sosa-Avalos R, Gaxiola-Castro G, Durazo R, Mitchell BG. 2005. Effects of Santa Ana winds on bio-optical properties off Baja California. *Ciencias Marinas*, 31:339-348.

Trasviña A, Ortiz-Figueroa M, Herrera H, Cosío MA, González E. 2003. “Santa Ana” winds and upwelling filaments off Northern Baja California. *Dynamics of Atmospheres and Oceans*, 37:113–129, doi: 10.1016/S0377-0265(03)00018-6.

Westerling, A.L. Cayan, D.R., Brown, TJ, Hall BL, and Riddle, LG. 2004. Climate, Santa Ana winds and autumn wildfires in Southern California. EOS,(85) No.31.p 289-300.

Wentz, F.J., J. Scott, R. Hoffman, M. Leidner, R. Atlas, J. Ardizzone, 2015: Remote Sensing Systems Cross-Calibrated Multi-Platform (CCMP) 6-hourly ocean vector wind analysis product on 0.25 deg grid, Version 2.0, [indicate date subset, if used]. Remote Sensing Systems, Santa Rosa, CA. Available online at  
[www.remss.com/measurements/ccmp](http://www.remss.com/measurements/ccmp)

Winant CD, Dorman CE. 1997. Seasonal patterns of surface wind stress and heat flux over the Southern California Bight. *Journal of Geophysical Research*, 102: 5641–5653, doi: 10.1029/96JC02801.

## **Acknowledgments**

The authors of this study would like to thank CICESE, Mexico. Particularly to Mr. Santiago Higadera Cervera and Dr. Modesto Ortiz Figueroa for providing the meteorological data used in this study. The University Autonomous of Baja California and the Institute for Oceanographic Research for their support and contribution in the realization of this project. The data obtained during the field work related to the currents was made possible thanks to the financing and appropriation under the following projects: CNA-CONACyT 143803 y CB-CONACyT 255602. CCMP Version-2.0 vector wind analyses are produced by Remote Sensing Systems. Data are available at [www.remss.com](http://www.remss.com).

## Figure Legends

Figure 1. Study area. The triangles show the location of the sites where the high-frequency radars were installed on the coast. The circle shows the position of the weather station. The contour lines indicate the depth of the bottom (m).

Figure 2. Time series of meteorological variables recorded between 2009 and 2016. (a) Air temperature ( $^{\circ}\text{C}$ ), (b) wind speed ( $\text{ms}^{-1}$ ) and (c) relative humidity (%). The gray line shows the hourly data and the thick line corresponds to the same data after the application of an average running filter of 18 hours.

Figure 3. A) Distribution of wind characteristics during winter, from 2009 to 2015; (b) only for data with magnitude greater than  $7 \text{ ms}^{-1}$  and in the first quadrant.

Figure 4. Six hours interval wind vectors from reanalysis data during May 13 2014 during a Santana wind event. contours dnote velocity magnitude ( $\text{ms}^{-1}$ )

Figure 5. Average winter currents for Todos Santos Bay. (a) Winter from 2010 to 2013 obtained with two CODAR system radars (b) Winter from 2014 to 2015 obtained with WERA radars system. Contours indicate the standard deviation. c) Santa Ana CODAR average currents (d) Santa Ana WERA average currents.

Figure 6. SAw event during December 14 to 21, 2011. (a) Mean surface currents. Color contours show the rms velocity variation (b) Wind velocity and frequency, during the period (c) Time series of wind speed (blue line  $\text{m/s}$ ), relative humidity (green, %) and average surface currents velocity, sampled hourly from HF radars (red,  $\text{cm/s}$ ).

Figure 7. Same as Figure 6 for April 29 to May 5, 2014.

Figure 8. Same as Figure 6 for May 10 to 15 2014.

Figure 9. A) Position of 4 points of observations of surface velocity currents in TSB and wind direction and frequency during the period aprit to may 16 2014, during SAw C) Winds (bold blue line) and surface current velocities for the points on the upper panel .

Figure 10. A) Aqua-MODIS images (1 day) for mass concentration of chlorophyll-a in sea water ( $\text{mg/m}^3$ ) during April 28 and 30 (Modis) in front of Todos Santos Bay. B) Mass concentration outside Todos Santos Bay ( $-116^{\circ} 48' \text{W}$ ,  $31^{\circ} 44' \text{N}$ ) of chlorophyll-a in sea water ( $\text{mg/m}^3$ ). Image is a daily global reanalysis average data (0.25degree x 0.25degree).

Figure 1

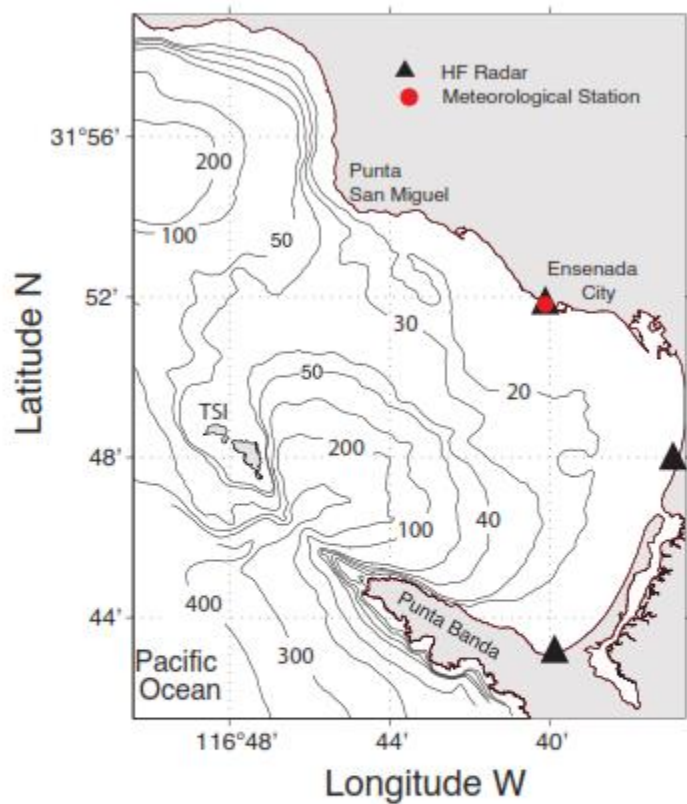


Figure 1

Figure 2

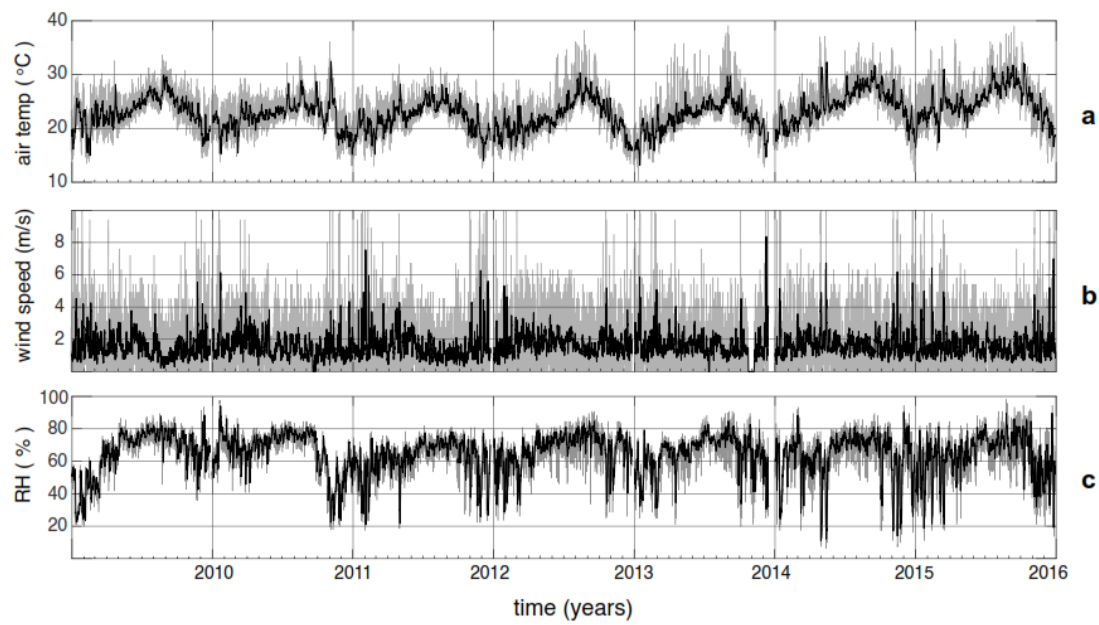


Figure 2

Figure 3

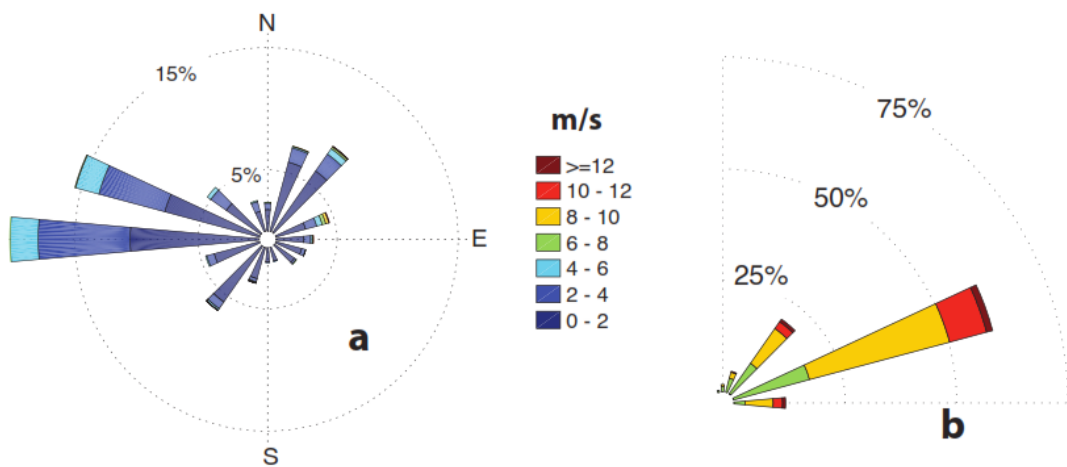


Figure 3

Figure 4

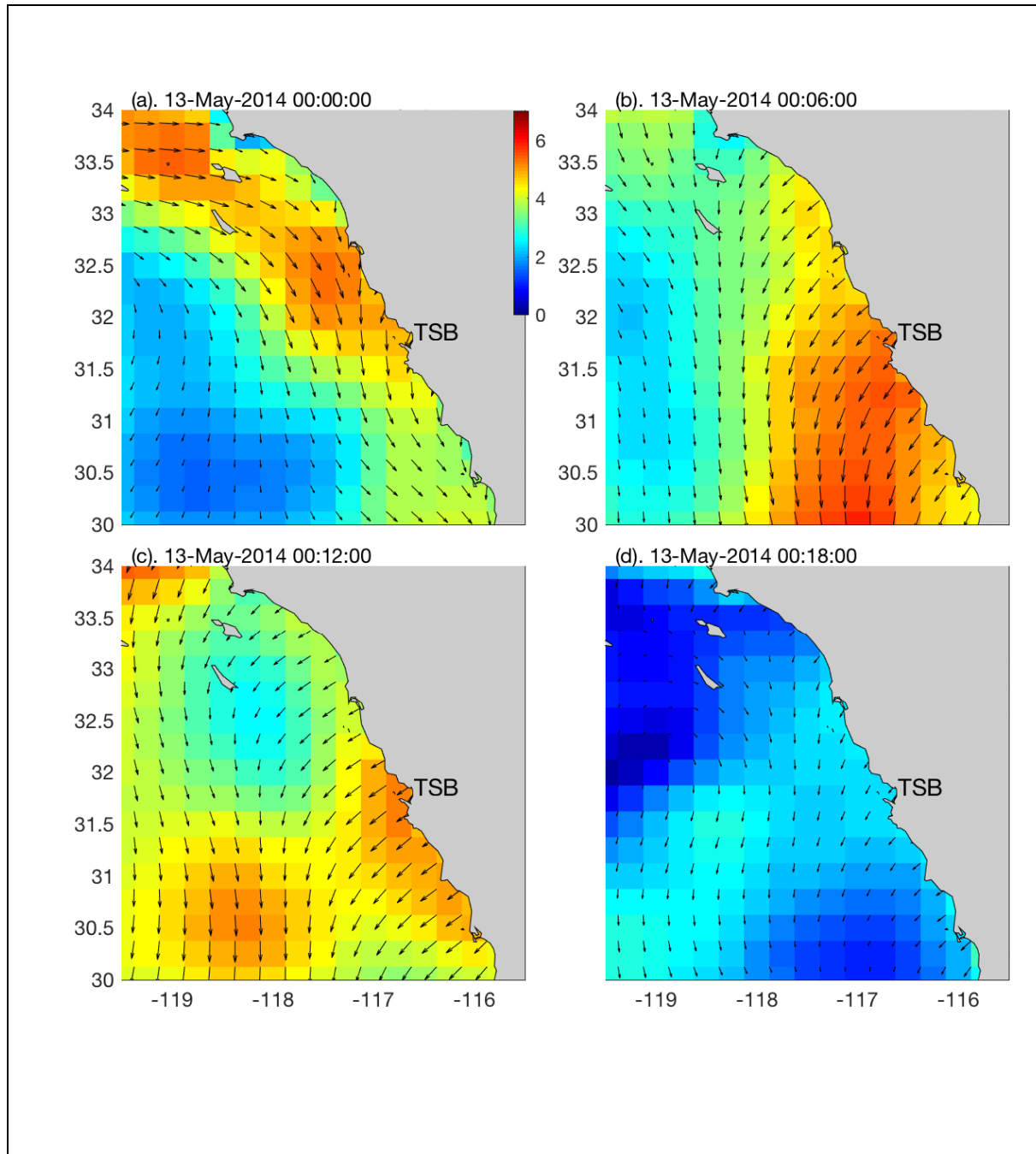


Figure 5

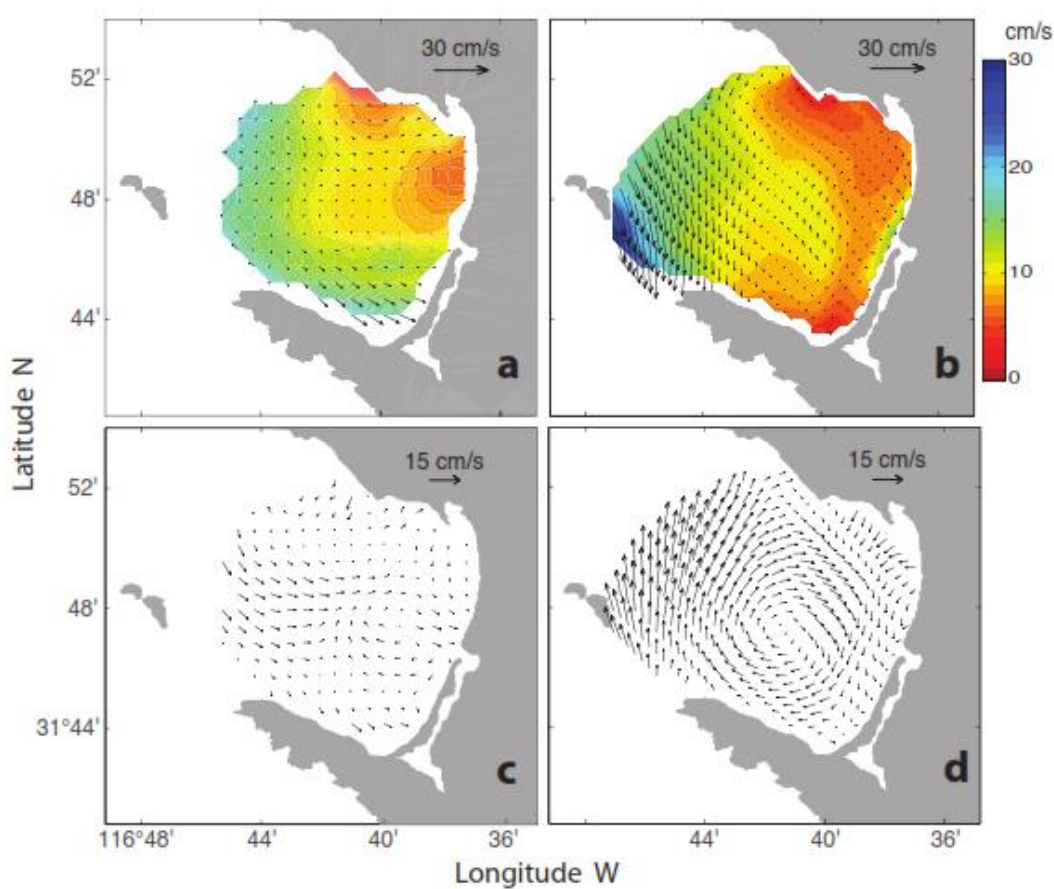


Figure 6

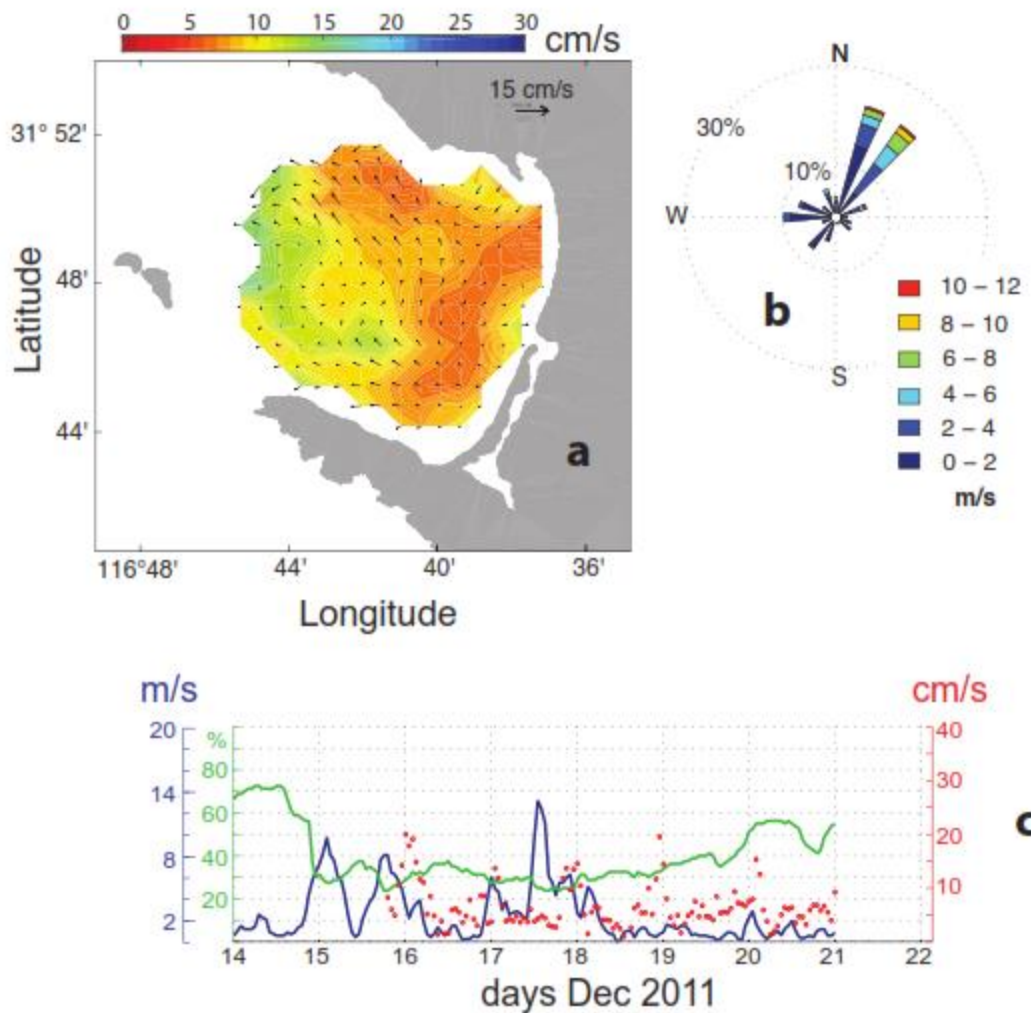


Figure 7

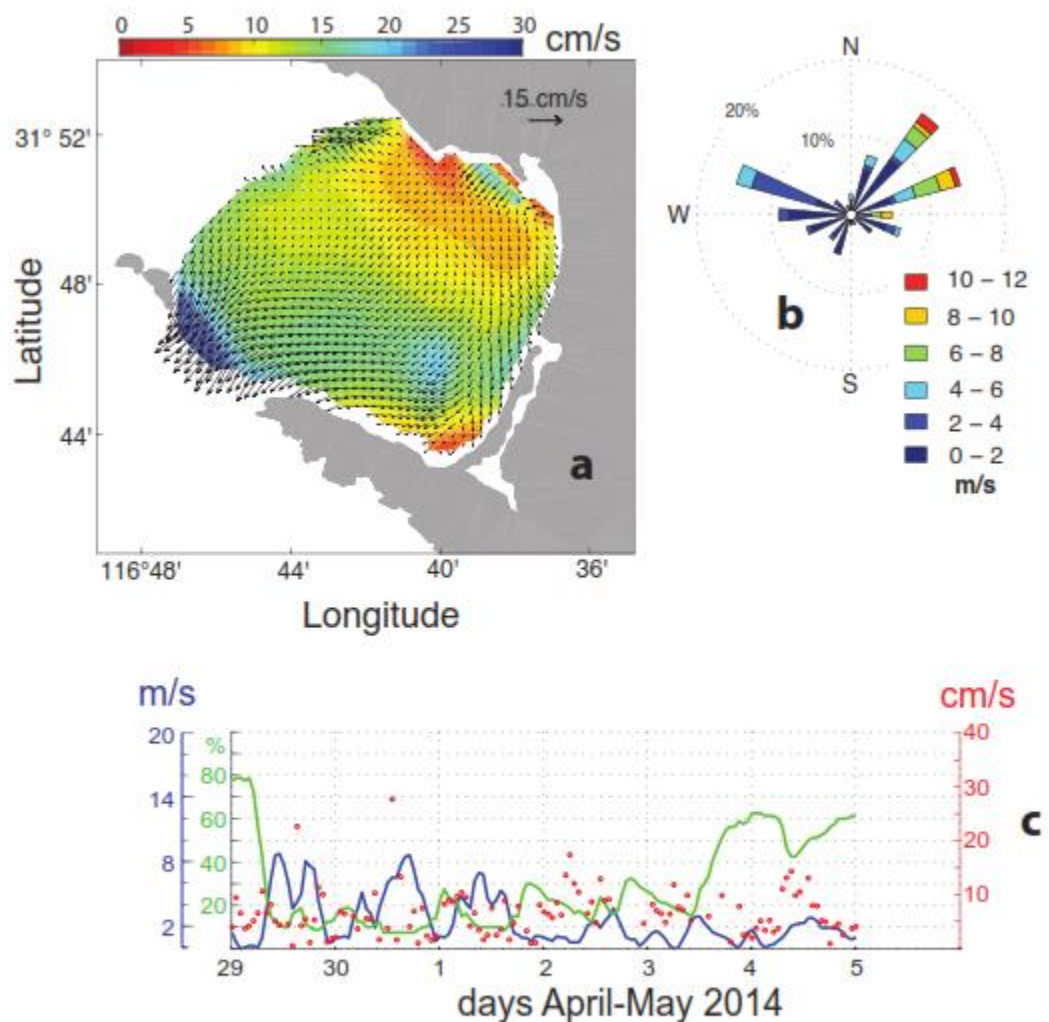


Figure 8

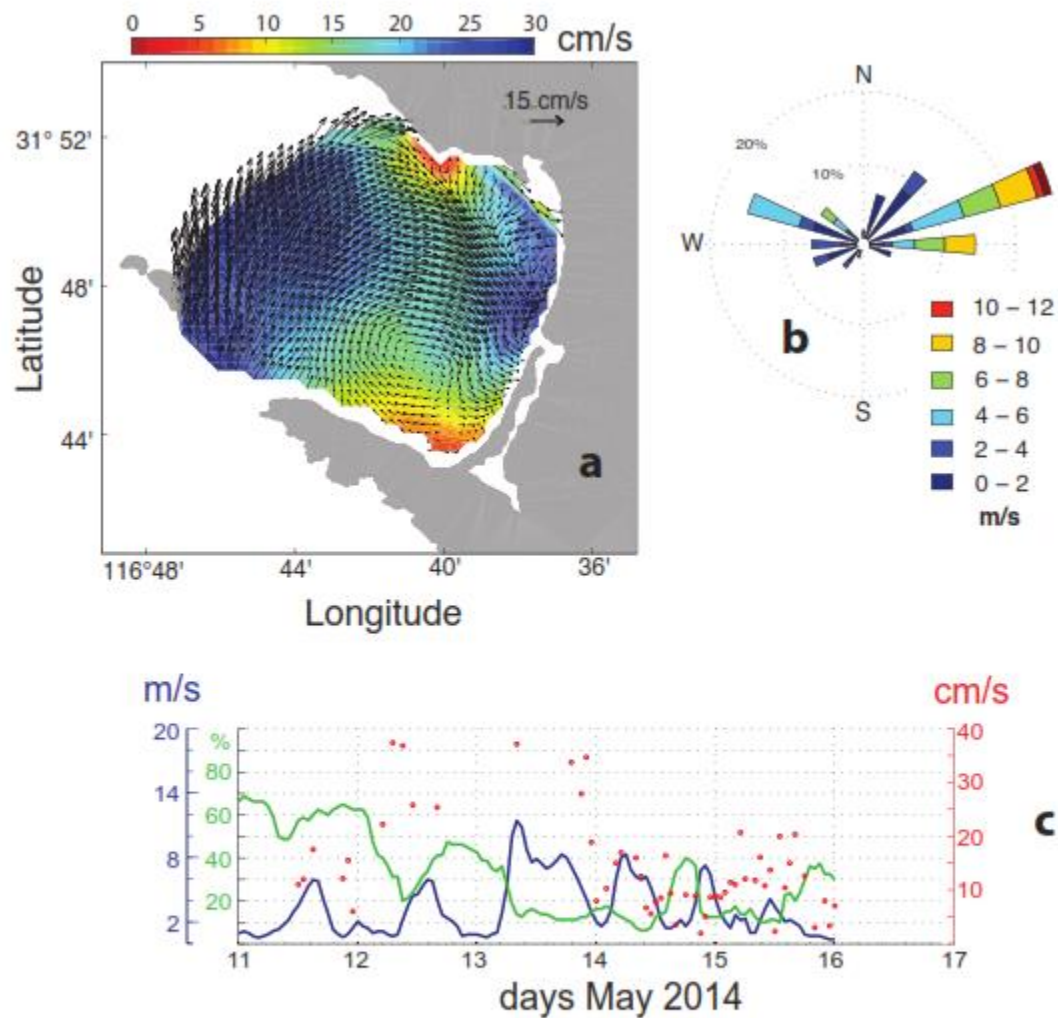


Figure 9

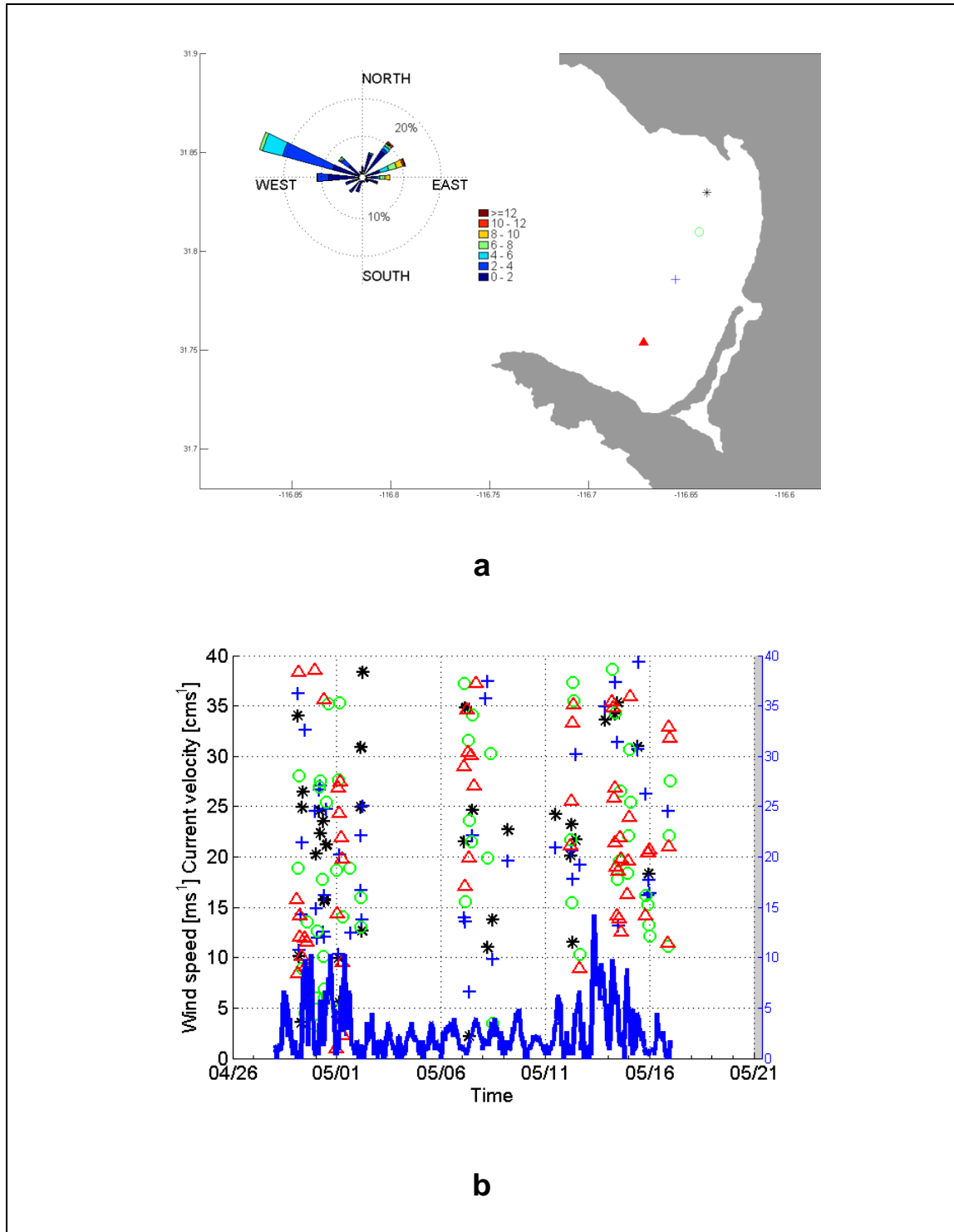
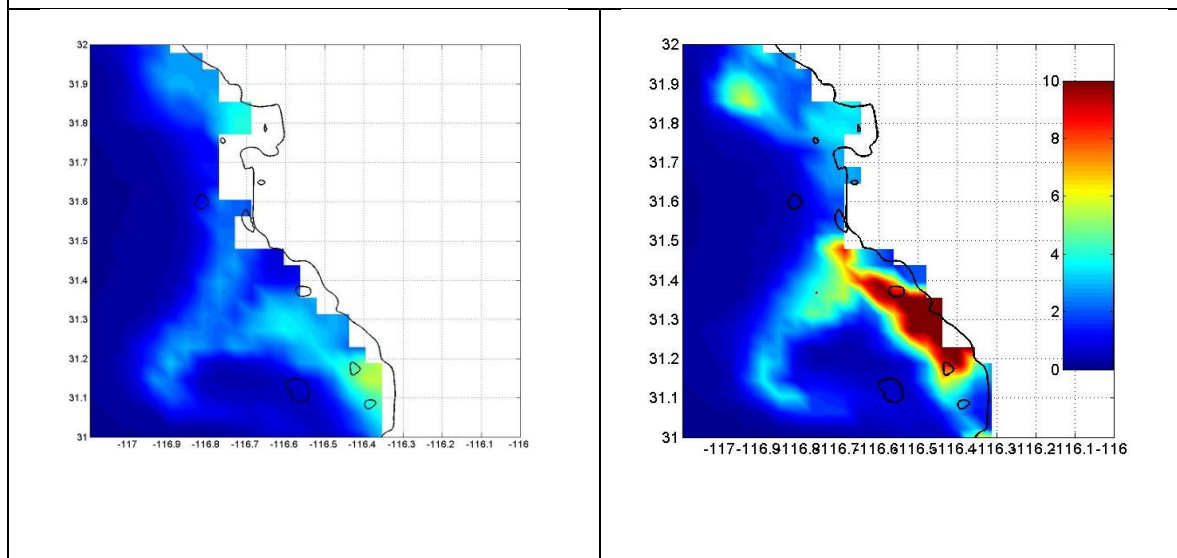
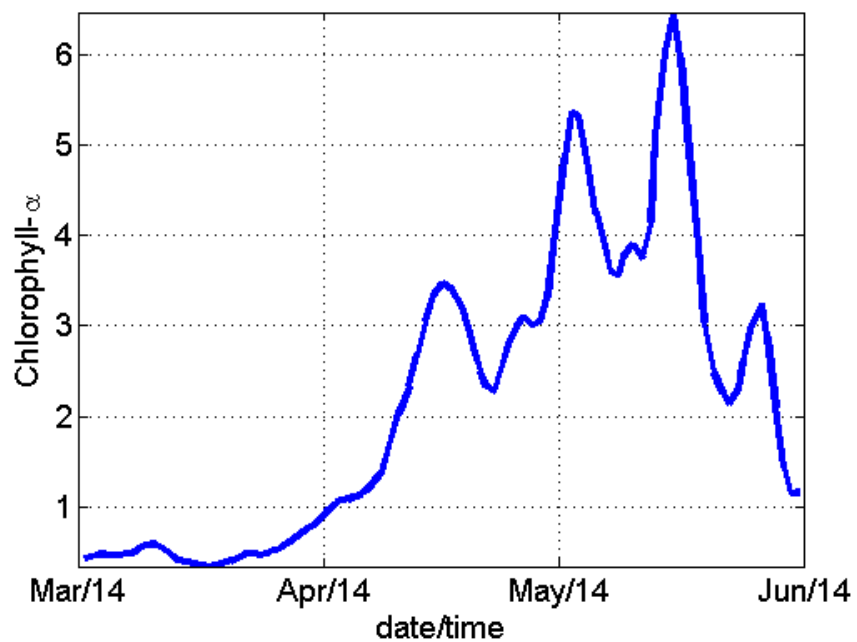


Figure 10

a



Lon = -116.7650461, Lat = 31.81091834



b



|  |  |
|--|--|
|  |  |
|  |  |

## **Capítulo III**

### **Kinematic parameters within Todos Santos Bay using the surface current velocity obtained with high frequency radars**

L.F. Navarro-Olache, R. Hernández-Walls, R. Durazo, A. Mejía R. Castro, A.L. Flores, X. Flores, and B. Martín-Atienza

Universidad Autónoma de Baja California, Ensenada, B.C., México

#### **Abstract**

The use of the Okubo-Weiss parameter to identify ocean eddies is a widely used tool in oceanography. This parameter uses the surface velocity field to perceive velocity closed contours that lead to the exposure of eddy like structures. Notwithstanding the efficiency of the method, a strong restriction is an assumption that the flow is non-divergent in numerical models calculations and also in observations from satellite altimeters, from which velocity fields are calculated. In this work, we used the surface velocity observations, obtained from high-frequency radars network. This data does not require the assumption of non-divergent flows, although it is of great importance to first ascertain whether or not the body of water under study is divergent. With this propose it is used the N2 parameter. The N2 parameter measures the relative importance of divergence in terms of the other kinematic parameters, such as vorticity and the deformation rate. This number is calculated inside the Todos Santos Bay in order to distinguish whether the flow within the bay was either divergent or non-divergent during the year 2010. It was found that calculating hourly values of surface velocity in a grid of 22 x 22 points in Todos Santos Bay, Baja California, Mexico during 2010, 70% of the flows in the area can be considered as non-divergent. This percentage includes extreme events condition, such as winter storms or Santa Ana wind in which kinematic parameters divergence, vorticity a deformation change considerably in Todos Santos Bay but maintaining the non-divergent condition  $N_2 >> 1$ . Cinematic parameters have shown that Todos Santos Bay rotates in a cyclonic direction most of the time, with

maximum positive divergent along the open boundary which presented the maximum deformations rate, in the direction north to south.

Keywords: High frequency radar data, surface circulation, Divergence, Rotational, Deformations, Determinant, Jacobian matrix, Parameter N<sub>2</sub>, Todos Santos Bay, Mexico

## Introduction

The use of high frequency (HF) radars network, along the West coast of the United States and some other regions on the world, has been developing as a method for observation the near coast surface ocean currents. A large and dense data base, with sufficient spatial and temporal resolution is being built to evaluate kinematic parameters such as divergence, vorticity and deformations of the surface layer of the ocean. This data, generated through surface velocities provide a comprehensively way to solve the chaotic nature of the surface flows<sup>1, 2, 3</sup>. With well resolved HF data, new techniques in oceanography have been incorporated for managing linear data systems that combine Lagrangian and Eulerian observations. The HF radar data enables vector operators such as the divergence, rotational or deformation of a fluid parcel<sup>4</sup> to be applied in such a way that the imprecision in the calculation of traditional techniques<sup>5</sup> is reduced to a reliable scale.

The distribution of properties on the surface of the ocean is associated with the intense activity of meso-scale structures<sup>6,7,8</sup>. These structures appear in the ocean in the form of vortices or eddies that often maintain their form for long periods of time, until they disappear or re-arranging themselves in lower scale structures. The energy of these structures has been associated with processes for mixing and redistributing the properties of the surface layers of the ocean and has awakened interest in studying their formation, evolution, decomposition and, above all, its detection. One of the most commonly used techniques for detecting eddy-shaped structures is perhaps the Okubo-Weiss (OW) parameter<sup>9,10</sup> which uses the velocity fields from numerical models, altimetry (sea level anomalies), and even drift elements, to detect coherent vortices on intermediate 100 to 200 km scales or lower, depending on the data resolution. The OW

parameter enables the differentiation of regions dominated by the vorticity ( $\text{OW} < 0$ ) from those dominated by deformation ( $\text{OW} > 0$ )<sup>11, 12</sup>. Considering that the method had been used successfully to detect and resolve eddies in the ocean, it also present some problems such as false eddies under strong vorticity flows. Another limitation of the method in both numerical and real data on eddy identification is based, on the assumption that the horizontal velocity field is non-divergent. It also assumes that vortices have axial symmetry, with maximum velocity on the edge of the eddy, in the maximum radius ( $\text{OW} = 0$ ). In this study we use a HF radar network located in Todos Santos Bay Baja California Mexico to obtain sea surface velocity vectors in 22x22 grid inside the bay. HF radar data do not require the assumption of divergence equal to cero, then using the parameter  $N_2$ <sup>11</sup> it is determined weather in the area of Todos Santos Bay this assumption is valid, under mean conditions or during some extreme weather events

## 1.1 Theoretical framework.

This study postulates that a flow could be defined in a vector field  $V(x,y)$  that represents the surface velocities. This velocities obtained by means of an HF radar system, with its two horizontal components:  $(u, v)$ . If  $V(x,y)$  is differentiable at any coordinate  $(x,y)$  within the  $\Omega$  domain, then this is the equivalent to each of its components also being differentiable.

If the positions of the surface velocities are known, it is possible to find the gradient values for each component, namely that it is possible to construct the 2-tensor gradient for the horizontal velocity (also known as the Jacobian matrix given by the gradient for the horizontal components of the vector field):

$$J = \begin{bmatrix} \frac{\partial u(x,y)}{\partial x} & \frac{\partial u(x,y)}{\partial y} \\ \frac{\partial v(x,y)}{\partial x} & \frac{\partial v(x,y)}{\partial y} \end{bmatrix} \quad (1)$$

This 2-tensor is used to detect flow characteristics (Haimes y Kenwright, 1999). It can be rewritten in the following form,

Here the divergence is defined as the trace of the matrix, this is

Positive values for divergence are characteristic of divergent flows while, on the contrary, negative values for the divergence indicate convergent flows.

The rotational of a vector field, for a bidimensional case, is defined in the following manner:

$$rot(\bar{v}) = \nabla \times \bar{v} = \left( \frac{\partial v(x, y)}{\partial x} - \frac{\partial u(x, y)}{\partial y} \right) \hat{k}$$

Namely the rotational for a bidimensional vector field has only one component, which is perpendicular to the  $(x,y)$  plane in a vertical direction . For the particular case in which the vector field is the surface velocity, the rotational is known as the relative vorticity, while positive values define positive (cyclonic) rotations, and negative values define negative (anticyclonic) rotations. In a more practical case, a scalar is defined for studying said vorticity as,

$$\zeta(\bar{v}) = \hat{k} \cdot (\nabla \times \bar{v}) = \left( \frac{\partial v(x,y)}{\partial x} - \frac{\partial u(x,y)}{\partial y} \right) \quad (4)$$

The following equations could be used to define the deformation<sup>14</sup>

$$\text{def}(\bar{v}) \sin(2\mu) = \frac{\partial u(x,y)}{\partial y} + \frac{\partial v(x,y)}{\partial x} \quad \dots \dots \dots \quad (5)$$

$$\text{def}(\bar{v}) \cos(2\mu) = \frac{\partial u(x,y)}{\partial x} - \frac{\partial v(x,y)}{\partial y} \quad (6)$$

where  $\mu$  is the angle towards the location of the greatest level of deformation. In order to calculate the magnitude of the deformation  $\text{def}(V)$ , the two equations (equations 5 and 6) can be divided,

$$\tan(2\mu) = \left( \frac{\frac{\partial u(x,y)}{\partial y} + \frac{\partial v(x,y)}{\partial x}}{\frac{\partial u(x,y)}{\partial x} - \frac{\partial v(x,y)}{\partial y}} \right) \quad (7)$$

Solving for  $\mu$  and substituting the result into either of the two equations (5 or 6), gives  $\text{def}(\bar{v})$  as a result.

Another way of calculating deformation is to square the two equations (5 and 6) and add them, thus eliminating the dependence on the angle..

$$\text{def}(\bar{v})^2 = \left( \frac{\partial u(x,y)}{\partial y} + \frac{\partial v(x,y)}{\partial x} \right)^2 + \left( \frac{\partial u(x,y)}{\partial x} - \frac{\partial v(x,y)}{\partial y} \right)^2 \quad \dots \dots \dots \quad (8)$$

It should be noted that the magnitudes given for the divergence, rotational and deformation are amounts invariant to the reference frame <sup>14</sup>.

The determinant of the Jacobian matrix, **det(J)**, provides information on the velocity gradient 2-tensor, which contains the divergence operators, vorticity and deformation,

$$\text{det}(J) = \frac{\partial u(x,y)}{\partial x} \frac{\partial v(x,y)}{\partial y} - \frac{\partial u(x,y)}{\partial y} \frac{\partial v(x,y)}{\partial x} \quad (9)$$

This could be rewritten in terms of the divergence operators, vorticity and deformation using equations 3, 4 and 8<sup>15</sup>:

$$\text{det}(J) = \frac{1}{4} [\zeta(\bar{v})^2 + \text{div}(\bar{v})^2 - \text{def}(\bar{v})^2] \quad 10)$$

The determinant of the Jacobian matrix **det(J)** provides information on the velocity gradient 2-tensor, which contains the divergence operators, vorticity and deformation, The parameter OW for divergent flow (Qd) is given <sup>17</sup> coincides with the positive eigenvalue of the acceleration gradient tensor. For the limit where the fields evolve slowly, without the divergence disappearing 17 we will have

$$Qd = \frac{1}{4} [\text{div}(\bar{v})^2 + \text{def}(\bar{v})^2 - \zeta(\bar{v})^2 + 2\text{div}(\bar{v})\sqrt{\text{div}(\bar{v})^2 - \zeta(\bar{v})^2}]$$

Mixing the previous equation with Equation (10) obtains the Okubo-Weiss parameter for divergent flows, written only in terms of the divergence and determinant, in the following manner

$$Q_d = \frac{1}{2} \left[ \operatorname{div}(\bar{v})^2 - 2\det(J) + \operatorname{div}(\bar{v})\sqrt{\operatorname{div}(\bar{v})^2 - 4\det(J)} \right] \quad (11)$$

while the following obtains non-divergent flows ( $Q_{nd}$ )<sup>17,18</sup>

$$Q_{nd} = \frac{1}{2} [ \operatorname{def}^2(\bar{v}) - \zeta(\bar{v})^2 ]$$

which, in terms of the determinant, could be written for non-divergent flows using Equation (11) as follows<sup>19</sup>:

$$Q_{nd} = -\det(J) \quad \dots \quad (12)$$

The  $Q_{nd}$  parameter for non-divergent flow is positive for values in which the deformation dominates and negative where the rotational is more important. The  $Q_{nd}$  parameter is often used for the detection of eddies<sup>20,12,15</sup>, even when the method is able to detect false positives, due to the fact that the shear effect is not eliminated from the velocity gradient tensor information<sup>21</sup>. It has also been used successfully for predicting the evolution of the flow's spectral properties<sup>22</sup>.

## 2 Methodologies

Data from 2 HF radars located in Todos Santos Bay was analyzed for the year 2010. The radars operate at a modulated frequency of 25 MHz, enabling the surface current information to be averaged to a depth of ~1 meter and a spatial resolution of 700 meters<sup>23</sup>. The radial velocity data are measured approximately every 20 minutes and averaged each hour. Details of the site and methodology can be seen in<sup>2</sup>. The Jacobian matrix was calculated using the surface velocity field obtained by the two radars. The measurements enable the construction of an hourly matrix comprising approximately 22x22 velocity nodes in a mesh positioned in a north-east direction. The vector operators for the horizontal divergence were calculated using Equation (2), while the vorticity was calculated using Equation (3). The terms for the deformation were first calculated using the angle of deformation obtained from Equation (6) in order to then apply it to Equation (7). The vector operators were used in some scenarios for

observing the kinematics of the average currents in the bay, taking into account all the data from 2010. The  $N_2$  parameter indicate the relative importance of divergence in terms of the kinematic parameters flow divergence, vorticity and deformation.  $N_2$  parameter was obtained hourly from the data and the information accumulated in each node on the TSA. For an overall analysis the  $N_2$  parameter was redefined as  $N_2=1$  if the divergence is not significant,  $N_2 = -1$  if the divergence is significant, and zero for places where no velocity values are recorded

### 3 Results

The surface velocity maps within Todos Santos Bay have good spatial and temporal resolution to calculate the kinematic characteristics of the fluxes. This database is used in terms of the components of the surface velocity ( $u, v$ ). The surface velocities are hourly data obtained in Todos Santos Bay in 2010, because this year presented a lesser amount of gaps in time and space from the whole series (2009 to 2016) and may be a good example of the behavior of the surface flow in the study area. In the first place we are going to present the characteristics of the mean surface flow inside Todos Santos Bay and its kinematic parameters of divergence, vorticity and deformation. Additionally it is examined the kinematic response of the bay to three extreme events occurred in the bay (a winter storm, and two Santa Ana event) to observe if under mean conditional and extreme condition the assumption of divergence equal to zero stand.

The annual surface currents in TSB, shows in the overall a cyclonic circulation around BTS and their behavior during extreme events that occurred in Todos Santos Bay. Firstly, the average of the velocities was calculated over the course of the year using a 22x22 mesh covering the surface of the bay (Figure 1A). The average shows the highest velocities and the highest level of variability on the open front and at the south of the bay. On this data scale, the bay presents a tendency to rotate in a cyclonic direction<sup>24,2</sup>, as observed in Figure (1C), with slightly positive values.

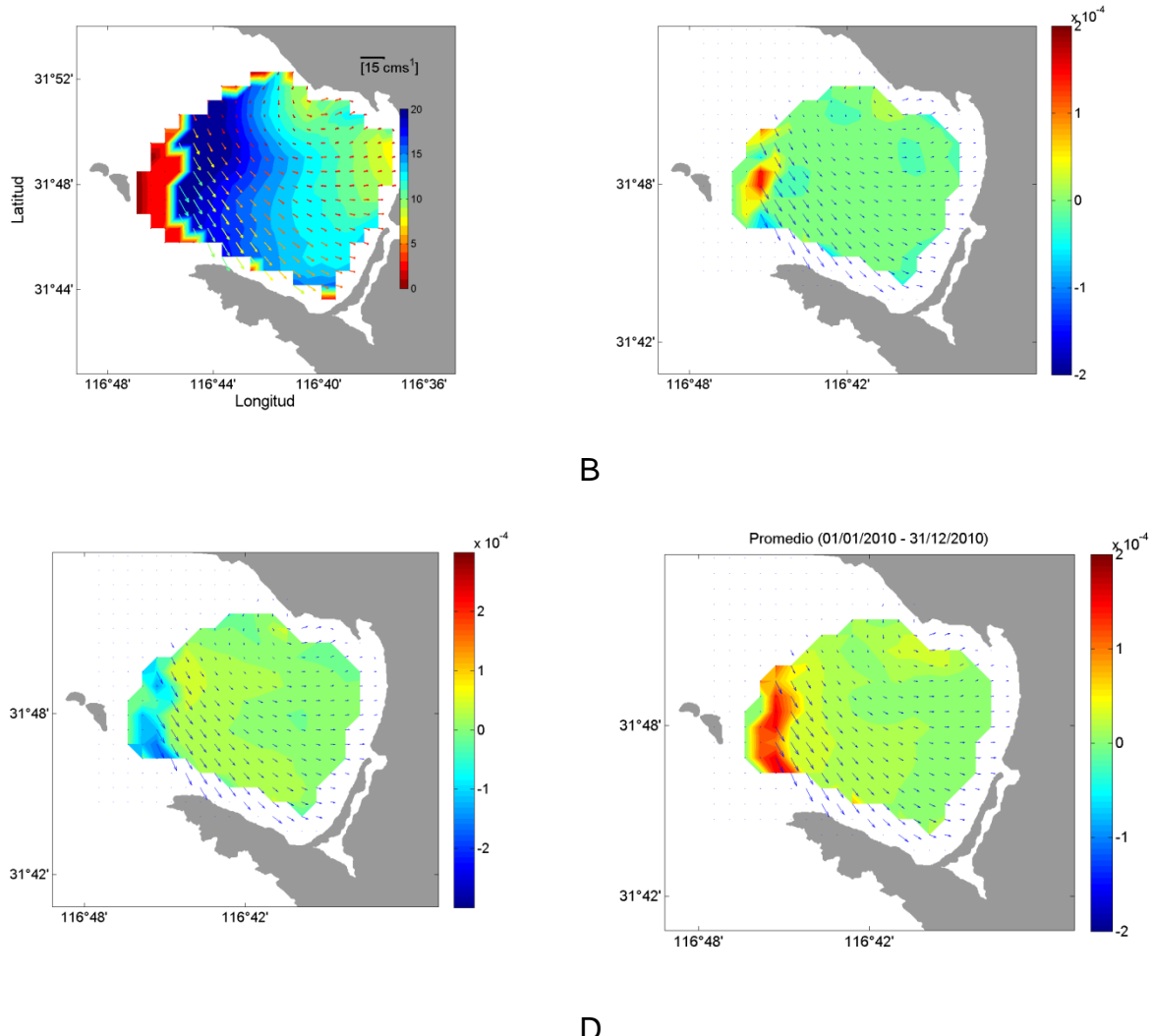


Fig. 1 Todos Santos Bay HF average velocities and RMS for 2010

Similar to the annual average, the maximum divergence is found on the open front and the southern part of the bay (1B), while the deformation presents a greater component along the length of the coast, in a north-south direction (1D).

The calculations for the kinematic parameters were applied to extreme event conditions with the objective of observing the response of the flows in the bay under these wind conditions. An event involving NE-E winds, known as Santa Ana winds, was first considered, as was a winter storm wind event (NW-W) and a SW-NE wind event . The

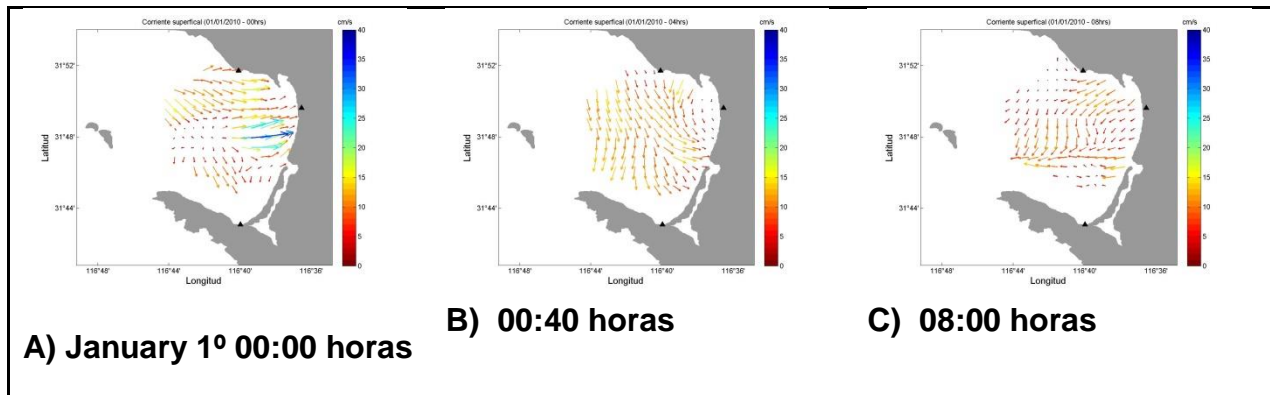
winds were measured in the northern section of the bay and were presented as daily averages.

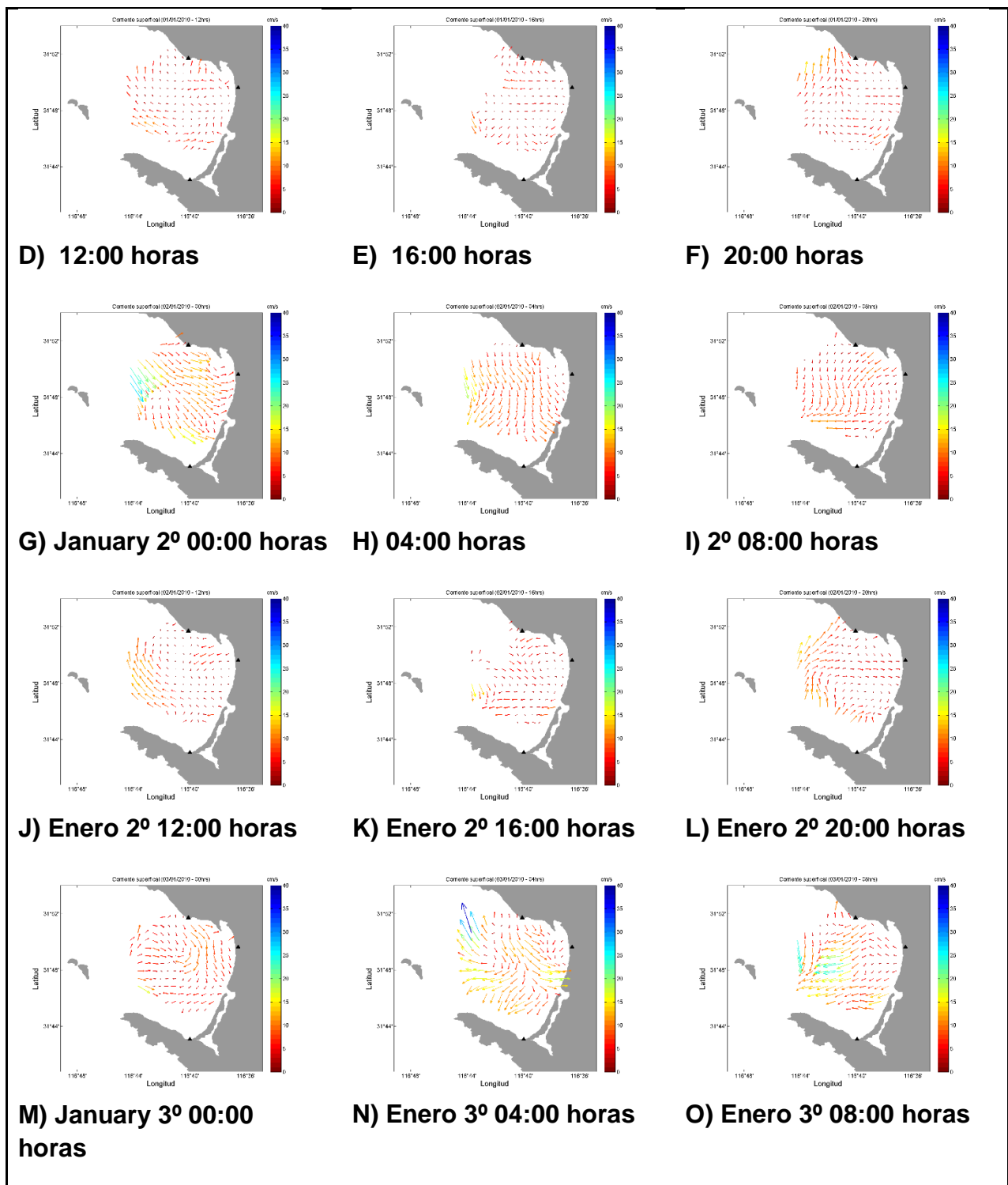
A sequence of the velocities of the currents during a Santa Ana event (Figure 2) shows the high level of variability in the currents of the zone. The event registered occurred during the first days of January 2010. The sequence begins on 1st January at 00:00 hours and at intervals of every four hours (Figure 2). The currents show, at the beginning, a circulation with a tendency to rotate cyclonically, maintaining that direction until 04:00 hours, at which time the flow was observed to begin rotating (Figure 2C), from the NE part of the bay, confirming the occurrence of flows away from the coast. This flow intensifies in accordance with the intensification of the wind in this same direction, thus marking the first day of Santa Ana winds (figures 2C and 2D). The sequence for the second day (2nd January 2010) is similar. At 00:00, the flow was observed moving toward the coast, while, from 0400 hours onwards, the flow began to rotate away from the coast, intensifying at 0800 hours and continuing until between 18:00 and 21:00 hours (figures 2 I-L). On the third day, the meteorological data shows a significant drop in relative humidity and an increase in wind velocity, thus marking the most intense moment of the Santa Ana wind event (Figure 3). On this day, surface flow in a direction away from the coast continued from 04:00 hours until 20:00 hours (Figure 2 N-R). On the following days, the 4th and 5th January, the event decreased in force until it could not be noted in the velocity data.

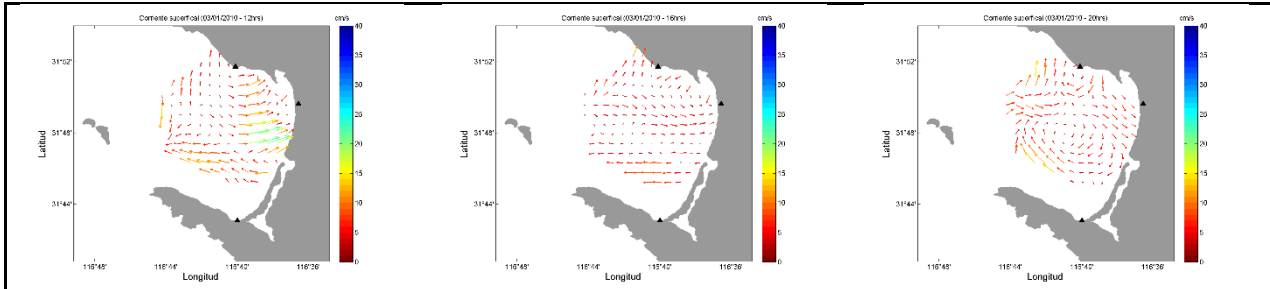
The kinematic parameters were calculated using the average velocities recorded during the Santa Ana wind event, in this first case of the 2nd to 5th January. The velocity component shows velocities moving away from the coast with a greater variability on the open front of the bay (Figure 4A). The divergence zone presents on the open front of the bay and in the zone close to the coast, demonstrating flows away from the coast with a tendency to negative rotation, namely anticyclonic circulation (Figure 4C), in the opposite direction to the average conditions (Figure 1C). The deformation has a component transverse to the bay (east to west), further to the longitudinal component running north to south (Figure 4D).

Another Santa Ana wind event was formed from 14th to 16th March, as presented in the figure presenting the meteorological data (Figure 3). The average flow pattern during the period (Figure 5A) shows a component of flows toward the bay on the open front and another component moving away from the coast, as a result of the arrival of the Santa Ana event. The divergence level is high in the coastal zone (Figure 5B), presenting a negative rotation (anticyclonic) close to the coast and a positive rotation (cyclonic) on the open front of the bay (Figure 5C). Deformation was shown with an east-west component and a north-south longitudinal component (Figure 5D). Although a total of 8 Santa Ana events presented in the year featured in the present research, from January to April and from November to December, those events that showed a similar distribution of velocity and range of time are not presented in this study.

The meteorological data for another extreme event, which presented from 19th to 22nd January, show that it is a winter storm event with high humidity and strong winds (Figure 3). The surface currents show a strong component moving toward the coast (Figure 6A) and values associated with winds of more than 35 cms<sup>-1</sup> (red dots shown in Figure 3). During this event, the highest level of divergence was found on the open front of the bay (Figure 6B), showing a cyclonic rotation, the same direction as the average annual circulation for the bay (Figure 1). While the deformation observed in the bay is greater on the open front, it has a component transverse to the coast, running west to east, forced, apparently, by the flows in this direction







P) Enero 3º 12:00 horas

Q) Enero 3º 16:00 horas

R) Enero 3º 20:00 horas

Figure 2. Sequence showing the arrival of a Santa Ana event in Todos Santos Bay on 1st and 4th January 2010. The event lasted for 5 days in total (1st to 5th January 2010) with a similar pattern of velocity.

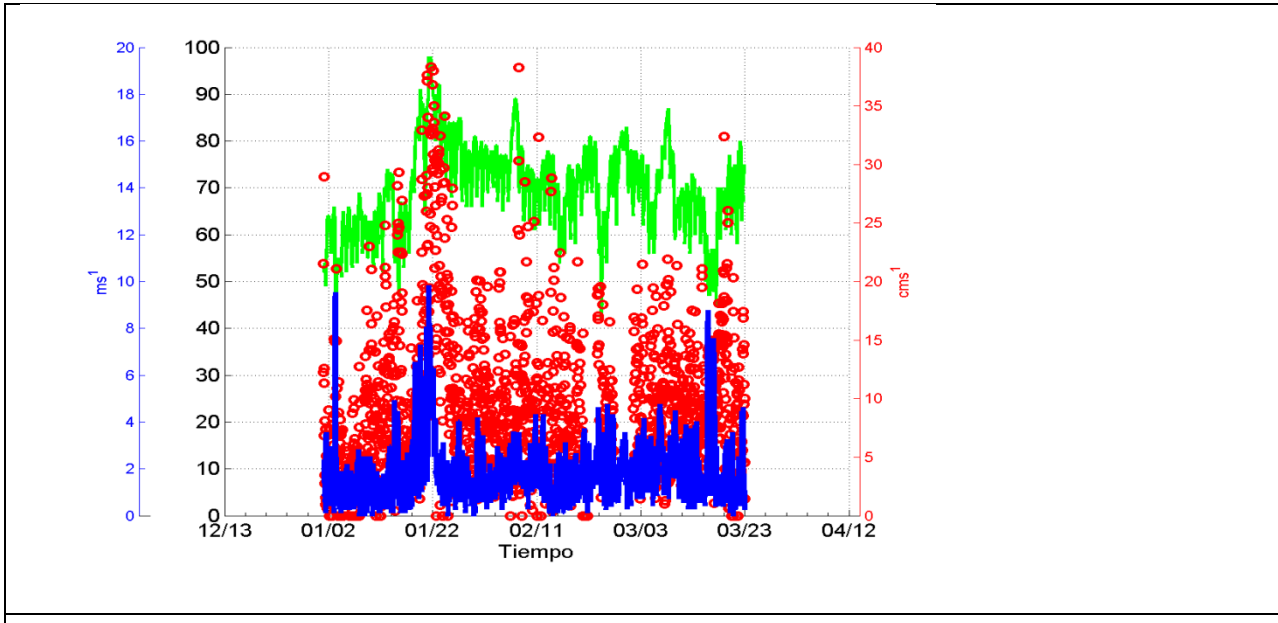
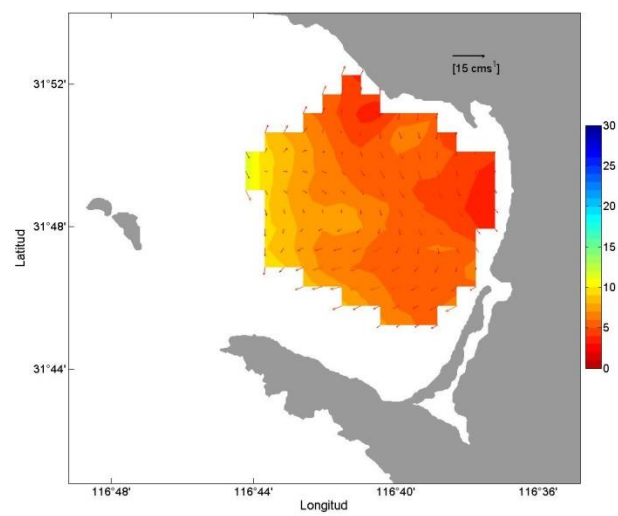
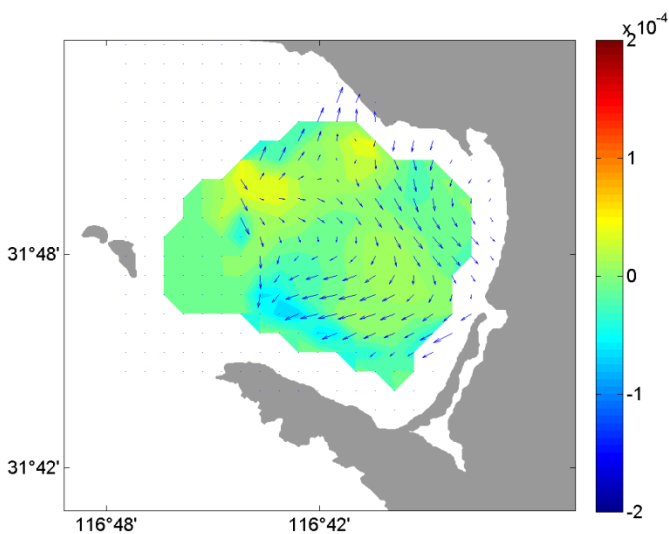


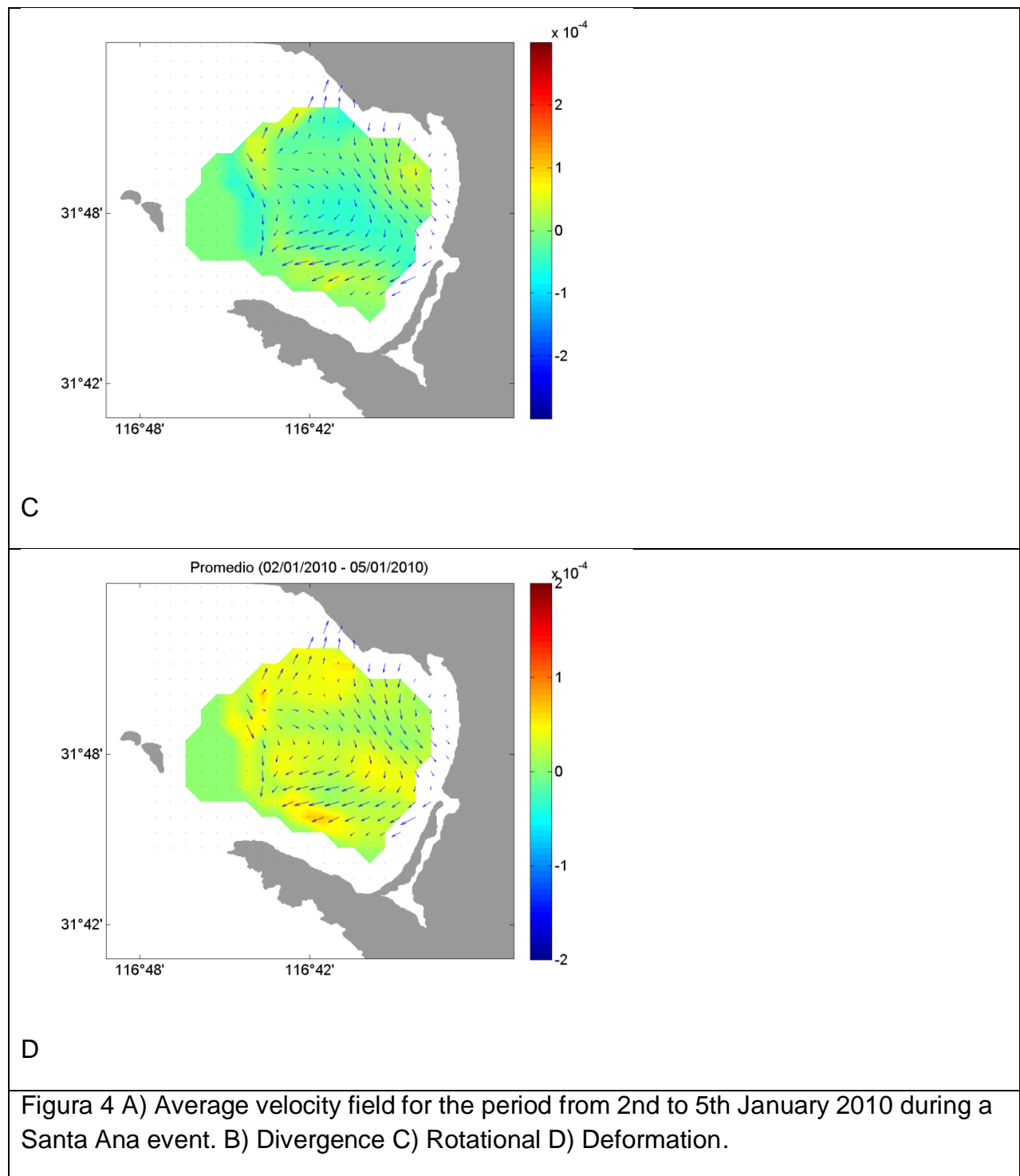
Figure 3 Meteorological data for January to March 2010. The green line represents the relative humidity, while the blue line represents the wind velocity ( $\text{ms}^{-1}$ ) and the red dots represent the surface current velocity data ( $\text{cms}^{-1}$ ) at one point of the bay. The peaks of 3rd January and 20th March indicate a Santa Ana event, while a winter storm can be observed on 20th January.

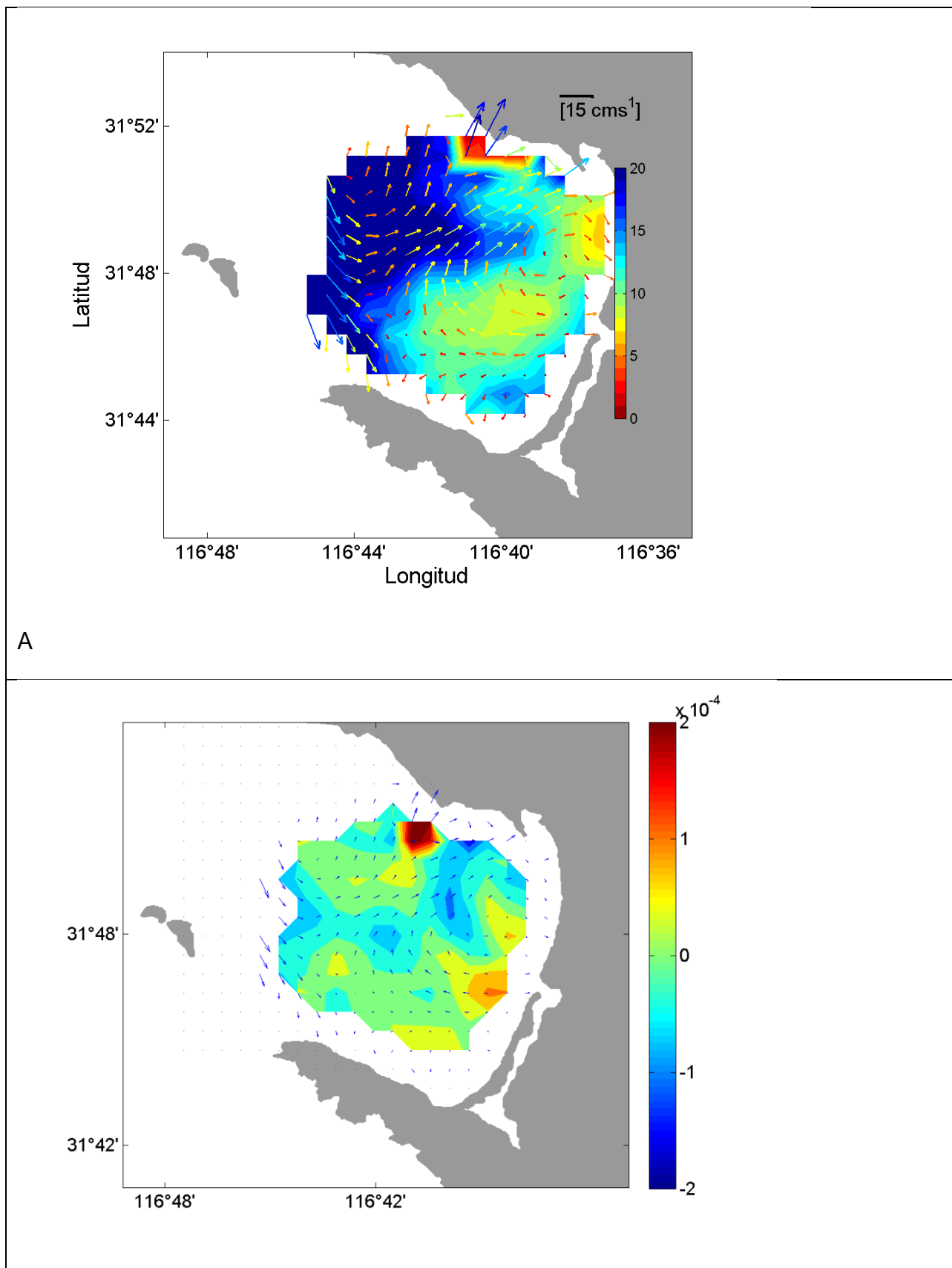


A

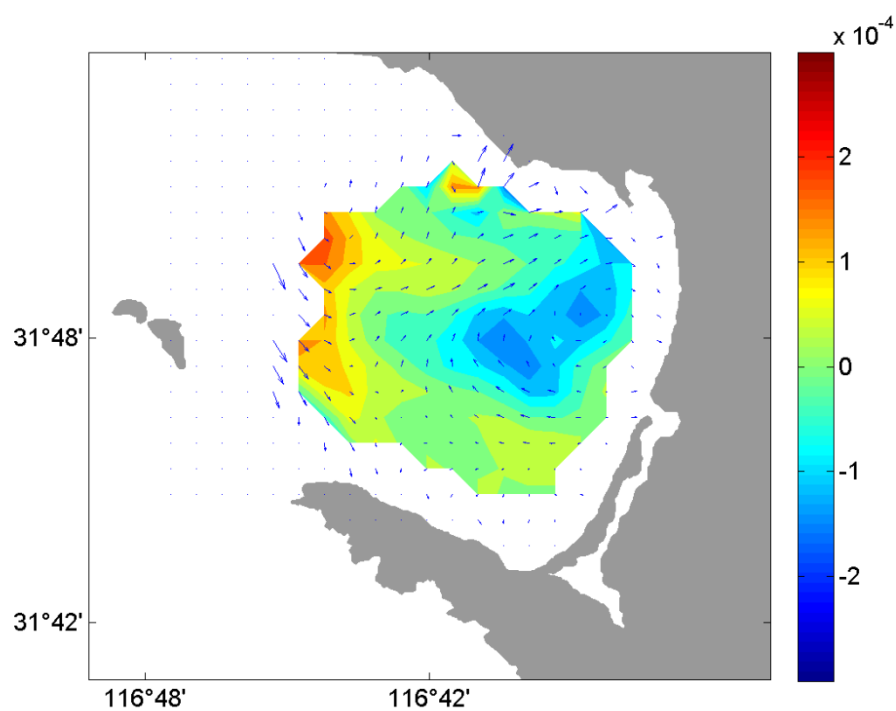


B

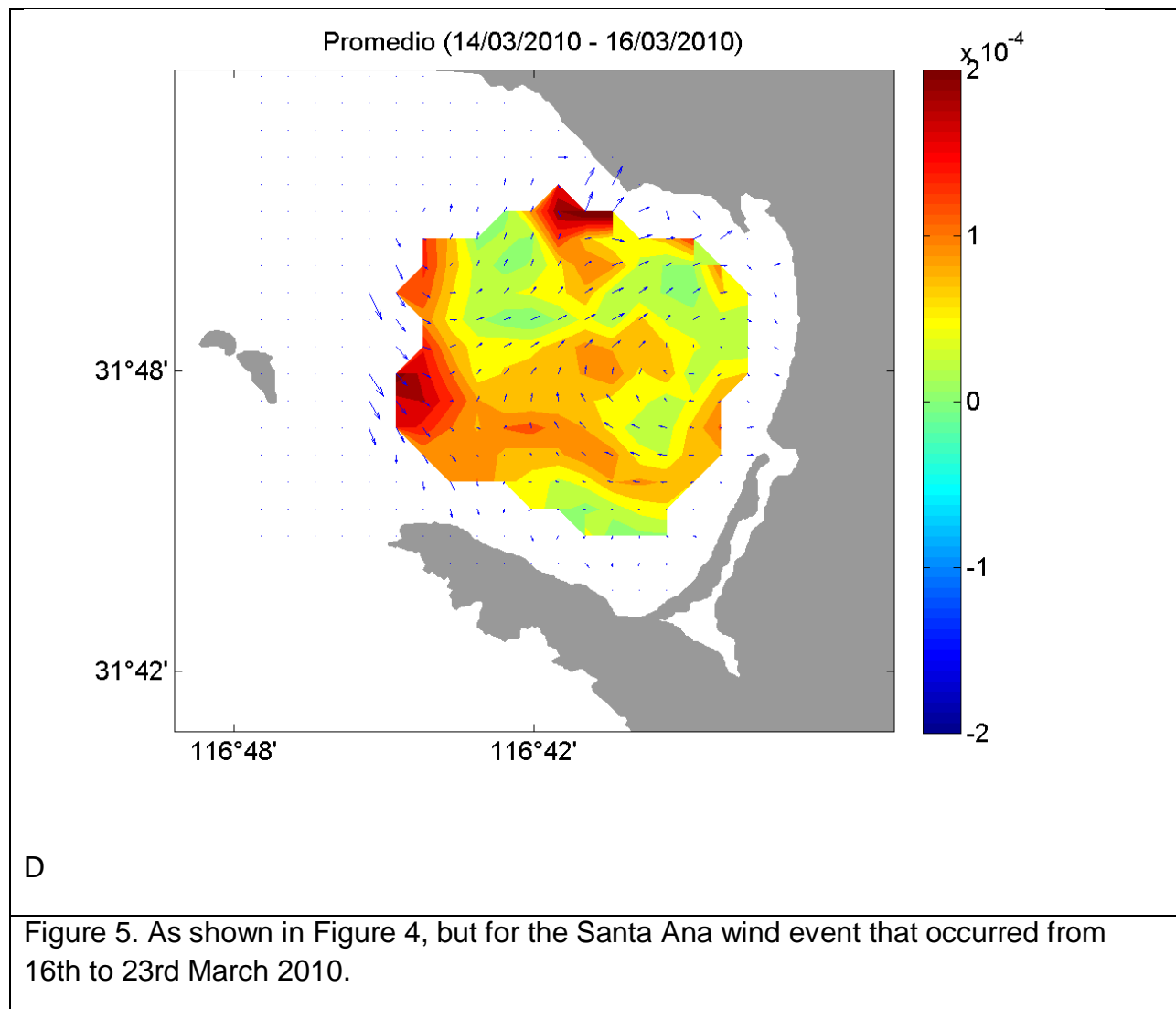


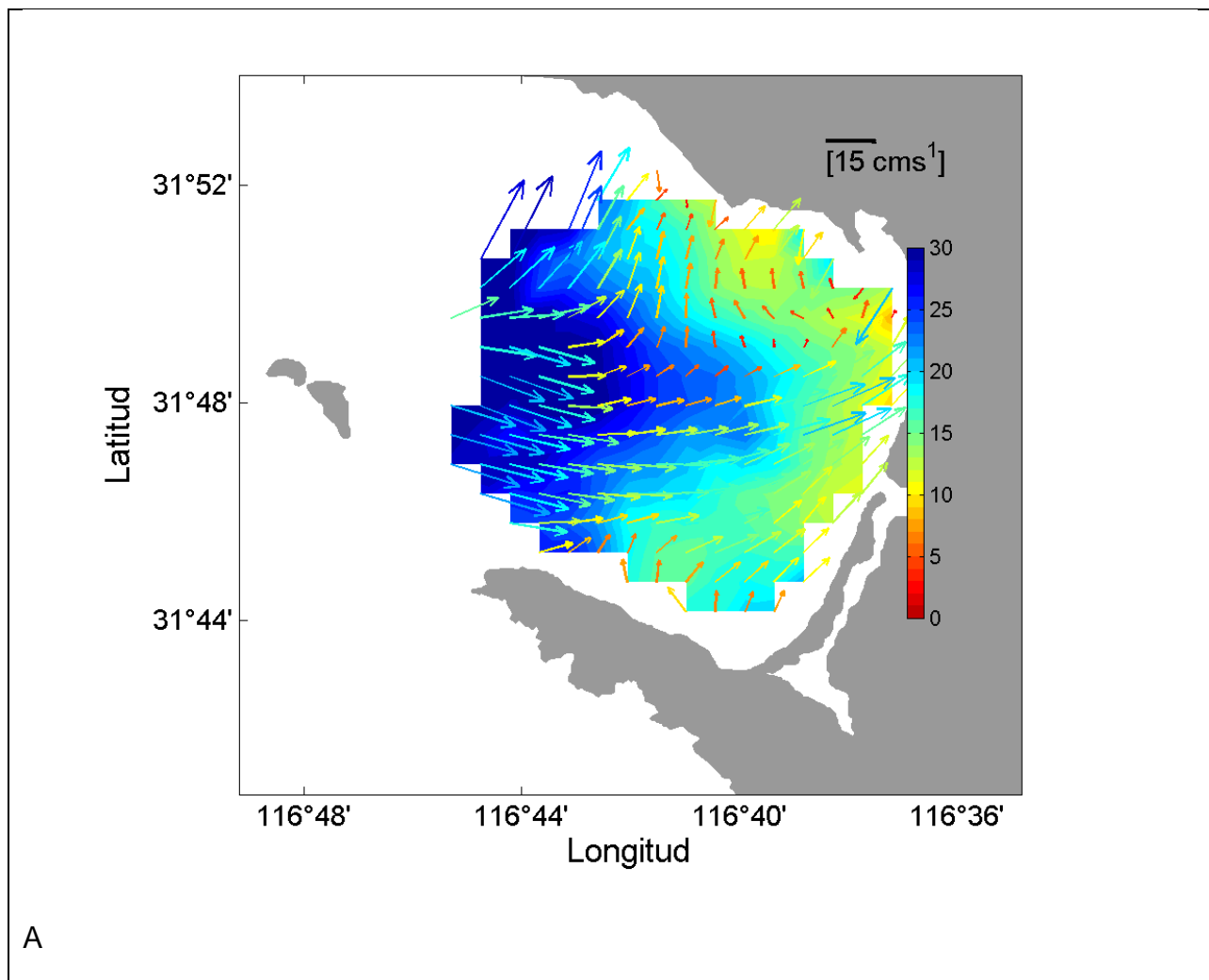


B

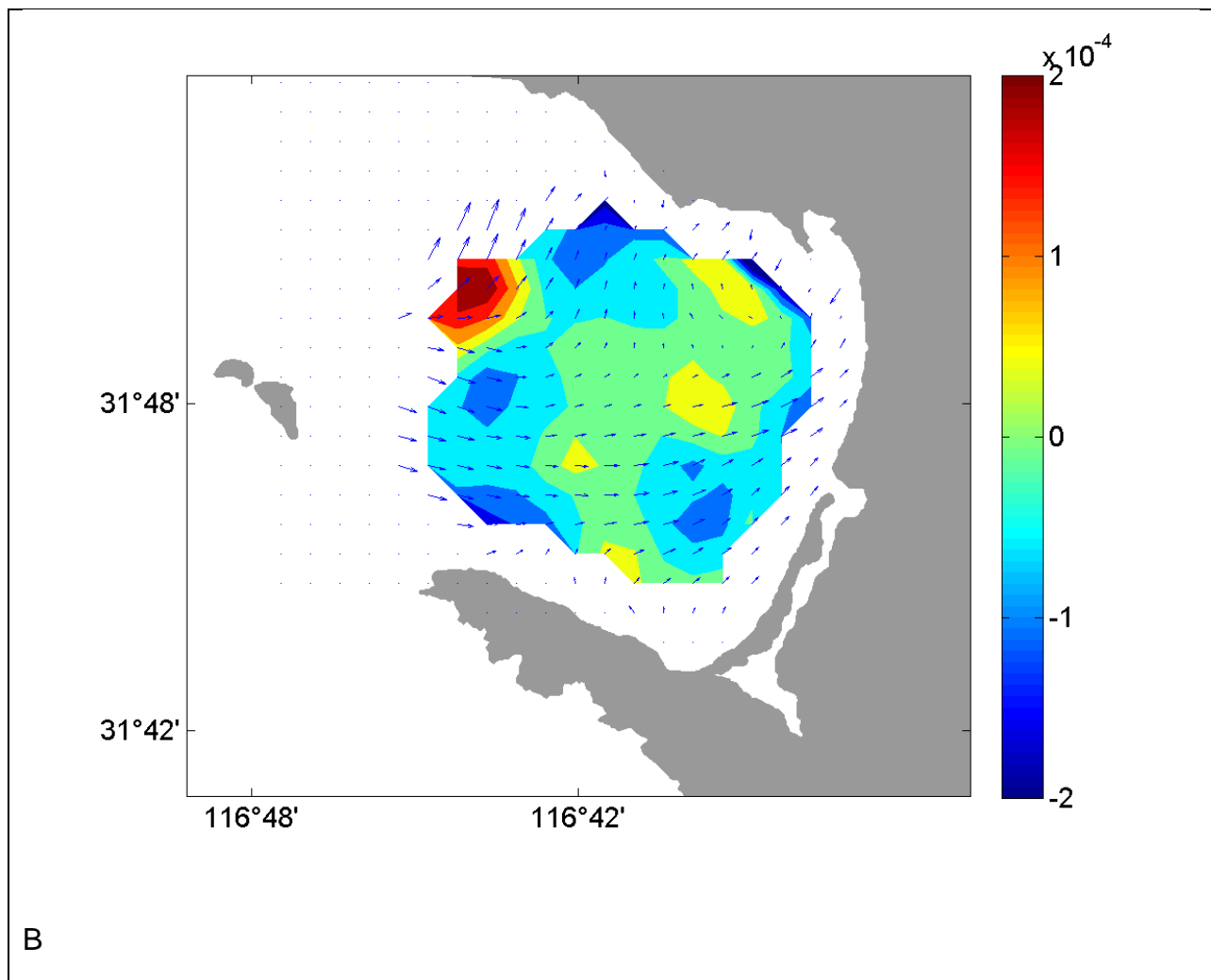


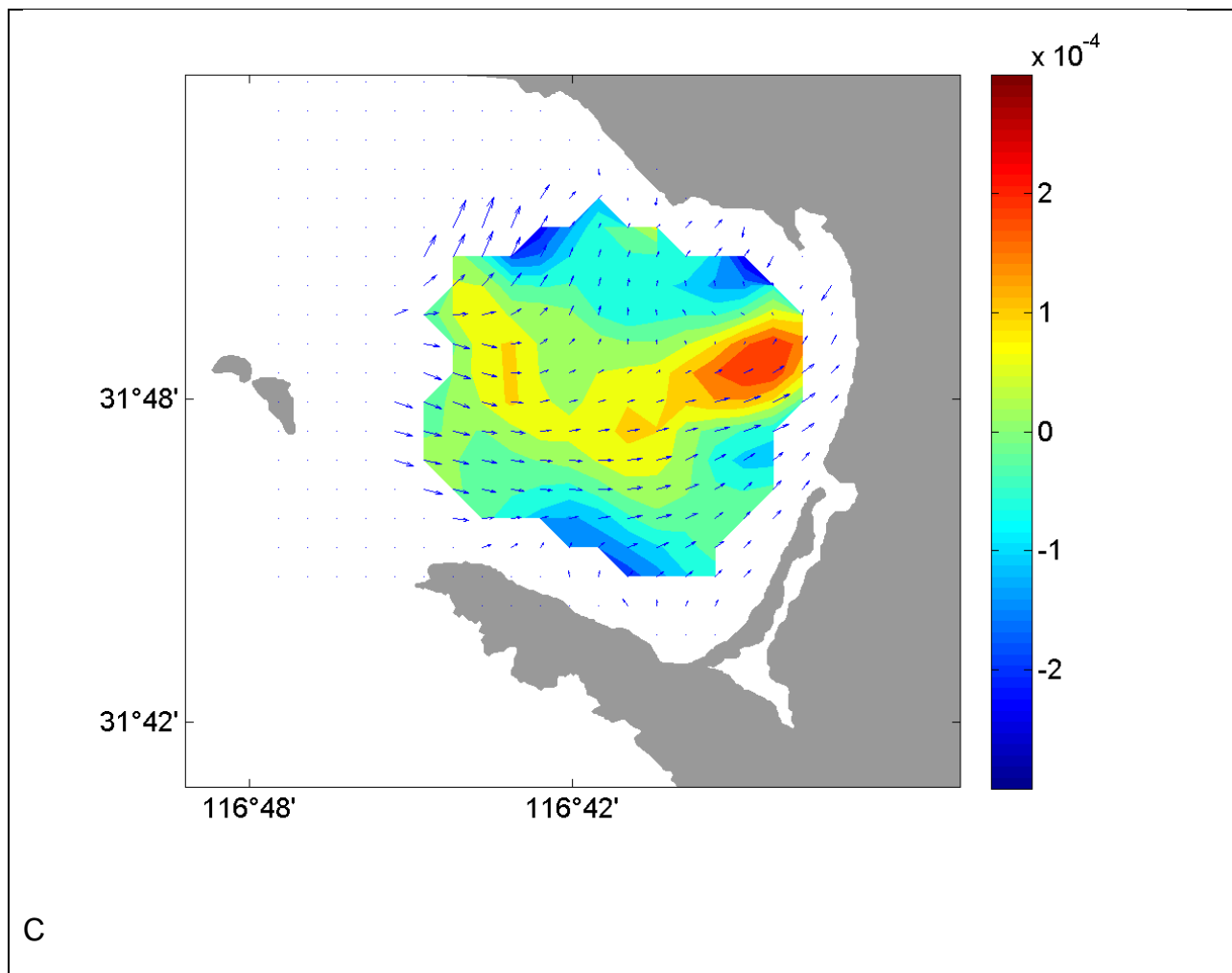
C

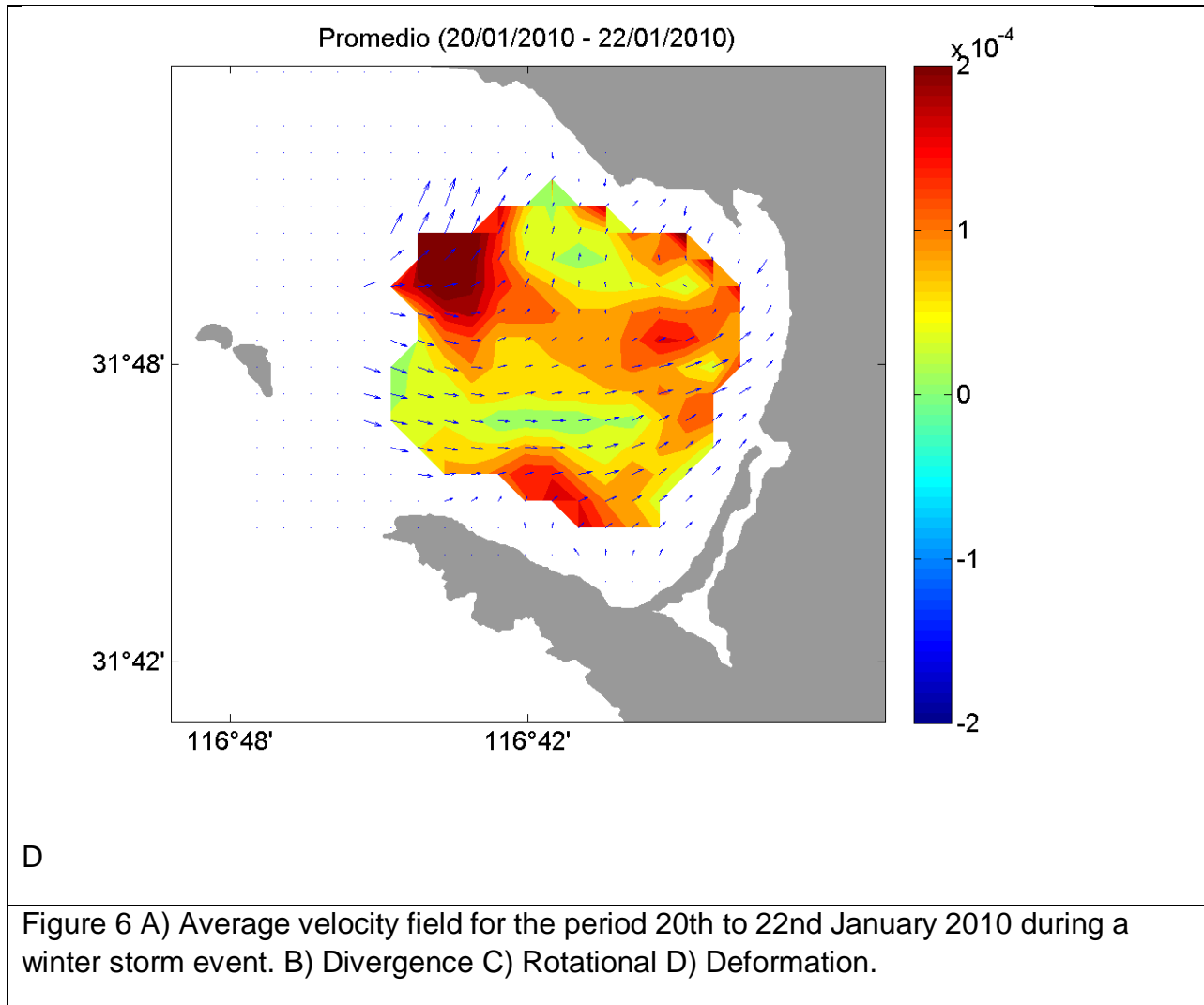




A







### III.A. Analysis of divergent flow fields using the N2 parameter

Due to the OW parameter differences for divergent and non-divergent flows, the relative importance of both the divergence and the determinant for the Jacobian matrix were analyzed, using the criteria proposed by Gan and Ho<sup>15</sup>, which compares the divergence in relation to the vorticity and deformation, as given by the following relation:

$$N_2 = \frac{4\det(J)}{\operatorname{div}(\bar{v})^2}$$

The divergence for the vector field could be underestimated if the N<sub>2</sub> value is found to be greater than 1 ( $N_2 \gg 1$ ) or negative ( $N_2 < 0$ ). Applying this criterion to the 2010 database compiled at Todos Santos Bay reveals that 70% of the data taken in the bay could lead to the underestimation of the divergence, as shown in figures 7A and B. The figure also shows that the data represents a good level of temporal coverage, for which reason the results obtained are considered reliable.

The figures also show that during extreme Santa Ana wind events or north-westerly storms, the N<sub>2</sub> values are also high, demonstrating that the non-divergent flow condition dominates the flows of the bay. In order to make a graphical analysis for the entire year, the N<sub>2</sub> parameter is redefined. N<sub>2</sub>=1 if the divergence is not significant, N<sub>2</sub> = -1 if the divergence is significant, and zero for places where no velocity values are recorded. The accumulative N<sub>2</sub> values within the Todos Santos Bay (Figure 7C) shows that in the majority of the areas inside the bay N<sub>2</sub>>1 for the period of 2010, supporting the non-divergent nature of Todos Santos Bay.

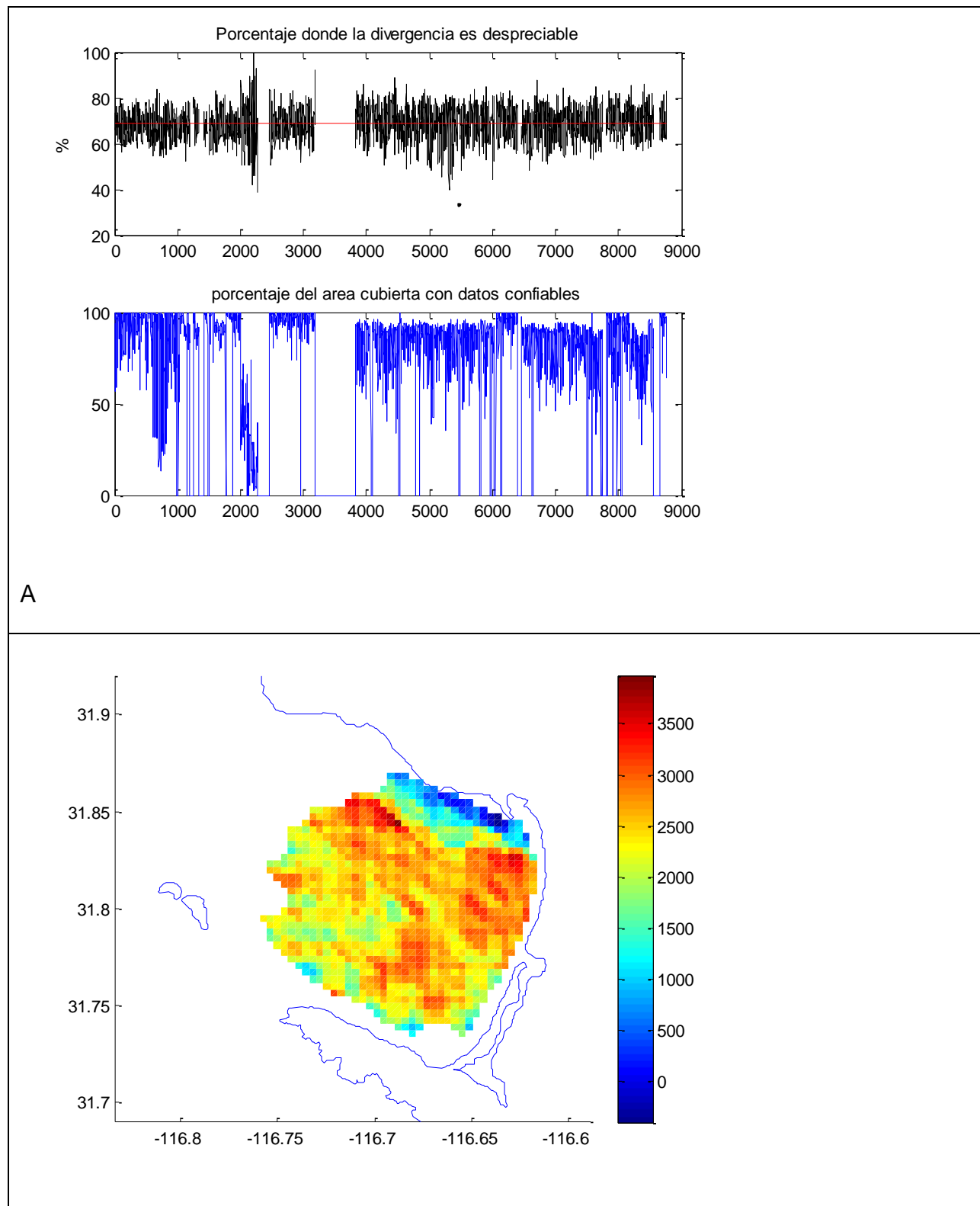
#### 4 Discussions

The year corresponding to the data presented in this study reveals the general form of circulation in the bay, as well as the response of the flows in the interior of the bay, under average and extreme wind conditions, such as winter storms and Santa Ana wind events, over the course of the year. Although previous studies on the circulation found in the bay<sup>25,26,2</sup> show a cyclonic rotation, it was not until the processing of radar data undertaken in the present study that more reliable evidence, based on said calculations, of the high divergence values on the open front and in the southern areas of the bay was available, values which cause the rotation to occur in this direction. This study also presents evidence of positive vorticity, with a  $1/3f$  velocity of rotation in average

conditions and an  $f$  reading (where  $f$  is the Coriolis parameter ( $7.3 \times 10^{-5} \text{ s}^{-1}$ ) for Santa Ana wind conditions. Larrañaga<sup>24</sup> showed that the average circulation in the summer consistently occurs in a cyclonic direction, while the circulation in winter divides into an anticyclonic rotation in the coastal area of the bay and a cyclonic rotation in the west of the bay. The results of the present study show that the anticyclonic coastal rotations, during the winter, are generated during Santa Ana events and, depending on their intensity and duration, cover the entire bay, inverting the flow for the duration of said Santa Ana event. On average, the circulation in the bay, in both winter and summer, indicates a cyclonic rotation.

The surface deformation values found for the bay are caused by the rate of shear, the deformations and the pattern of lateral mixing that occurs during the flow. The highest level of deformation presents on the open front of the bay along the length of the coast, which was also where the highest divergence values in the bay were observed. The high levels of divergence and deformation on the open front could prevent the surface flows from remaining within the bay, as has been observed in the high number of drift elements found in the bay<sup>2</sup>, elements which circulate around the bay for days without leaving it. On the other hand, the deformation and possible mixing of the surface lie transverse in relation to the bay (E-W) during Santa Ana events, facilitating not only the water's egress from the bay but also the mixing of internal and external water, due to the rate of shear .

Todos Santos Bay is an important aquaculture and maricultural zone, into the coastal areas of which are dumped large amounts of domestic wastewater in three official discharges from the city's treatment plants. A significant amount of stormwater discharge and clandestine wastewater discharge is deposited, untreated, into its coastal areas and streams and eventually arrives to the waters of the bay. In 2018, a desalination plant, located in the center of the bay, began operating, releasing a sporadic flow of brine. Given this perspective, it is important to ascertain the response of the internal flows of the bay under both normal and extreme conditions in order to be able to understand the possible impacts that these inputs could have on the economic and tourism activities undertaken in the zone



C

Figure 7 A) The upper panel represents the percentage of hourly data, which could lead to the underestimation of the divergence  $N_2 \gg 1$  or  $N_2 < 0$ , B) Coverage of velocity data for 2010, C) Accumulated  $N_2$  data for 2010, which could lead to the underestimation of the divergence.

## 5 Conclusion

The present study found that the Okubo-Weiss parameter could be written in two different forms, firstly, for divergent flows as:

$$Q_d = \frac{1}{4} \left[ \mathbf{div}(\bar{v})^2 + \mathbf{def}(\bar{v})^2 - \zeta(\bar{v})^2 + 2\mathbf{div}(\bar{v})\sqrt{\mathbf{div}(\bar{v})^2 - \zeta(\bar{v})^2} \right]$$

and

$$Q_d = \frac{1}{4} \left[ 2\mathbf{div}(\bar{v})^2 - 4\det(J) + 2\mathbf{div}(\bar{v})\sqrt{\mathbf{div}(\bar{v})^2 - 4\det(J)} \right]$$

For non-divergent flows, the above equations are reduced to:

$$Q_{nd} = \frac{1}{4} [ \mathbf{def}^2(\bar{v}) - \zeta(\bar{v})^2 ]$$

or as:

$$Q_d = -\det(J)$$

The kinematic parameters showed that, during Santa Ana wind events, the bay presents higher deformation values, generating a shear vorticity with the flows found on the open front. The high level of deformation found in the output flows during these events could indicate a higher level of mixing in the surface layer.

The values for the  $N_2$  parameter showed that the flows within the bay are non-divergent (within 70 percent), even for extreme flow conditions with velocities higher than the average for the bay.

## **ACKNOWLEDGEMENTS**

The authors wish to thank the students involved in the retrieval of information from the HF radar system. This study was made possible thanks to the support received as a result of the successful participation of the project Circulation in Todos Santos Bay in the 17th internal UABC scholarship process. The authors also wish to thank the UABC (PREDEPA) and the SEP (PRODEP) for the support received via the mobility program in 2017.

## **References**

- [1] Abraham, E. R., Law, C. S., Boyd, P. W., Lavender, S. J., Maldonado, M. T., Bowie, A., 2000. Importance of stirring in the development of an iron-fertilized phytoplankton bloom. *Nature* 407, 727–730.
- [2] Alvarez-Sanchez, L. G., Hernandez W. R, and Durazo A. R. (1988). Patrones de deriva de trazadores lagrangeanos en la Bahía de Todos Santos. In “Ciencias Marinas”. Vol. 14,(No. 4,):pp. 135-162. UABC, México..

- [3]Argote-Espinoza, M.L., Gavidia-Medina, F., Amador-Buenrostro, A. (1991). Wind induced circulation in Todos Santos Bay, B. C. México. In “Atmósfera” , Vol. 4, pp. 101-115.
- [4]Beltrami, E.J. 1987. Mathematics for dynamic modelling. Academic Press, Inc. London UK
- [5]Blanch-Mercader, C., V. Yashunsky, S. Garcia, G. Duclos, L. Giomi, and P. Silberzan. 2018. Turbulent Dynamics of Epithelial Cell Cultures. Physical Review Letters, 120, 208101 Published 17 May 2018.
- [6]Cipolla, R. and A. Blake. 1997. Image divergence and deformation from closed curves. International Journal of Robotics Research 16: 77-96.
- [7]Chang, Y.L. and Lie-Yauw Oey. 2014. Analysis of STCC eddies using the Okubo-Weiss parameter on model and satellite data. Ocean Dynamics (2014) 64:259271
- [8]Dong, Y., Y. Yan and C. Liu. 2016. New visualization method for vortex structure in turbulence by lambda2 and vortex filaments. Applied Mathematical Modelling, Volume 40(1):500-509. <https://doi.org/10.1016/j.apm.2015.04.059>
- [9]Flores-Vidal, X., R. Durazo, R. Castro, L.F. Navarro, F. Dominguez, E. Gil. 2014. Fine-Scale Tidal and Subtidal Variability of an Upwelling-Inuenced Bay as Measured by the Mexican High Frequency Radar Observing System. Y. Liu, H. Kerkering and R.H. Weisberg (Eds.). Coastal Ocean Observing Systems: Advances and Syntheses. Elsevier.209-228.
- [10]Flores-Vidal, X., S. Gonzlez-Montes, R. ZertucheChanes, I. Rodrguez-Padilla, C.L. Marti, J. Imberger, A. Meja-Trejo, R. Durazo-Arvizu, L. Navarro-Olache. 2018. Three-dimensional exchange ows in a semi-enclosed bay: Numerical simulations and high frequency radar observations. Estuarine, coastal and Shelf Science, 201(2018):2635
- [11]Gan J.and H. S. Ho. 2007. Identfcation of spatial variability and eddies in the circulation of the South China Sea. Advances in Geosciences, Vol. 12: Ocean Science: 243-260.

- [12]Haimes, R. and D. Kenwright. 1999. On the velocity gradient tensor and uid feature extraction. Conference, Fluid Dynamics and Co-located Conferences, <https://doi.org/10.2514/6.19993288>
- [13]Hollis 2002]Selwyn Hollis. 2002. Differential Equations with Boundary Value Problems. ISBN-10: 0130159271, ISBN-13: 9780130159274. Pearson Higher Education.
- [14]Hua, B.L. and P. Klei. 1998. An exact criterion for the stirring properties of nearly two-dimensional turbulence. *Physica D* 113(1998):98-110
- [15]Isern-Fontanet, J., Garcia-Ladona, Font, J., 2003. Identification of marine eddies from altimetry. *J. Atmos. Oceanic Technol.* 20, 772–778.
- [16]Isern-Fontaneta J, J. Fonta, E. Garcia-Ladonaa, M. Emelianova, C. Millotb, I. Taupier-Letage. 2004. Spatial structure of anticyclonic eddies in the Algerian basin (Mediterranean Sea) analyzed using the Okubo-Weiss parameter. *Deep-Sea Research II* 51 (2004): 30093028.
- [17]Jeong, J. and F. Hussain. 1995. On the identification of a vortex. *Journal Fluid Mechanics*, 285:69-94.
- [18]Kim, S.Y. 2010. Observations of sub meso-scale eddies using high frequency radar-derived kinematic and dynamic quantities. *Continental Shelf Research*, 30(2010):1639-1655.
- [19]Kolar V and J. Sistek. Recent progress in explicit shear eliminating vortex identifcation. 19 Australasian Fluid Mechanics Conference Melbourne, Australia (2014).
- [20]Liao, Y. and N. T. Ouellette. 2015. Correlations between the instantaneous velocity gradient and the evolution of scaleto-scale fluxes in two-dimensional of. *Physical Review E* 92, 033017.
- [21]Lukovich, J.V. and T.G. Shepherd. 2005. Stirring and mixing in two-dimensional divergent ow. *Journal of the Atmospheric Science*, 62:3933-3954.

- [22]Mantovanelli, A., S. Keating, L. R. Wyatt, M. Roughan, and A. Schaefer 2017. Lagrangian and Eulerian characterization of two counter-rotating submesoscale eddies in a western boundary current, *J. Geophys. Res. Oceans*, 122, 49024921, doi:10.1002/2016JC011968.
- [23]Mateos, E., Marinone, S.G., and Parés-Sierra, A. (2009). Towards the numerical simulation in the summer circulation in Todos Santos Bay, Ensenada, B. C., México. In “Ocean Modeling”, vol. 27, pp. 107-112.
- [24]Mathworks, 2006. Gradient function. Merikoski, J. and A. Virtanen. 1997. Bounds for eigenvalues using the trace and determinant. *Linear Algebra and its applications*, 264:101-108. <https://www.mathworks.com/help/matlab/ref/gradient.html>
- [25]Miller, H., D. Jerison and J. French. 2013. MIT 18.03 Ordinary Differential Equations 18.03 Extra Notes and Exercises. [http://math.mit.edu/jorlo/\\_suppnotes/suppnotes03/la8.pdf](http://math.mit.edu/jorlo/_suppnotes/suppnotes03/la8.pdf)
- [26]Okubo, A., 1970: Horizontal dispersion of oatable particles in the vicinity of velocity singularities such as convergences. *Deep-Sea Res.*, 17, 445454.
- [27]Paduan, J.D., P.M. Kosro, S.M. Glenn. 2004. A national coastal ocean surface current mapping system for the United States. *Marine Technology Society Journal*, 38(2):102-108
- [28]Robinson, A. R. et al., 1993. Mesoscale and upper ocean variabilities during the 1989 JGOFS bloom study. *Deep-Sea Res. II* 40, 9–35.
- [29]Schaefer, A., A. Gramouille, M. Roughan, and A. Mantovanelli (2017), Characterizing frontal eddies along the East Australian Current from HF radar observations, *J. Geophys. Res. Oceans*, 122, 39643980, doi:10.1002/2016JC012171.
- [30]Suarez-Molina D. y L. Garca-Weil. 2009. Detección y seguimiento automático de vórtices en la Cuenca Canaria con altímetros. Aplicación del parámetro Okubo-Weiss. XIII Congreso de la Asociación española de Teledetección. pp. 157-160. Editores: S. Montesinos Aranda y L. Fernández Fornos.

[31]Weiss, J. The dynamics of enstrophy transfer in two dimensional hydrodynamics.  
Physica D Nonlinear Phenomena 48 (March 1991), 273294.

## **Capítulo IV.**

### **Efecto de estructuras Coherentes Lagrangeanas de meso-escala sobre la circulación superficial de la Bahía de Todos Santos**

Autores: Luis Felipe Navarro Olache, Rafael Hernández Walls, Reginaldo Durazo, Rubén Castro

#### **Resumen**

Se utilizan los campos de velocidad de altímetros de satélite y las velocidades superficiales generadas radares de alta frecuencia, para observar los efectos de estructuras Lagrangeanas del Océano Pacífico sobre la capa superficial del océano y la región costera de la bahía de Todos Santos, Baja California. Estructuras coherentes Lagrangeanas son calculadas diariamente a través Exponentes de Lyapunov de Tamaño Finito (ELTF) y comparado con los campos de divergencia superficial dentro de la Bahía de Todos Santos calculadas a partir de velocidad superficiales generadas por un arreglo de radares de alta frecuencia. Las estructuras de meso escala observadas frente a las costas de Baja California muestran flujos convergentes y divergentes que logran impactar cerca de la costa generando condiciones de circulación dentro de la bahía de Todos Santos. Estas estructuras parecen ser agentes de forzamiento adicional a los forzamientos internos de la bahía, tales como sistemas de brisas, mareas y el traslado del sistema de la corriente de California cercanos a la costa. Los datos muestran que bajo situaciones conocidas como Eventos Santa Ana y condiciones de tormentas, los campos flujos del Océano Pacífico generado por las estructuras coherentes Lagrangeanas son coincidentes y logran modificar la circulación de la bahía.

#### **1 Introducción**

El sistema de la corriente de California (SCC) localizada en la costa oeste de los Estados Unidos y México es una corriente de frontera Este caracterizada por su amplia y permanente flujo superficial en dirección norte a sur y flujos sub superficiales hacia los polos (Chelton, 1982, Lynn et al., 2002, Durazo, 2015). Esta corriente ha sido estudiada extensivamente bajo diferentes

programas y perspectivas (CalCOFI, CODE, SMILE, IMECOCAL) y su dinámica sigue presentando más incógnitas que respuestas, sobre todo a partir de mejores formas de muestrear la capa superficial del océano y los avances en el poder de cómputo. El SCC se encuadra en un sistema de corrientes derivadas por los vientos del giro subtropical del Océano Pacífico Norte, el cual fluye a lo largo de la costa oeste de América del Norte (McCreary et al., 1987). Con las nuevas observaciones la forma en que esta corriente transporta masa, calor y propiedades se presenta cada vez más compleja, en relación a las estructuras de meso y submeso escala que se observan en la superficie. Frentes, eddies, filamentos son observados a lo largo de esta corriente, denotando la naturaleza caótica de flujos superficiales (Figura 1). Estructuras superficiales en forma vórtices coherentes, filamentos, chorros y dipolos tanto en cuencas oceánicas como en las zonas costeras se presentan en escala de 10 a 100 km y una duración de alrededor de algunos días a meses (Griffies et al., 2015). Recientes esfuerzo computacional muestra estas estructuras sobre un dominio numérico en alta resolución ( $1/10^\circ \approx 12$  km de numérica, modelo GFDL's CM2.6, <https://www.gfdl.noaa.gov/ocean-mesoscale-eddies/>) los cuales revelan la forma y en que estas estructuras distribuyen de propiedades en los océanos y son importantes para comprender las escala de balances térmicos y biogeoquímicos.

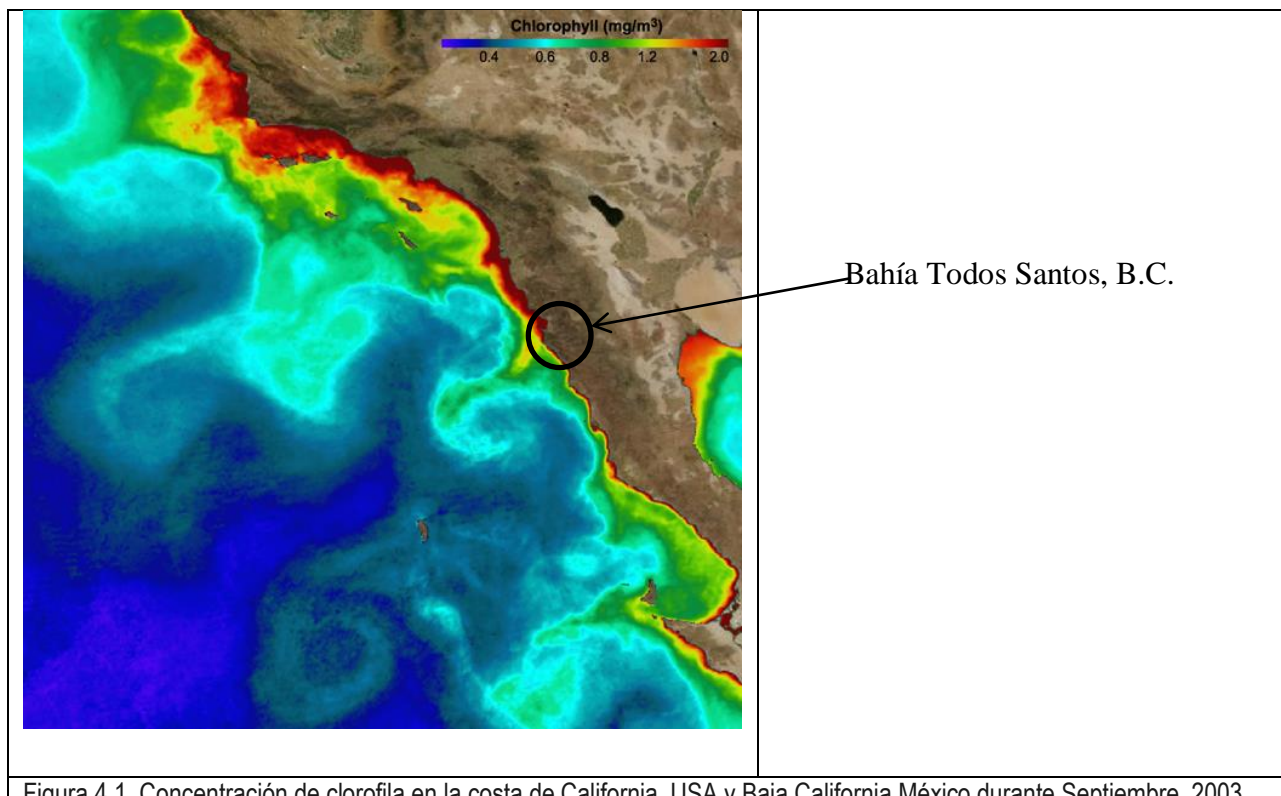


Figura 4.1. Concentración de clorofila en la costa de California, USA y Baja California México durante Septiembre, 2003,

se muestra el transporte superficial hacia afuera de la costa en estructuras superficiales en forma de eddies y filamentos (imagen MODIS Aqua (<http://oceancolor.gsfc.nasa.gov/>)).

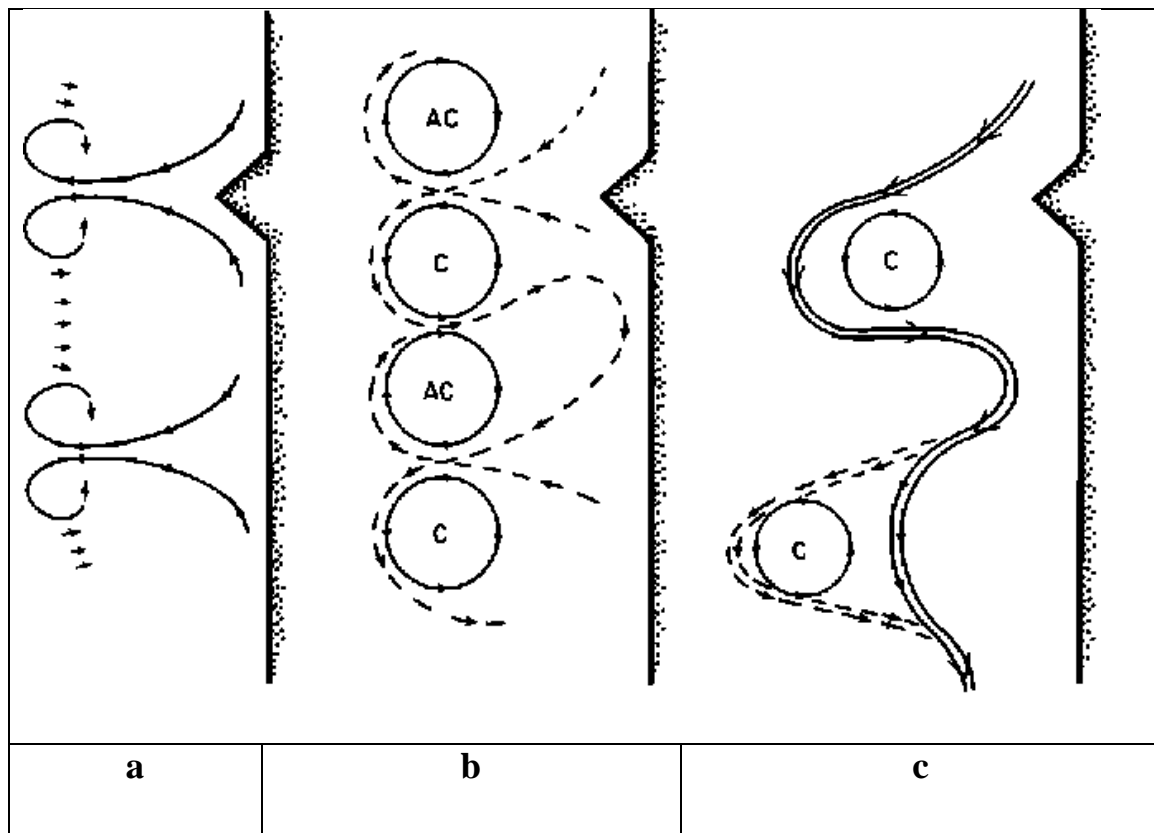


Figura 4.2 Esquema conceptual de estructura de flujo asociado con los filamentos frios (Strub et al., 1991) del sistema de la corriente de California. De izquierda se identifican a) dipolos o chorros costeros (squirts), b) eddies de mesoescala y c) menadros. El prefijo **C** en los esquemas identifica circulacion ciclonica (dextrogiro) y **AC** anticiclonica (levogiro)

Las imágenes de satélite tanto en clorofila, temperatura muestran a lo largo de la corriente de California estructuras ordenadas, como filamentos (Fig. 2) eddies de mesoescala (Fig.2 b) o meandros a lo largo de la costa ((Fig. 2c) con al parecer algunas propiedades de transporte como se muestra imagen de la Fig. 1. A pesar de este la alta variabilidad de las estructuras y flujos, las imágenes muestran estructuras que perduraban en el tiempo, a las cuales se les llamo estructuras Coherentes Lagrangeanas (ECL) en un flujo caótico. Las ECL pueden definirse como entidades individuales en un flujo, que persiste suficientemente, como para ser visualizadas, es decir tiene

coherencia temporal (Adrian, 2007) o que contribuye significativamente en la estructura media de flujo. (Adrian y Marusic, 2012) a lo que se le llama coherencia espacial.

Las estructuras Lagrangeanas coherentes puedes ser vistas como líneas o barreras materiales en las cuales elementos de fluido al no poder cruzar son atraídos o repelidos a lo largo de líneas de divergencia o convergencia (Haller y Yuan, 2000). El concepto teórico emerge de sistemas dinámicos que evolucionan con el tiempo y que han sido eficaces en detectar transporte en fluidos, un esquema de estas líneas de flujo se presenta en la figura 4.3. En estas estructuras es frecuente que se formen zonas donde los elementos quedan atrapados, por periodos de tiempo en estructuras concéntricas o vórtices. Las flechas en la figura 4.3a señalan la trayectoria del flujo generado por la barrera y la deformación lateral de una parcela de fluido cercano a la línea repelentes (Fig. 4.3b). En cualquier escenario de flujos en el océano, identificar estos puntos atrayentes o repelentes es claramente necesario para estimar con mayor precisión trayectorias de objetos en la superficie del océano, o predecir con mayor grado de certeza el destino de elementos en la capa superficial, tales como de plumas de contaminantes, derrames de petróleo e incluso en la dispersión de propiedades biogeoquímicas. En este trabajo se identifican estructuras coherentes Lagrangeanas a partir del cálculo de exponentes de Lyapunov de tamaño finito (ELTF o FSLE). Los exponentes se generan mediante mallas de velocidad superficial y miden la razón del estiramiento de partículas contiguas, usando las velocidades adquiridas por los altímetros de satélite y provistos por el sistema AVISO+. Esta información de estructuras de meso escala se proyecta en la cercanía de la Bahía de Todos Santos con el objetivo de observar el papel de transporte advectivo en trazadores tanto pasivos como reactivos. En la bahía se generan mallas velocidad superficial de alta resolución mediante radares de alta frecuencia que pueden distinguir el papel de las estructuras externas dentro de la bahía. Se compara bajo diferentes esquemas el impacto de flujos de meso-escala divergente o convergente en la circulación de la bahía observada en alta resolución, actuando como agente externo a la circulación de la bahía de Todos Santos.

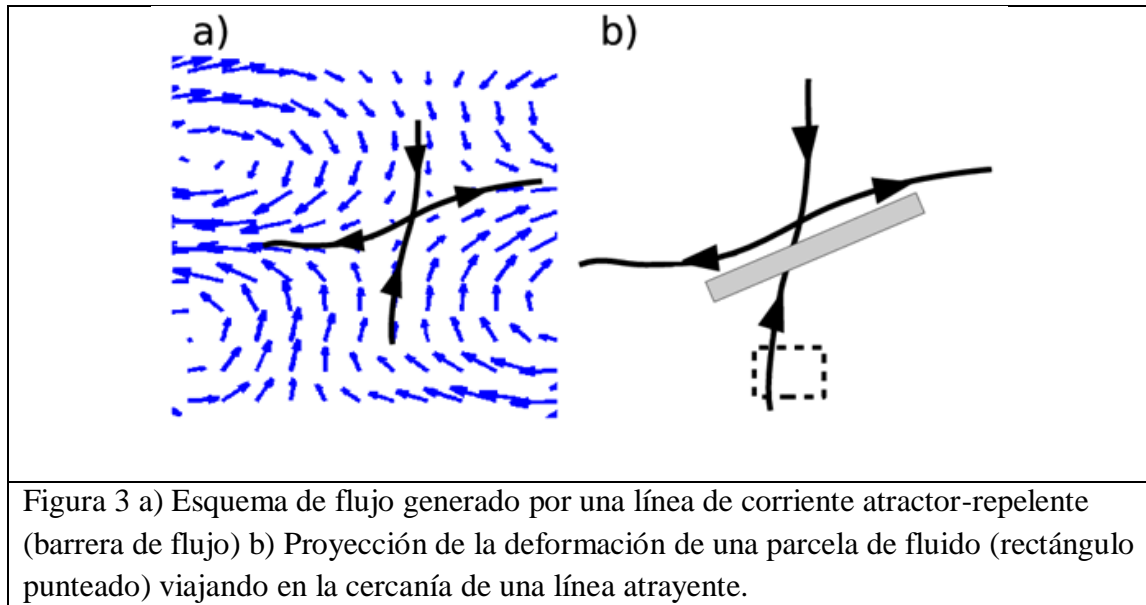


Figura 3 a) Esquema de flujo generado por una línea de corriente atractor-repelente (barrera de flujo) b) Proyección de la deformación de una parcela de fluido (rectángulo punteado) viajando en la cercanía de una línea atrayente.

## 2 Metodología

La organización espacial de estructuras de flujo caóticas tanto en la atmósfera como en los océanos se ha distinguido desde que la escala de observaciones de estos movimientos ha incrementado su resolución. Seguir a estas estructuras y sus movimientos es fundamental para comprender los procesos de transporte, mezcla y agitación de partículas dentro de un flujo. Las Estructuras Coherentes Lagrangeanas (ECL) son identificadas como líneas materiales de atracción o repulsión (figura 2) y se calculan a través de un campo de velocidad, en el presente caso en dos dimensiones, utilizando las técnicas denominadas estructuras de Lyapunov de tamaño finito ELTF y estructuras de Lyapunov de tiempo finito ELTF los cuales se explicaran más adelante.

### 2.1 Datos de velocidad

Se generaron independientemente dos campos de velocidad uno gran escala a lo largo de la costa de California y Baja California y el otro dentro de la Bahía de Todos Santos. El campo de velocidad  $v(x,t)$  entre el paralelo 34 y 28 norte, que distingue al sistema de la Corriente de California es obtenida de la ecuación siguiente:

$$v(\mathbf{x}, t) = \left[ -\frac{g}{f} \frac{\partial \eta(\mathbf{x}, t)}{\partial y}, \frac{g}{f} \frac{\partial \eta(\mathbf{x}, t)}{\partial x} \right] \quad (1)$$

Aquí  $\mathbf{x} = (x, y)$  es la posición en el plano Cartesiano, donde  $x$  es la coordenada zonal, mientras que  $y$  en la dirección meridional;  $\eta(\mathbf{x}, t)$  es la altura de nivel de mar de datos de altímetro (SSH);  $f$  es el parámetro de Coriolis (dos veces el componente vertical de la velocidad angular de la tierra);  $y g$  la aceleración de la gravedad. El componente  $\eta$  esta dado por la topografía dinámica construida de datos de altímetro, (Rio y Hernández, 2004, 2005). La perturbación  $\eta$  es una componente transitoria dada por la anomalía del altímetro, generada en forma diaria a una resolución de  $0.25^\circ$ .

Los datos de corrientes superficiales en la bahía de Todos Santos fueron medios por un arreglo de radares de alta frecuencia, localizado en el margen de la Bahía de Todos Santos. Para este trabajo se utilizó el año 2010 por contener la serie más completa de datos de velocidad, aunque también se usaron series cortas durante eventos específicos como la serie de Abril y Mayo 2014 que discutiremos más adelante con relación a las estructuras Lagrangeanas afuera de la bahía. La resolución espacial de los datos es de 1 km y la temporal es de 1 hr. Los radares operan a una frecuencia modulada de alrededor de 25 MHz capaz medir la velocidad de la corriente a una profundidad de alrededor de un metro, a una distancia de 20 km. Las velocidades radiales son medidas cada 20 minutos y promediadas cada hora. (Flores-Vidal et al., 2015). Con los datos de velocidad se calculó la matriz Jacobiana:

$$J = \begin{bmatrix} \frac{\partial u(x,y)}{\partial x} & \frac{\partial u(x,y)}{\partial y} \\ \frac{\partial v(x,y)}{\partial x} & \frac{\partial v(x,y)}{\partial y} \end{bmatrix} \quad (2)$$

Usando una malla de 22X22 , posicionada en el eje norte-sur dentro de la bahía.

De la ecuación 2, la traza define la divergencia horizontal como sigue:

Este operador permite comparar la similitud de patrones generados las velocidades el océano pacífico.

## 2.2 Estructuras de Lyapunov de tamaño finito (ELTF)

El cálculo de exponentes de tamaño finito de Lyapunov (ELTF) es una herramienta prácticas y robustas para identificar cambio espaciales en un flujo, debidos a procesos de advección. Los exponentes miden la razón de separación entre partículas contiguas en un flujo, promediadas sobre un tiempo y se usan para detectar y visualizar estructuras Lagrangeanas (barreras de transporte, Koh y Legras, 2002).

Los cambios se calculan integrando el campo de velocidad utilizando una interpolación bilineal de las velocidades del altímetro para generar un suavizado efectivo con una resolución menor a 1/8 de grado (D’Ovidio et al., 2004). Los bordes donde los exponentes de Lyapunov son máximos, calculados hacia atrás, definen las llamadas estructuras coherentes Lagrangeanas o barreras de transporte (Fig. 1) que son una generalización de trayectorias hiperbólicas estables de un flujo independiente del tiempo. Se definen como en máximo eigenvalor del tensor de esfuerzo Cauchy-Green. Estas estructuras están fuertemente ligadas a la razón de separación  $\lambda$  de dos partículas transitando en un flujo durante un lapso de tiempo ( $t$ ):

Donde  $\delta_o$  (respecto de  $\delta_f$ ) es distancia de separación inicial fijada antes de iniciar los cálculos. El método es un producto proporcionado por AVISO (d’Ovidio et al 2014) calculado en una malla (nivel 4) de velocidades geostrofica de la topografía dinámica del nivel de mar (ADT) por el Servicio Marino Copernicus (CMEMS, <http://marine.copernicus.eu/>). Los detalles de entrada y procesamiento pueden ser consultados en los manuales de usuarios (<http://cmems-resources.cls.fr/documents/PUM/CMEMS-SLPUM-008-032-051.pdf>) y documentos de validación (<http://cmemsresources.cls.fr/documents/QUID/CMEMS-SL-QUID-008-032-051.pdf>). El producto tiene cobertura global desde 1994 a 2018. La separación inicial de 0.2 grados y la final es de 0.6 grados con una resolución temporal de un día y espacial de 0.04 grados. El producto visualiza estructuras de meso-escala por lo que la distancia final  $\delta_f$  representa un grado es decir cerca de 110 km. Los FSLE representan el inverso de la escala de mezcla entre las distancias inicial y final ( $\delta_o$  y  $\delta_f$ ) d’Ovidio et al. (2004).

## 2.1 Estructuras de Lyapunov de tiempo finito (FTLE)

Los ELTF son también escalares que miden la separación de partículas de fluido en tiempos finitos (Shadden et al., 2005, Beron-Vera, et al., 2008). Esta herramienta calcula el tiempo promedio en que ocurre la máxima razón de separación entre dos partículas en el flujo, es una analogía matemática de seguir elementos a la deriva ya que a miden a partir de una distancia inicial entre elementos en el flujo el transporte en el espacio, esta distancia se denominado razón de separación. Cada partícula será afectada por el flujo que desplazara a ambas a posiciones nuevas, después de un tiempo T, las cuales deformaran la línea entre ambas partículas. El máximo desplazamiento está relacionado con el máximo eigenvalor del tensor de deformación de Cauchy-Green. El método descrito por Shadden et al 2005 muestra que el máximo estiramiento ocurre cuando se elige un desplazamiento alineado con el eigenvector de la máximo eigenvalor, bordeando zonas máximas donde el flujo diverge o converge como se muestra en la figura 4.2.

$$\sigma_{to}^T(x) = \frac{1}{|T|} \ln \sqrt{\lambda_{\max}(\Delta)}$$

En este trabajo se presentan exponentes Lyapunov de tamaño finito (ELTF) ya que a no se esperan diferencias significativas entre cualquiera de los dos métodos para localizar estructuras Lagrangeas coherentes, a la escala y parámetros de este trabajo (Tew Kai et al., 2008).

### **3 Resultados y Discusiones**

En este trabajo se estudia estructuras coherentes Lagrangeanas, visualizadas de los campos de estructuras de exponentes de Lyapunov integradas hacia adelante y hacia atrás (d'Ovidio et al 2004,2009). Las figuras revelan una serie de estructuras Lagrangeanas con dimensiones dominada por la mesoscala de alrededor de 100 km. Las estructuras de Lyapunov de tamaño finito se utilizan en este trabajo para visualizar movimientos de partículas en un fluido no estacionario, es decir donde las partículas se separan o se atraen en forma continua. Dentro de la Bahía de Todos Santos se registran los datos meteorológicos mediante una estación meteorológica la cual registro los rasgos dominantes y detalles durante el año 2010, de los cuales mostramos los primeros y últimos meses, ya se describirán algunos rasgos dinámicos ocurridos durante estos períodos. Los datos de temperatura para la zona fueron de un promedio de 22°C, magnitud de velocidad de viento en el rango promedio de  $2 \text{ ms}^{-1}$  con una humedad relativa promedio de 70% (Figura 4). En el primer panel (fig. 4a) se presentan los datos de enero a abril y

se observan 4 eventos marcados por la velocidad del viento, la temperatura y la humedad relativa. En tres de los eventos la velocidad se incrementa a  $10 \text{ ms}^{-1}$ , un decremento de la humedad relativa y aumento en la temperatura del ambiente, este comportamiento fu generado por eventos Santana. Uno de los eventos la velocidad es similar pero la humedad relativa se incrementa con una reducción de la temperatura ambiente, marcando una tormenta de invierno. En la figura 4b se muestran una serie de eventos Santana, de aproximadamente la misma magnitud de velocidad de viento y fuerte decrementos de la humedad relativa con un notable incremento de la temperatura del aire, estos datos son características que marcan la entrada a la costa de eventos Santana (Castro et al., 2003, 2006, Guzmán-Morales et al., 2013). En esta graficas se observa también la llegada de tormentas de invierno a finales de enero y diciembre 2010 correspondientes a dirección de W (Fig. 4c y 4d). El máximo de temperatura para eventos de Santana, fue  $36^{\circ}\text{C}$  durante noviembre. La magnitud máxima de las velocidades de viento para eventos de Santana y tormentas es  $10 \text{ ms}^{-1}$  (Figs. 4 a y b), con ráfagas de hasta  $16 \text{ ms}^{-1}$  en eventos Santana.

Las secuencias que se presentan a continuación mostraran la distribución espacial de exponente de Lyapunov de tamaño finito durante eventos notables en la zona costera. Eventos de vientos intensos (NE-E, continente a oceano) de corta duración conocidos como Santana y tormentas invernales, de magnitud similar, pero dirección contraria (oceano a continente, NW-W). Los exponentes marcan regiones donde partículas se separan (divergen) o se atraen a una razón máxima, relativa al campo de velocidades proporcionado por los altímetros. La región costera seleccionada mide aproximadamente 350 km de ancho por 800 km de largo (Fig. 4.5 a). La figura muestra ELTF para los primeros días del mes de enero 2010. Líneas de altos valores de exponentes de Lyapunov marcan los bordes de estructuras coherentes Lagrangeanas, donde los contornos colores indica flujos que se atraen (azul) o flujo que se repelen (tonos rojo). Destacan en esta figura una estructura en forma de vórtice dipolo en la línea del paralelo  $27^{\circ}\text{N}$ , giros ciclónicos y anticiclónicos en los paralelos 30, 31 y 32.5 de aproximadamente 100 km de diámetro. Estructura en forma de filamentos costeros parecen desarrollarse en las costas de California y Baja California. Sobre la costa algunas estructuras aparentemente formadas en el océano se proyectan a la BTS, en líneas convergentes y divergentes (Fig. 4.5b). En esta figura muestra una marcada zona de divergencia negativa en la BTS, utilizando la velocidad de radares de alta frecuencia esta zona también muestra una divergencia negativa (fig. 4.5c) y velocidades

saliendo por la región sur de la bahía. En estas regiones se marcan zonas de maximas de movimiento en la cercanía de estructuras coherentes Lagrangeanas. Las curvas filamentos y estructuras en forma de eddies que son resueltas en las imágenes diarias de FSLE revelan la naturaleza caótica de los flujos superficiales en el océano pacífico. La distribución espacial de FSLE para los primeros días del mes de Enero 2010 se presenta en la figura 4.3. Valores típicos están en el orden de 0-0.14 (atractores negativo) y 0-0.04 (repelentes positivos) que corresponden a tiempos de mezcla de 7 a 24 días. Estas estructuras son responsables de la capacidad de las corrientes para captar y retener partículas y organismos que estén a la deriva de sus corrientes, existe evidencia de que predadores (Tew Kai et al, 2008) y aves utilizan estos campos de corriente para desplazarse en busca de alimento o (Hernandez-Garcia et al., 1997, Weimerskirch et al., 2010),

En la siguiente imagen se presentan los flujos divergentes y convergentes para el 21 de enero del 2010. Durante este periodo se registró en la zona una tormenta invernal. En la región norte, mar abierto ( $31-33^{\circ}\text{N}$ ) se puede observar un flujo hacia el norte generado por una estructura en forma de vórtice de aproximadamente 200 km. A lo largo de la costa esta estructura forma un flujo hacia el sur paralelas a la costa, con una fuerte zona de convergencia dividiendo ambas estructuras. (Fig. 4.6 a). La amplificación, cercana a la BTS (Fig. 4.6 b) muestra un flujo hacia el sur, paralelos a la costa y las componentes de velocidades de los radares muestran flujos hacia dentro de la bahía (Fig. 4.6c), en el sentido de la dirección dominante (W). Estos datos de corriente superficial, mostraron además valores intensos de divergencia horizontal, en el centro de la bahía.

En las figuras 4.7 a 4.9 mostramos tres eventos de Santana más intensos que los de enero. El primero se presentó en marzo y los otros dos en noviembre 4 y 16 del 2010. Las estructuras en el océano pacífico muestran la misma escala, vórtices de 100 km de diámetro evolucionando en todo el dominio y modificando la estructura de trayectorias superficiales. Cerca de la costa en una franja de entre 50 a 100 km se observa aparentemente la influencia de los vientos Santana (Fig. 4.4 c y d) del continentales hacia mar. Mientras que el flujo de las velocidades del altímetro indican una dirección hacia el sur (Figs. 4.7b y 4.8b) los eventos Santana de noviembre muestran un flujo a lo largo de la costa hacia el norte. Dentro de la bahía los valores de ELTF son pequeños a negativas, marcando una zona de divergencia horizontal, misma que se refleja en la

estructura de divergencia negativa , en el centro de la bahía, generada por las velocidades superficiales de los radares de alta frecuencia (Figs 4.7c, 4.8c y 4.9c).

La figura 4.10 muestra la influencia de uno de los eventos de Santana más intensos de los registrados en la BTS, entre 2009 al 2018. El panel para el 13 de mayo muestra dos giros de sentido contrario cerca de la costa, aproximadamente centrados en 31 y 33°N. En la BTS puede notarse una zona de divergencia con flujos hacia afuera de la costa, más notoria en la amplificación (Fig. 4.10b). En este día los flujos de viento fueron preferentemente hacia afuera de la costa (Fig 4.10c) marcando una fuerte divergencia de tanto las corrientes del altímetro como las velocidades medidas por los radares dentro de la bahía (Fig. 4.11).

Las estructuras coherentes Lagrangeanas proveen el esqueleto de transporte horizontal, escala en la que se comparan los eventos son diferente, sin embargo considerando la alta resolución para detectar la separación de partículas bajo este método ( $\sim 2.2$  km) (d'Ovidio et al, 2004,2009) podríamos sugerir que las coincidencias no son fortuitas Los valores de mezcla para estructuras atrayentes fueron de alrededor de 7 días mientras que para valores cercanos a la costa de estructuras repelentes fue de 24 días. La cantidad de información que se obtiene de las estructuras Lagrangeanas podría utilizarse en una gran variedad de aplicaciones como conocer la trayectoria de objetos flotantes, o partículas disueltas (Olascoanga et al, 2004) búsqueda y recate entre otras ya mencionadas. Investigaciones sobre el comportamiento de animales marinos sugiere fuertemente que utilizan las trayectorias de estructuras coherentes para usar zonas de acumulación de material, diferencias de temperatura o rutas más favorables para el vuelo (Ruijter et al., 2004, Weimerskirch et al., 2004)

## 4 Conclusiones

Los exponentes de Lyapunov de tamaño finito son una herramienta robusta en la observación del movimiento de partículas marcando regiones donde las partículas continuamente se alejan o atraen, marcando estructuras coherentes Lagrangeanas en un campo de flujo caótico. En la región de estudio que corresponden al sistema de la corriente de California podrían explicar parte de las estructuras que frecuentemente se observan en imágenes de satélite. Estas estructuras en zonas costeras podrían aportar patrones de movimiento externos a cuerpos costeros, como es el

caso de la bahía de Todos Santo, aunque las escalas y metodología para encontrar las velocidades fue diferente.

El uso del concepto de estructuras coherentes Lagrangeanas se utilizó con aproximaciones de exponentes de Lyapunov de tamaño y tiempo finito. En ambos métodos se puede observar que las estructuras separan fluido de diferente dinámica y por tanto realizan diferentes trayectorias. Las estructuras coherentes no solo controlan la advección caótica del fluido, mediante líneas que se atraen o repelen sino que parecen influir en forma remota, es decir desde el océano abierto a la dinámica cercana a la costa como se observa en algunos eventos dentro de la bahía de Todos Santos.

## Bibliografia

- Aref, H.1984. Stirring by chaotic advection. *J. Fluid Mech.*, 143:1–21.
- Artale, V G. Boffetta, VG, Celani,A, Cencini, M and Vulpiani, A. 1997. Dispersion of passive tracers in closed basins: Beyond the diffusion coefficient. *Phys. Fluids*, 9:11, 1997.
- Beron-Vera F.J. and M. J. Olascoaga, (2008). Oceanic mesoscale eddies as revealed by Lagrangian coherent structures. *Geophys. Res.* 35, L12603, doi:10.1029/2008GL033957.
- Chelton, D. B., M. G. Schlax, R. M. Samelson, and R. A. de Szoeke (2007), Global observations of large oceanic eddies, *Geophys. Res. Lett.*, 34, L15606, doi:10.1029/2007GL030812.
- Conkright, M. E., et al. (2002), World Ocean Database 2001, Volume 1:Introduction, 152 pp., NOAA Atlas NESDIS 42, U.S. Government Print-ing Office, Washington, D.C.
- D'Ovidio, F., V. Fernández, E. Hernández-Gracia, and C. López(2004), Mixing structures in the Mediterranean Sea from finite-sizeLyapunov exponents, *Geophys. Res. Lett.*, 31, L17203, doi:10.1029/2004GL020328.
- D'Ovidio, F., Taillandier, V., Taupier-Letage, I. and Mortier, L. 2009. Lagrangian validation of the mediterranean mean dynamic topography by extraction of tracer frontal structures. *Mercator Ocean Quarterly Newsletter* 32: 24–32
- Ducet, N., P.-Y. Le Traon, and G. Reverdin (2000), Global high resolutionmapping of ocean circulation from TOPEX/Poseidon and ERS-1 and -2,J. *Geophys. Res.*, 105, 19,477– 19,498.
- Franco, E., D. N. Pekarek, J. Peng, and J. O. Dabiri (2007), Geometry ofunsteady fluid transport during fluid-structure interactions, *J. FluidMech.*, 589, 125–145.
- Goni, G., and W. Johns (2001), Census of warm rings and eddies in theNorth Brazil Current retroflection region from 1992 through 1998 usingTOPEX/Poseidon altimeter data, *Geophys. Res. Lett.*, 28, 1–4.
- Green, M. A., C. W. Rowley, and G. Haller (2007), Detection of Lagrangiancoherent structures in three-dimensional turbulence, *J. Fluid Mech.*, 572, 111–120, doi:10.1017/S0022112006003648.
- Griffies, Stephen M.,Michael Winton, Whit G Anderson, Rusty Benson, Thomas L Delworth, C O Dufour, John P Dunne, P Goddard, A K Morrison, Andrew T Wittenberg, J Yin, and

- Rong Zhang, February 2015: Impacts on ocean heat from transient mesoscale eddies in a hierarchy of climate models. *Journal of Climate*, 28(3), doi:10.1175/JCLI-D-14-00353.1.
- Haller, G. (2001), Lagrangian structures and the rate of strain in a partition of two-dimensional turbulence, *Phys. Fluids*, 13, 3365–3385.
- Haller, G., and G. Yuan (2000), Lagrangian coherent structures and mixing in two-dimensional turbulence, *Physica D*, 147, 352–370.
- Hernandez Garcia E., J.H. Bettancourt, V. Garcon, L. Hernandez Carrasco, C. Lopez V. Rossi, J. Sudre y E. Tew Kai. Biological Impact of Ocean transport: a finite size lyapunov characterization. DOI: 10.13140/2.1
- Isern-Fontanet, J., E. García-Ladona, and J. Font (2003), Identification of marine eddies from altimetric maps, *J. Atmos. Oceanic Technol.*, 20, 772–778
- Le Traon, P.-Y., F. Nadal, and N. Ducet (1998), An improved mapping method of multisatellite altimeter data, *J. Atmos. Oceanic Technol.*, 15, 522–534.
- McCreary, J. P. and S.-Y. Chao, 1987: On the dynamics of the California Current system. *J. Mar. Res.*, 45, 1–32
- Mathur, M., G. Haller, T. Peacock, J. E. Ruppert-Felsot, and H. L. Swinney (2007), Uncovering the Lagrangian skeleton of turbulence, *Phys. Rev. Lett.*, 98, 144,502, doi:10.1103/PhysRevLett.98.144502.
- Morrow, R., F. Birol, and D. Griffin (2004), Divergent pathways of cyclonic and anti-cyclonic ocean eddies, *Geophys. Res. Lett.*, 31, L24311, doi:10.1029/2004GL020974.
- Okubo, A. (1970), Horizontal dispersion of floatable particles in the vicinity of velocity singularity such as convergences, *Deep-Sea Res. Oceanogr. Abstr.*, 12, 445–454.
- Olascoaga, M. J., Beron-Vera, F. J., Brand, L. E. and Kocak, H. 2008. Tracing the early development of harmful algal blooms on the west Florida shelf with the aid of lagrangian coherent structures. *J. Geophys. Res.* **113**(C12014).
- Olascoaga M.L. y G. Haller. 2012. Forecasting sudden changes in environmental pollution patterns. *PNAS* (109)13, 4738-4743.
- Rio, M.H. and Hernandez F., 2004. A mean dynamic topography computed over the world ocean from altimetry, in situ measurements, and geoid model. *Journal of Geophysical Res.* Vol 109 C12032, 1-19.
- Rio, M.H., Schaefer, P., Lemoine, J.M. y Hernandez, F. 2005. Estimation of the ocean Mean Dynamic Topography through the combination of altimetric data, in-situ measurements and GRACE geoid: From global to regional studies. Paper presented at GOCINA International Workshop, Eur. Cent. for Geodyn. and Seismol, Luxembourg, 13-15 April
- Scott, R. B., and F. Wang (2005), Direct evidence of an oceanic inverse kinetic energy cascade from satellite altimetry, *J. Phys. Oceanogr.*, 35, 1650–1666.
- Shadden, S. C., F. Lekien, and J. E. Marsden (2005), Definition and properties of Lagrangian coherent structures from finite-time Lyapunov exponents in two-dimensional aperiodic flows, *Physica D*, 212, 271–304.
- Shadden, S. C., J. O. Dabiri, and J. E. Marsden (2006), Lagrangian analysis of fluid transport in empirical vortex ring flows, *Phys. Fluids*, 18, 47, 105.
- Stammer, D. (1997), Global characteristics of ocean variability estimated from regional TOPEX/POSEIDON altimeter measurements, *J. Phys. Oceanogr.*, 27, 1743–1769.

- Strub, P. T., and C. James, 2000: Altimeter derived variability of surface velocities in the California Current System: 2. Seasonal circulation and eddy statistics. Deep-Sea Res. II, 47B, 831–870.
- Strub, P. T., P. M. Kosro, and A. Huyer, 1991: The nature of the cold filaments in the California Current System. J. Geophys. Res., 96, 14 743–14 768.
- Tew Kai, E., V. Rossi, J. Sudre, H. Weimerskirch, C. Lopez, E. Hernandez-Garcia, F. Marsac y V. Garcon. 2008. Top Marine predators track Lagrangian coherent structures. PNAS (16) 20, 8245-8250. [www.pnas.org/cgi/doi/10.11073/pnas.0811034106](http://www.pnas.org/cgi/doi/10.11073/pnas.0811034106)
- Weimerskirch, H., M. Le Corre, E. Tew Kai , F. Marsac. 2010. Foraging movement of greater frigatebirds from Aldabra Inland: relationship with environmental variables and interactions with fisheries. Progress in Oceanography 86:204-213. doi:10.1016/j.pocean.2010.04.003
- Weiss, J. (1991), The dynamics of enstrophy transfer in two-dimensional hydrodynamics, Physica D, 48, 273–294, doi:10.1016/0167-2789(91)90088-Q.
- Witter, D. L., and A. L. Gordon (1999), Interannual variability of the South Atlantic circulation from 4 years of TOPEX/POSEIDON satellite altimeter observations, J. Geophys. Res., 10, 20,927–20,948.

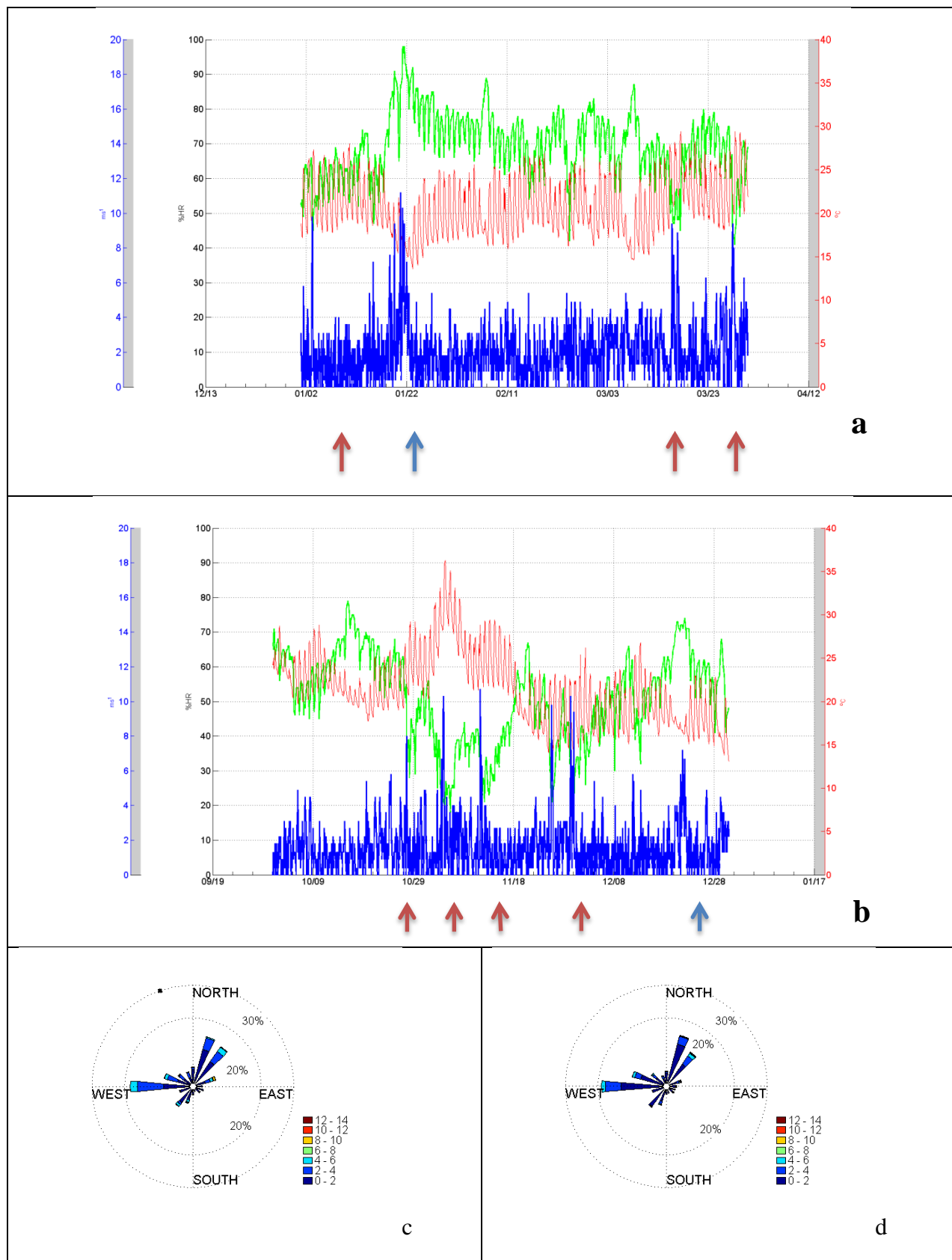
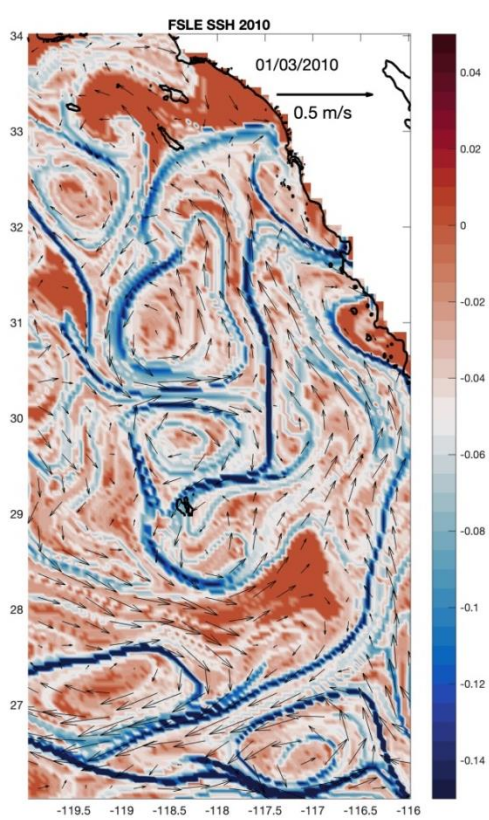
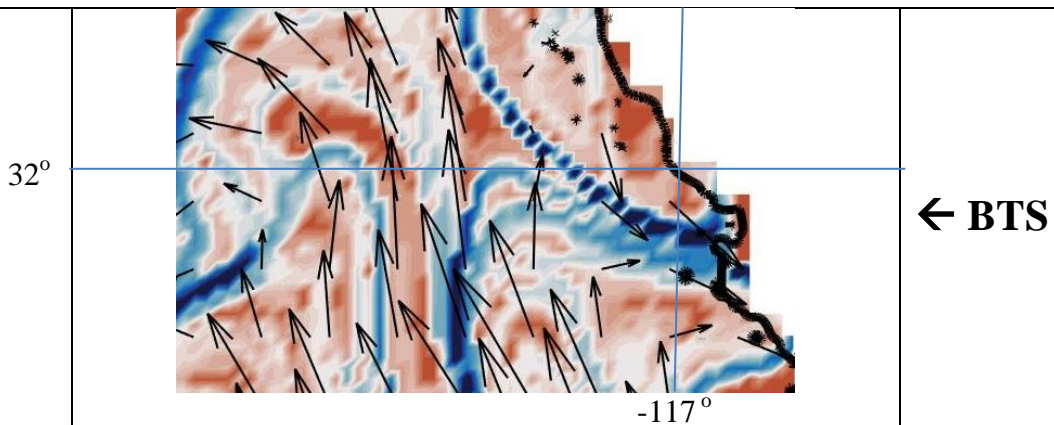


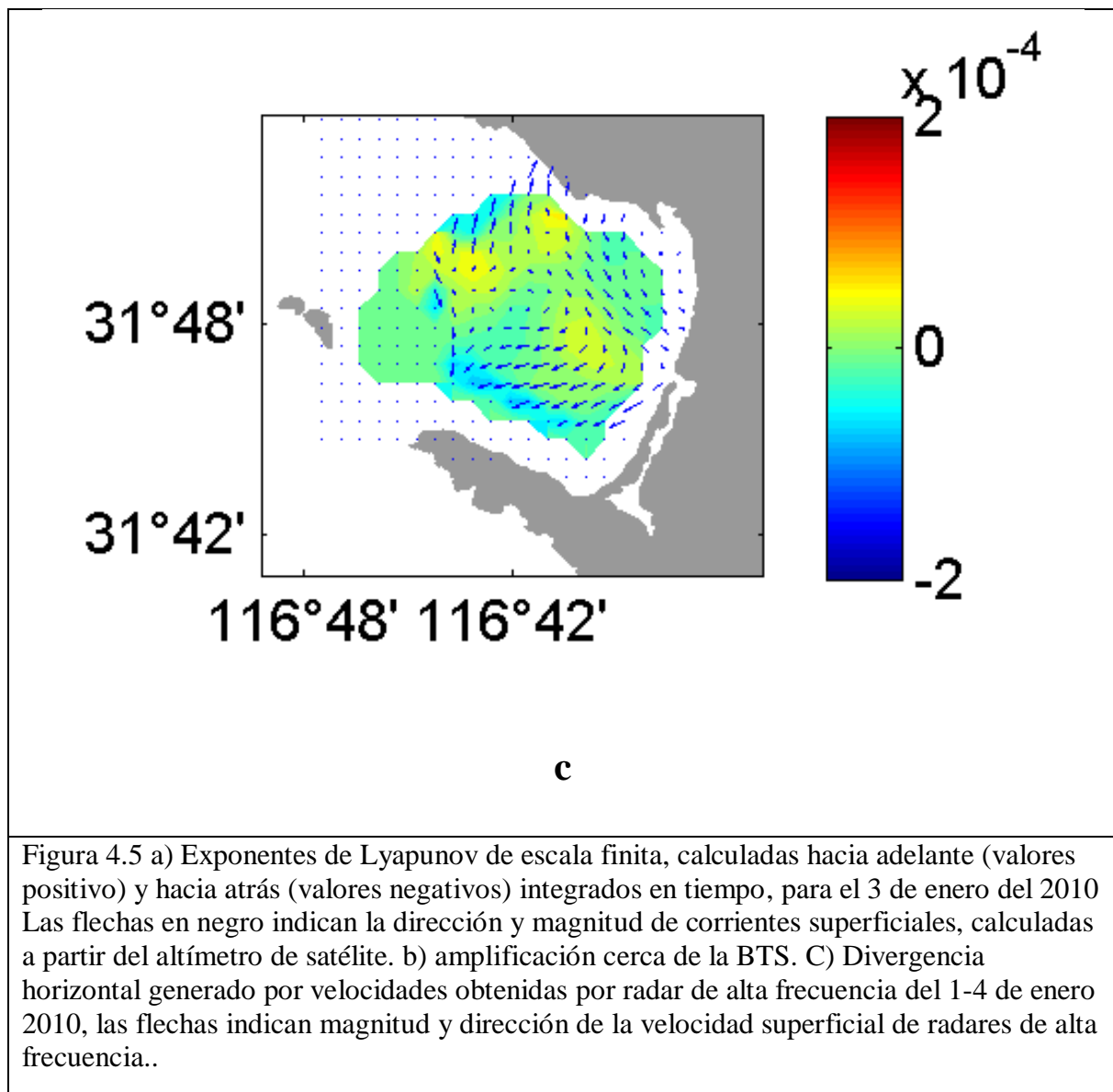
Figura 4.4 Variables meteorologicas sobre la costa humedad relativa (verde), temperatura del aire (rojo) y velocidad de viento para los primeros a) los primeros 4 meses del año b) ultimos 4 meses del año 2010. Las flechas en azul señalan eventos tormentas de dirección NW-W mientras que las flechas en rojo señalan de alta temperatura, generados vientos de Santana del NE a E conocidos como Santana. Rosa de direcciones de viento para c) panel superior, d) panel inferior

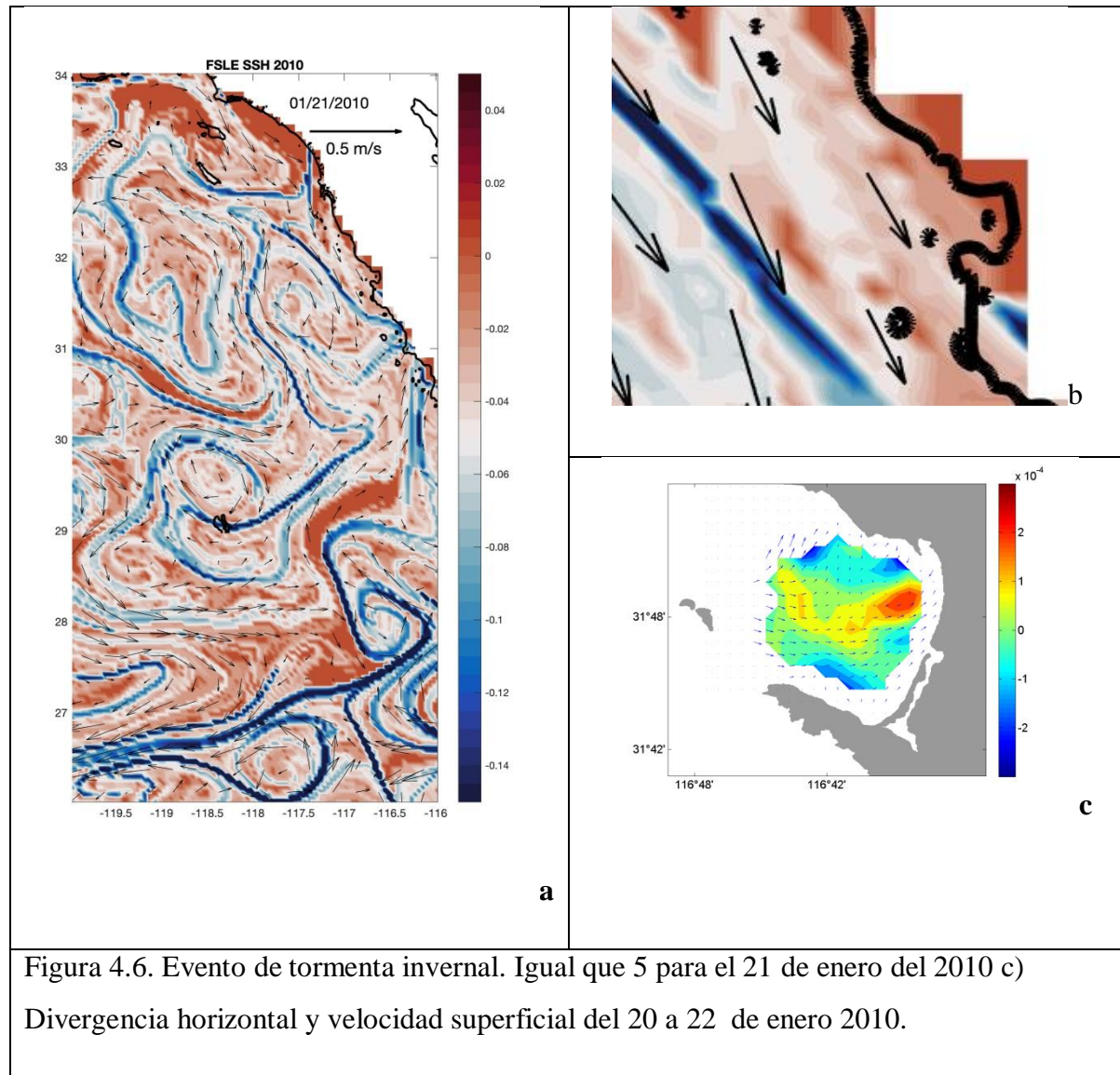


**a**



**b**





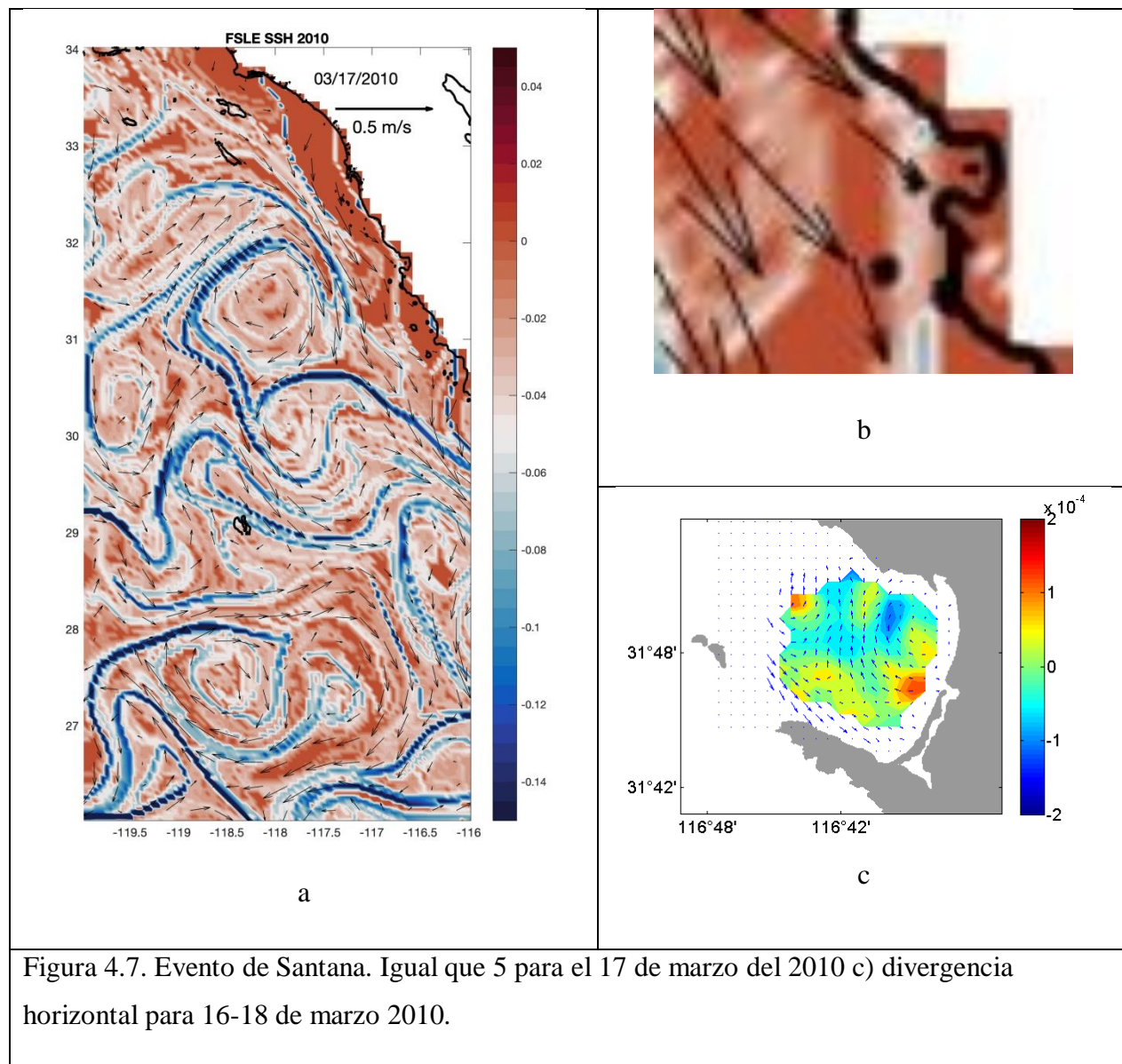
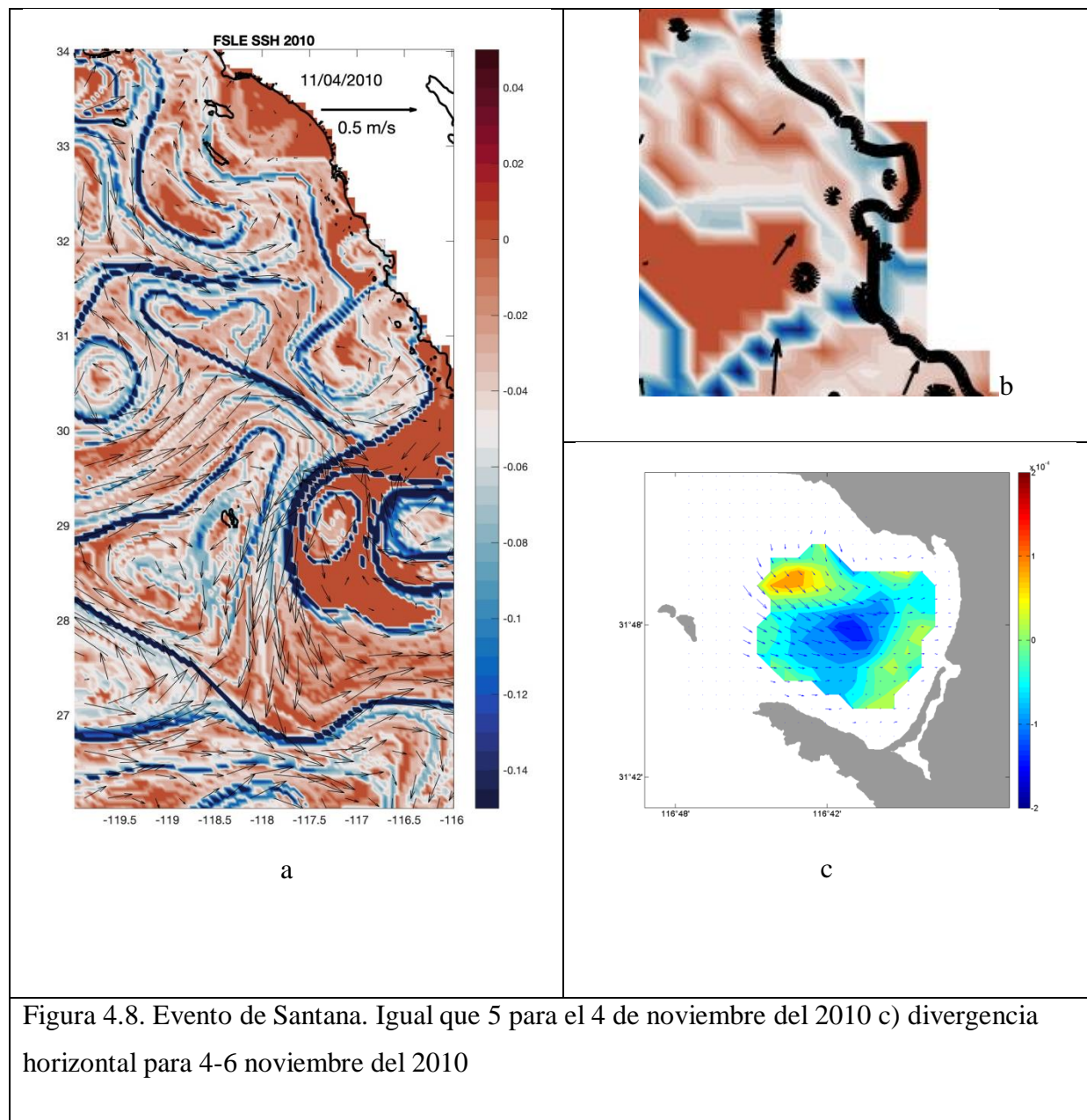
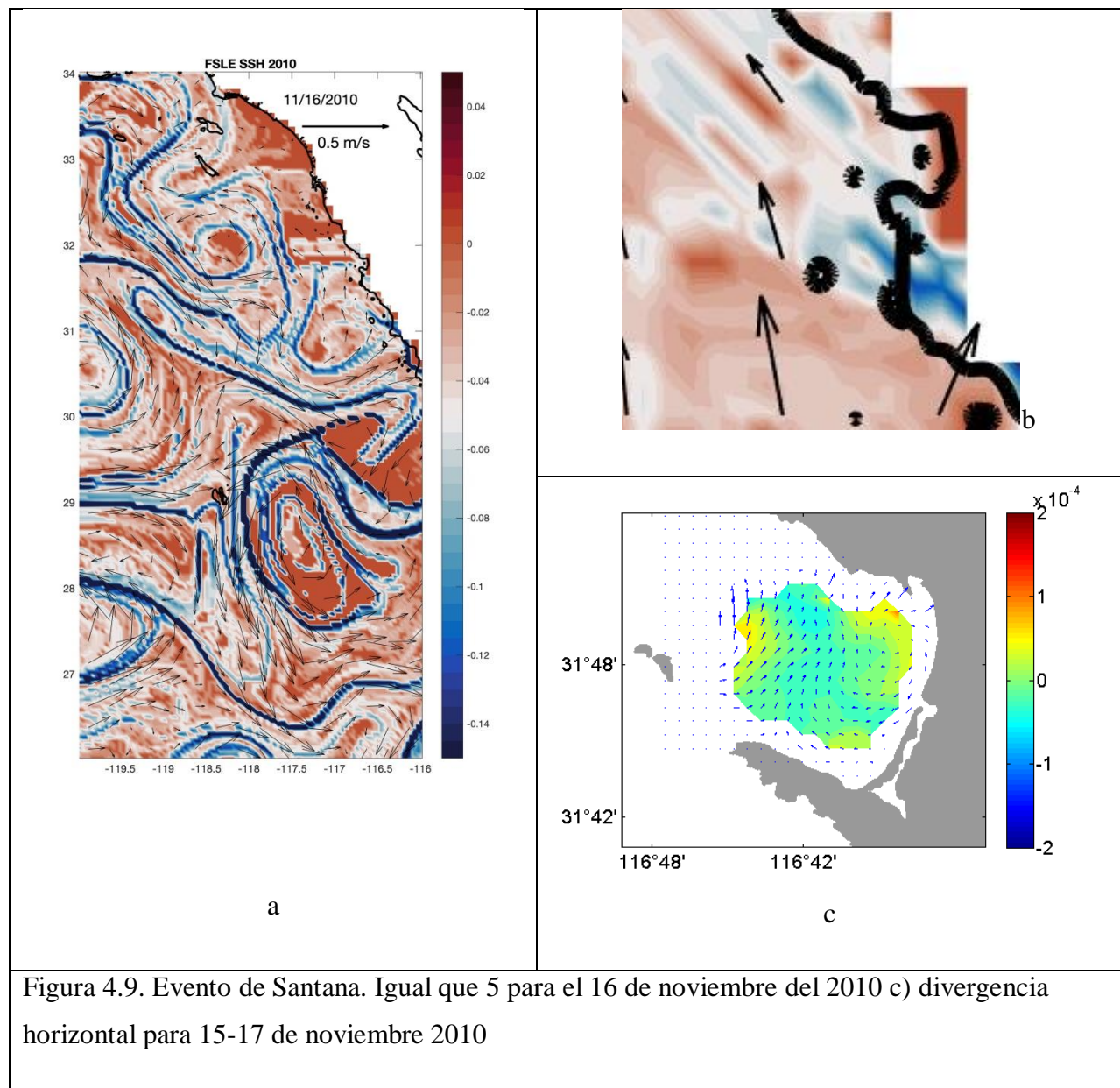
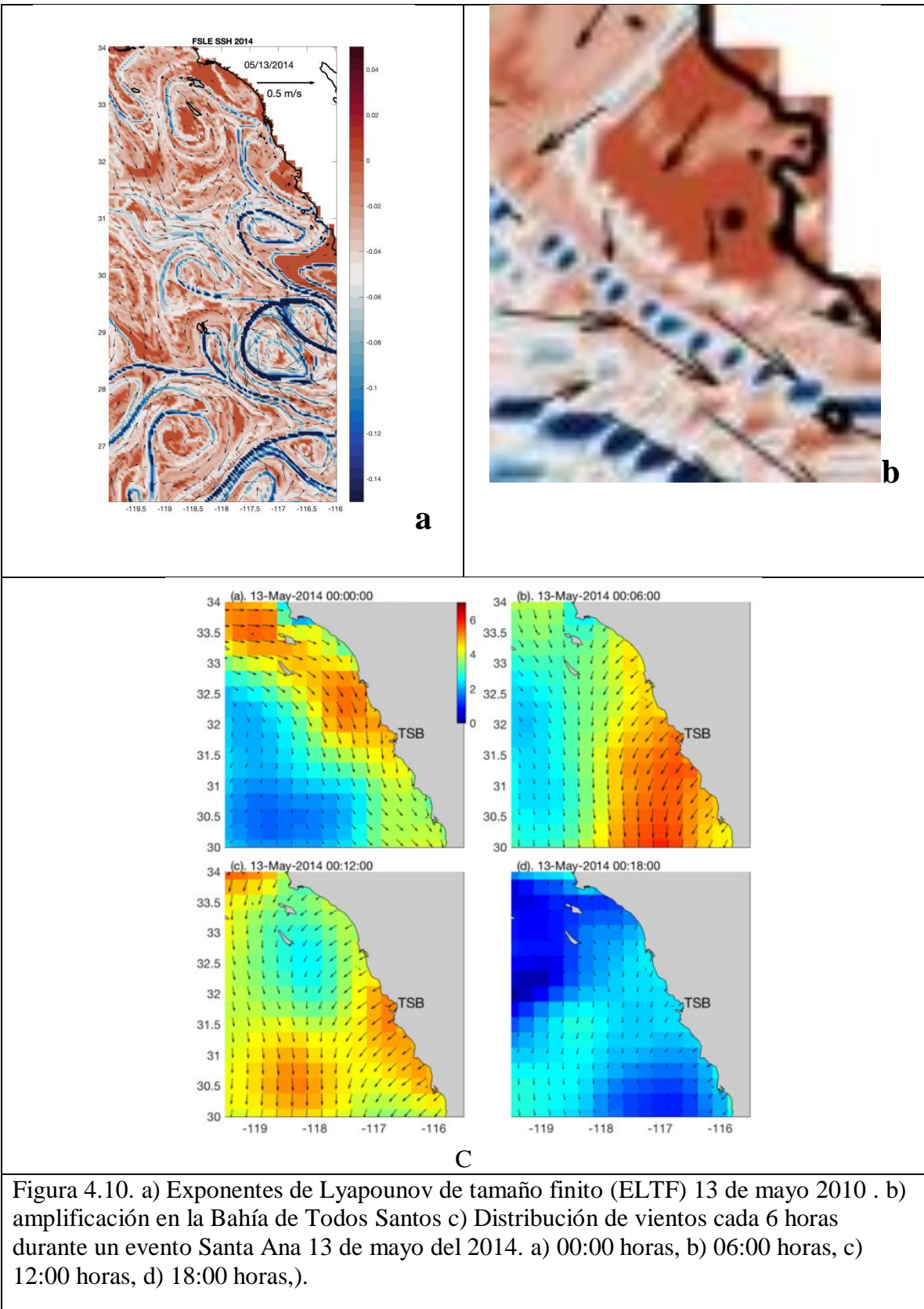
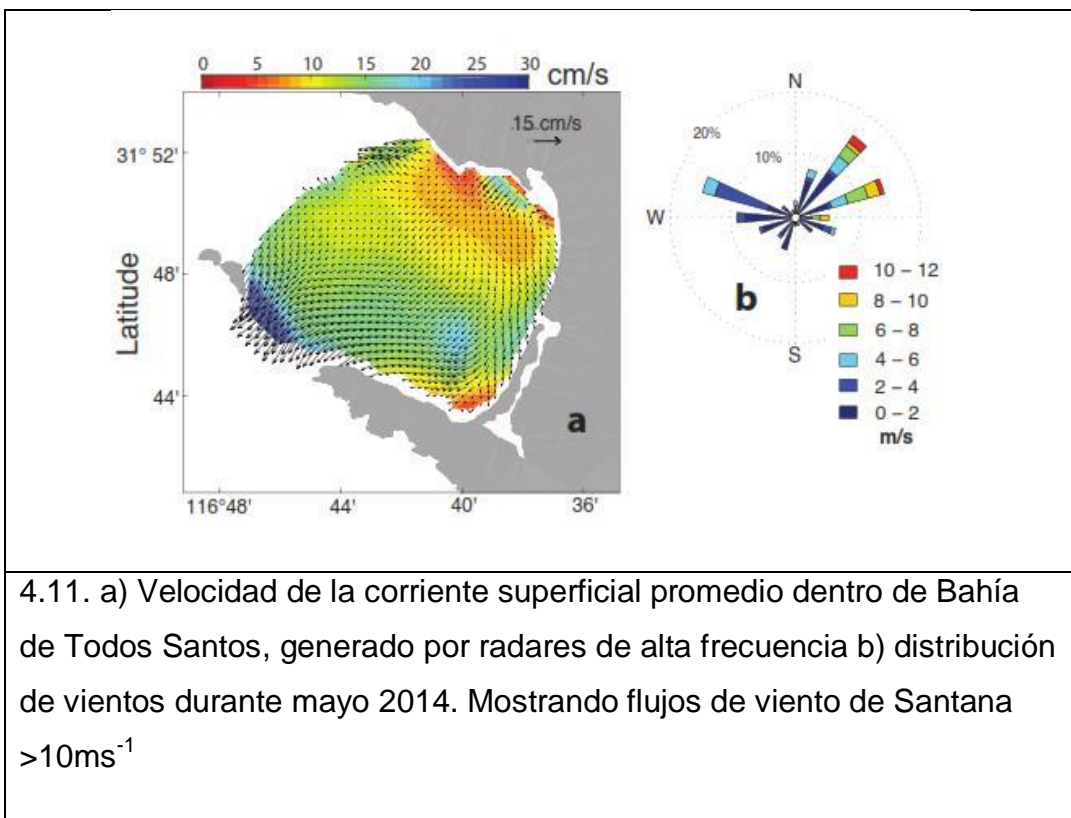


Figura 4.7. Evento de Santana. Igual que 5 para el 17 de marzo del 2010 c) divergencia horizontal para 16-18 de marzo 2010.









4.11. a) Velocidad de la corriente superficial promedio dentro de Bahía de Todos Santos, generado por radares de alta frecuencia b) distribución de vientos durante mayo 2014. Mostrando flujos de viento de Santana >10ms<sup>-1</sup>